VILNIUS GEDIMINAS TECHNICAL UNIVERSITY

Veronika MALYŠKO-PTAŠINSKĖ

DEVELOPMENT AND RESEARCH OF INVASIVE AND NON-INVASIVE ELECTRODES FOR ELECTROCHEMOTHERAPY

DOCTORAL DISSERTATION

TECHNOLOGICAL SCIENCES,
ELECTRICAL AND ELECTRONIC ENGINEERING (T 001)

Vilnius, 2023

The doctoral dissertation was prepared at Vilnius Gediminas Technical University in 2019–2023.

Supervisor

Prof. Dr Vitalij NOVICKIJ (Vilnius Gediminas Technical University, Electrical and Electronic Engineering – T 001).

The Dissertation Defence Council of the Scientific Field of Electrical and Electronic Engineering of Vilnius Gediminas Technical University:

Chairman:

Prof. Dr Artūras SERACKIS (Vilnius Gediminas Technical University, Electrical and Electronic Engineering – T 001).

Members:

Dr Baltramiejus JAKŠTYS (Vytautas Magnus University, Biology – N 010),
Dr Oliver LIEBFRIED (French-German Research Institute of Saint-Louis, France, Electrical and Electronic Engineering – T 001),
Prof. Dr Voitech STANKEVIČ (State Research Institute Center for Physical Sciences and Technology, Electrical and Electronic Engineering – T 001),
Prof. Dr Nerija ŽURAUSKIENĖ (Vilnius Gediminas Technical University, Electrical and Electronic Engineering – T 001).

The dissertation will be defended at the public meeting of the Dissertation Defence Council of the Scientific Field of Electrical and Electronic Engineering in the Senate Hall of Vilnius Gediminas Technical University at **10 a. m. on 22 May 2023.**

Address: Saulėtekio al. 11, LT-10223 Vilnius, Lithuania.
Tel.: +370 5 274 4956; fax +370 5 270 0112; e-mail: doktor@vilniustech.lt

A notification on the intended defence of the dissertation was sent on 21 April 2023. A copy of the doctoral dissertation is available for review at the Vilnius Gediminas Technical University repository http://dspace.vgtu.lt, the Library of Vilnius Gediminas Technical University (Saulėtekio al. 14, LT-10223 Vilnius, Lithuania) and the Wroblewski Library of Lithuanian Academy of Sciences (Žygimantų st. 1, LT-01102, Vilnius, Lithuania).

Vilnius Gediminas Technical University book No 2023-010-M

doi:10.20334/2023-010-M

veronika.malysko-ptasinske @vilniustech.lt

VILNIAUS GEDIMINO TECHNIKOS UNIVERSITETAS

Veronika MALYŠKO-PTAŠINSKĖ

INVAZINIŲ IR NEINVAZINIŲ ELEKTRODŲ ELEKTROCHEMOTERAPIJAI KŪRIMAS IR TYRIMAS

DAKTARO DISERTACIJA

TECHNOLOGIJOS MOKSLAI,
ELEKTROS IR ELEKTRONIKOS INŽINERIJA (T 001)

Vilnius, 2023

Disertacija rengta 2019–2023 metais Vilniaus Gedimino technikos universitete.

Vadovas

prof. dr. Vitalij NOVICKIJ (Vilniaus Gedimino technikos universitetas, elektros ir elektronikos inžinerija – T 001).

Vilniaus Gedimino technikos universiteto elektros ir elektronikos mokslo krypties disertacijos gynimo taryba:

Pirmininkas

prof. dr. Artūras SERACKIS (Vilniaus Gedimino technikos universitetas, elektros ir elektronikos inžinerija – T 001).

Nariai:

dr. Baltramiejus JAKŠTYS (Vytauto Didžiojo universitetas, biologija – N 010),
dr. Oliver LIEBFRIED (Saint-Louiso Prancūzijos-Vokietijos tyrimų institutas, Prancūzija, elektros ir elektronikos inžinerija – T 001),
prof. dr. Voitech STANKEVIČ (Valstybinis mokslinių tyrimų institutas Fizinių ir technologijos mokslų centras, elektros ir elektronikos inžinerija – T 001),
prof. dr. Nerija ŽURAUSKIENĖ (Vilniaus Gedimino technikos universitetas, elektros ir elektronikos inžinerija – T 001).

Disertacija bus ginama viešame Elektros ir elektronikos mokslo krypties disertacijos gynimo tarybos posėdyje **2023 m. gegužės 22 d. 10 val.** Vilniaus Gedimino technikos universiteto senato posėdžių salėje.

Adresas: Saulėtekio al. 11, LT-10223 Vilnius, Lietuva.
Tel.: (8 5) 274 4956; faksas (8 5) 270 0112; el. paštas doktor@vilniustech.lt

Pranešimai apie numatomą ginti disertaciją išsiųsti 2023 m. balandžio 21 d.

Disertaciją galima peržiūrėti Vilniaus Gedimino technikos universiteto talpykloje http://dspace.vgtu.lt, Vilniaus Gedimino technikos universiteto bibliotekoje (Saulėtekio al. 14, LT-10223 Vilnius, Lietuva) bei Lietuvos mokslų akademijos Vrublevskių bibliotekoje (Žygimantų g. 1, LT-01102 Vilnius, Lietuva).

Abstract

Electroporation-based biomedical treatment has proven to be an efficient method for treating cancer, gene administration or tissue ablation. However, due to the limitations, i.e., inhomogeneous treatment leading to tumour regression, muscle contractions, pain, etc., further optimisation is necessary for the electrodes and pulsed electric field protocols to be performed before clinical use. The dissertation is focused on developing novel electrode structures to ensure uniform treatment and optimal electrical pulsing protocols.

The objective of this dissertation is an adequate simulation of electroporation-based treatments by estimating electric field distribution using accurate tissue models and applied electroporation research.

The introduction presents the investigated problem, research objects, relevance and importance of the dissertation, describes the research methodology, scientific novelty and the defended statements.

The first Chapter introduces the survey of scientific publications on electroporation-based biomedical treatments focusing on the importance of spatial electric field distribution in the tissue, dielectric properties of the tissue and response to the pulsed electric field. Various electrode types used for electrochemotherapy, gene electrotransfer and irreversible electroporation procedures are analysed in terms of electric field distribution and fields of application. It specifies limitations and improvement options regarding previously introduced electrode structures. Also, it shows the influence of pulsed power properties for electroporation-based procedures.

The second Chapter presents the developed superficial tumour and skin models to estimate electric field distribution. The tumour model is used to evaluate the efficacy of the treatment in terms of electric field distribution with the proposed electrode structures, positioning technique and the influence of conductive gel. It analyses the adequacy of the developed electrodes to the experimental setup.

The third Chapter introduces the experimental application of the developed electrode structures positioning strategy for *in vivo* electrochemotherapy treatments. Simultaneously, the efficacy of sub-microsecond electric pulses is demonstrated for different tumour cell lines *in vitro* and *in vivo*. The skin model and simulation results are employed for successful wound treatment with acetic acid. The conclusions are formed according to the obtained results.

Research results on the dissertation's subject were published in five scientific articles in CA Web of Science database journals with an impact factor and 13 presentations have been made at international conferences in Lithuania, Latvia, Slovakia, Slovenia, Poland and Denmark.

Reziumė

Elektroporacija pagrįstas biomedicininis gydymas gali būti efektyviai taikomas vėžiui gydyti, genų terapijai ar audinių abliacijai. Dėl šiuo metu išskiriamų metodikos trūkumų, t. y. nehomogeniško gydymo, sukeliančio naviko regresiją, raumenų susitraukimų ar skausmo, būtina optimizuoti elektrodų ir impulsinio elektrinio lauko protokolus prieš taikant kliniškai. Disertacijoje pagrindinis dėmesys skiriamas naujų elektrodų struktūrų, užtikrinančių efektyvų gydymą, kūrimui ir optimalių impulsinio lauko protokolų tyrimui.

Šios disertacijos tikslas – adekvatus elektroporacija grįsto gydymo modeliavimas, įvertinant elektrinio lauko pasiskirstymą naudojant tikslius audinių modelius ir taikomuosius elektroporacijos tyrimus.

Įvade pristatoma tiriamoji problema, tyrimo objektai, disertacijos aktualumas ir svarba, aprašoma tyrimo metodika, mokslinis naujumas ir ginamieji teiginiai.

Pirmajame skyriuje pateikta mokslinių publikacijų elektroporacija pagrįsto biomedicininio gydymo srityje apžvalga. Išanalizuota elektrinio lauko pasiskirstymo audinyje svarba, audinio elektrinės savybės ir atsakas į impulsinį elektrinį lauką. Skyriuje analizuojami įvairūs elektrodų tipai, naudojami elektrochemoterapijos, genų terapijos ir negrįžtamos elektroporacijos procedūroms, atsižvelgiant į elektrinio lauko pasiskirstymą ir taikymo metodus. Nurodomi esamų elektrodų konstrukcijų apribojimai ir tobulinimo galimybės, parodyta impulsinės galios savybių svarba elektroporacija pagrįstoms procedūroms biomedicinos srityje.

Antrajame disertacijos skyriuje sukurtas po oda esančio auglio ir odos modeliai skirti elektrinio lauko pasiskirstymo analizei. Auglio modelis naudojamas sukurtų elektrodų efektyvumui vertint remiantis elektrinio lauko pasiskirstymo vaizdais. Taip pat įvertinta elektrinio lauko homogeniškumo priklausomybė nuo laidaus gelio, naudojant tik plokštelinius elektrodus ir plokštelinius elektrodus su pasyvia adata. Analizuojamas sukurtų elektrodų tinkamumas eksperimentiniams tyrimams.

Trečiajame skyriuje aprašomas sukurtų elektrodų struktūrų ir jų padėties nustatymo metodo eksperimentinis pritaikymas *in vivo* elektrochemoterapijai. Eksperimentinių tyrimų rezultatai rodo submikrosekundžių elektrinių impulsų veiksmingumą skirtingoms naviko ląstelių linijoms *in vitro* ir *in vivo*. Odos modelis ir modeliavimo rezultatai pritaikyti sėkmingam žaizdų gydymui acto rūgštimi. Remiantis gautais rezultatais suformuluotos disertacijos išvados.

Disertacijos tema paskelbti penki straipsniai *Clarivate Analitics Web of Science* duomenų bazėje referuojamuose moksliniuose žurnaluose su citavimo indeksu. Disertacijos tema perskaityta 13 pranešimų tarptautinėse konferencijose Lietuvoje, Latvijoje, Slovakijoje, Slovėnijoje, Lenkijoje ir Danijoje.

Notations

Symbols

C_m – cell membrane capacitance;
E – electric field;
J – current density;
l – tumour length;
r – radius of the biological cell;
R – impedance;
R_{EMC} – extracellular medium resistance;
R_{IMC} – intracellular medium resistance;
v – tumour volume;
V – voltage;
$V_{overshoot}$ – voltage overshoot;
V_p – effective voltage;
$V_{terminal}$ – terminal voltage;
$V_{undershoot}$ – voltage undershoot;
t – time;
t_{delay} – pulse delay time;
t_{fall} – pulse fall time;
t_{rise} – pulse rise time;
t_w – pulse width;

T – period;
T_P – on time of the pulses;
w – tumour width;
$\Delta\Psi_{ext}$ – potentials inside the cell;
$\Delta\Psi_{int}$ – potentials outside the cell;
$\Delta\Psi_m$ – induced transmembrane potential;
θ – the angle between the cell surface and electric field direction;
σ – initial specific conductivity;
σ_{max} – maximum value of the specific conductivity;
ε_r – relative permittivity;
τ_m – time constant.

Abbreviations

DNA – deoxyribonucleic acid;
E_{RE} – reversible electroporation electric field threshold;
Cp – cut plane;
E_{IRE} – irreversible electroporation electric field threshold;
ECM – extracellular medium;
ITMV – induced transmembrane voltage;
ECT – electrochemotherapy;
ESOPE – European Standard Operating Procedures for Electroporation;
FEM – finite element method;
GET – gene electro-transfer;
HF – high frequency;
H-FIRE – high-frequency irreversible electroporation;
ICM – intracellular medium;
IRE – irreversible electroporation;
LF – low frequency;
LLC – Lewis lung carcinoma;
nsPEF – nanosecond pulsed electric field;
RE – reversible electroporation;
RLU – relative light units;
ROI – the region of interest;
RTMV – resting transmembrane voltage;
PEF – pulsed electric field;
PI – propidium iodide;
TMV – transmembrane voltage;
YO-PRO – oxazole yellow iodide;
µsPEF – microsecond pulsed electric field.

Contents

Introduction

Problem Formulation

Nowadays, the electroporation phenomenon is applied in different areas, including such biomedical treatments as electrochemotherapy, gene electro-transfer or irreversible tissue ablation. The effectiveness of electroporation-based technologies for biomedical applications directly depends on electric pulse parameters, dielectric tissue properties and, especially, spatial pulsed electric field (PEF) distribution in tissue. The key element in distributing and controlling PEF in the tissue is the pulse applicator or electrode, hence, the continuous research of novel electrode structures is executed.

Electroporation of mammalian tissue is still relatively abstruse in terms of cancerous and healthy cells' response to PEF and unique target tissue morphology. The mechanisms of tissue electroporation can be partially explained through numerical models. Therefore, the development of realistic numerical models of cutaneous or deep-seated targets is in demand.

Currently, in the cancer treatment context, tissue heterogeneity leads to electroporation-based procedures exhibiting various negative factors, such as muscle contractions, pain sensation, Joule heating or non-uniform spatial electric field distribution. These aspects result in insufficient tissue of interest response and, therefore, potentially incomplete treatment, as well as delayed healing and

discomfort in patients. The appropriate electrode structure must be selected and contemplated with suitable PEF properties to minimise the unfavourable effects.

Electrochemotherapy, by far, is performed with microsecond range electrical pulses according to ESOPE (100 μs × 8 pulses) procedures, which, however, are associated with higher exposure energy and muscle contractions or pain. Recent studies have demonstrated that sub-microsecond pulses have a role in reducing these side effects, therefore, are under the scope. Nonetheless, conventional sub-microsecond PEF protocols must be derived experimentally *in vitro* and *in vivo* before applying in clinics.

Relevance of the Dissertation

The structures of the most commonly applied electrodes are trivial; though, state-of-art technologies are becoming more sophisticated and more efficient electrodes allow for more precise control of the anti-cancer effect of electric fields. However, the development of such applicators requires detailed research. At the moment, forecasting and minimisation of negative factors (thermal effects in tissues, bioimpedance distortions, muscle contractions, insufficient field homogeneity, volume, etc.) are among the main technological problems in the field of electrochemotherapy. Therefore, developing new electrodes and pulsed electric field protocols allows for addressing these issues by controlling the locality of anti-cancer effects and reproducibility of results by influencing further biomedical development in the field of electroporation.

Research Object

The dissertation's object is the research of invasive and non-invasive electrodes and parametric protocols for cancer treatment with the electrochemotherapy procedure.

Aim of the Dissertation

The aim of the dissertation is to investigate various electrode structures applicable for biomedical electroporation-based technologies, analyse spatial electric field distribution considering tissue inhomogeneity and electrical tissue properties, and propose new electrode structures and sub-microsecond parametric protocols for electrochemotherapy.

Tasks of the Dissertation

To achieve the objective of the dissertation, the following problems had to be solved:

1. To review different commercially available electrodes, electrode prototypes and *in silico* models used for electroporation-based biomedical applications *in vivo*.
2. To develop the numerical model of a superficial tumour for spatial electric field evaluation for more accurate pretreatment planning based on the finite element method (FEM).
3. To develop electrode structures suitable for more efficient electrochemotherapy treatment *in vivo*.
4. To propose novel sub-microsecond PEF parametric protocols, which are efficiency-wise equivalent to or better than the standard clinical ESOPE procedures.
5. To perform parametric drug transport *in vitro* analysis and develop new sub-microsecond protocols for applied electrochemotherapy research.
6. Apply the analysed electrode structure in electrochemotherapy research *in vivo*.

Research Methodology

This work used numerical and experimental methods. Spatial electric field distribution was modelled using the COMSOL software. The calculations and detailed model investigation were done using MATLAB and COMSOL LiveLink for the MATLAB software. Results were verified experimentally *in vivo* and *in vitro*.

Scientific Novelty of the Dissertation

The scientific novelty aspects in the theoretical and experimental investigation of the dissertation are as follows:

1. The developed model of the superficial tumour was successfully utilised to precisely evaluate treatment outcomes and determine the electrochemotherapy protocols.
2. A superficial skin model was used to evaluate the suitability of PEF for bacteria-killing on the skin surface. The appropriate PEF properties

were selected based on obtained results to achieve superficial treatment without damaging the deep tissues.

3. The efficacy of developed invasive electrode structures with the repositioning technique in the ECT context was verified with SP2/0 tumour *in vivo*.
4. Non-invasive plate electrode model was supplemented with a passive syringe needle to inject chemotherapeutic drugs. This approach allows for amplifying the electric field and ensures a more homogeneous spatial electric field distribution.
5. The proposed sub-microsecond high repetition frequency (up to 1 MHz) PEF protocols were tested on LLC1 and SP2/0 tumour cell lines. The results showed efficiency-wise ESOPE-equivalent or better overall treatment.

Practical Value of the Research Findings

The dissertation's results will contribute to a safer and more effective cancer treatment therapy, minimising muscle contraction, thermal effects and other negative factors that occur during electroporation-based treatments. The dissertation's results were used in three projects: "Development of High-Frequency Dielectrophoresis and Electrosensitization Based Nanoelectroporation Technologies for Targeted Drugs and Genes Delivery", S-MIP-19-13, Research Council of Lithuania"; "The influence of electrochemotherapy and its combination with dendritic cell vaccination for murine tumour eradication and formation of immune response", S-MIP-19-22, Research Council of Lithuania and "Electroporation-based manipulation of drug resistance in cancer using novel nanosecond asymmetrical pulse sequences" S-LL-21-4, Research Council of Lithuania.

Defended Statements

The following statements are to be defended:

1. The developed numerical models of a superficial tumour and skin allow for an accurate (with ±10% deviation) prediction of the spatial electric field distribution and tissue response to various pulsed electric field conditions.

2. The developed plate electrode structure with a passive centre electrode amplifies the electric field strength at the central part of the tumour, improving the tumour response to electrochemotherapy.
3. The proposed small gap tweezer electrodes and the repositioning technique is suitable for wound treatment to overcome superficial infections and result in a successful wound sterilisation method without affecting deeper tissue.
4. The proposed sub-microsecond range (100–900 ns) pulsed electric field protocols are efficiency-wise superior to ESOPE treatments.

Approval of the Research Findings

Research results have been published in five scientific articles; in Clarivate Analytics Web of Science journals with impact factor. The author gave 13 presentations at ten international scientific conferences:

- The Fourth International Wroclaw Scientific Meetings. 2020. Wroclaw, Poland.
- International Scientific Workshop. Electroporation-Based Technologies and Treatments (EBTT 2020). 2020. Ljubljana, Slovenia.
- The Sixty-Fourth International Conference for Students of Physics and Natural Sciences. Open Readings 2021. 2021. Vilnius, Lithuania.
- The Eighth International IEEE Workshop on Advances in Information, Electronic and Electrical Engineering. 2021. Vilnius, Lithuania.
- The Thirteenth International Conference on Measurement Science, Technologies and Devices (MEASUREMENT 2021). 2021. Bratislava. Slovakia.
- The First International Scientific Conference. Advances in biomedical research with the use of in vitro methods. 2021. Lublin, Poland.
- The Ninth International IEEE Workshop on Advances in Information, Electronic and Electrical Engineering. 2022. Riga. Latvia.
- The Sixty-Fifth International Conference for Students of Physics and Natural Sciences. Open Readings 2022. 2022. Vilnius, Lithuania.
- The Fourth International Baltic Biophysics Conference (BBC2022). 2022. Vilnius, Lithuania.
- The Fourth World Congress on Electroporation & Pulsed Electric Fields in Biology, Medicine, Food, and Environmental Technologies. 2022. Copenhagen. Denmark.

The Structure of the Dissertation

The dissertation is structured around three main chapters.

The First Chapter explains the basic mechanism of electroporation and electroporation-based technologies, including electrochemotherapy, for application on mammalian tissues and reviews its dielectric properties focusing on the influence of electric pulses. Then, the review is performed, focusing on different electrodes for biomedical treatments, such as electrochemotherapy, gene delivery or irreversible tissue ablation. The first Chapter concludes by formulating the main objective and tasks of the dissertation.

The Second Chapter focuses on the developed superficial tumour model for a more precise evaluation of spatial electric field distribution. The model evaluates separate skin layers and the dependence of tissue dielectric properties on PEF. Invasive and non-invasive electrodes are researched using the finite element method. The adequacy of the electrodes to the dissertation aims is studied based on the results.

The Third Chapter presents experimental results on electrochemotherapy treatments of Lewis lung carcinoma LLC1, mouse myeloma Sp2/0 and murine melanoma B16 tumour cell lines *in vitro* and *in vivo* using the developed electrode structures and proposed PEF protocols. Also, it researches the capabilities of using electroporation for superficial wound sterilisation.

General conclusions and recommendations for further research are presented in the final section.

The volume of the dissertation is 109 pages. The dissertation contains 67 figures, 12 tables, two numbered formulas, and 170 used references.

Acknowledgement

For guidance and support during PhD studies, I am grateful to my supervisor Prof. Dr Vitalij Novickij. Also, my appreciation is extended to my internship supervisor Dr Bor Kos for his guidance and collaboration.

I am thankful to all my colleagues in the Department of Electrical Engineering and Innovative Medicine Centre for valuable contribution and discussions on topics related to my dissertation.

1

Electroporation and Electroporation-based Technologies

This Chapter reviews the electroporation phenomenon and the biomedical applications of electroporation-based technologies for electrochemotherapy, gene electrotransfer and tissue ablation procedures. It summarises the main principles of mammalian tissue electroporation, the composition of superficial and various deep-seated tissues and their dielectric properties and the dependency on the pulsed electric field. The Chapter also covers the review of various electrodes and *in silico* models used for electroporation-based treatments, evaluation of the spatial electric field distribution, advantages, disadvantages and options for improvement. One scientific publication was published on the First Chapter's topic (Malyško-Ptašinskė et al., 2023).

1.1. Electroporation Phenomenon and Basic Applications

Electroporation is a phenomenon of the cell membrane becoming permeable due to the applied pulsed electric field (PEF). The process is controlled by pulsed

electric field parameters, and thus, the effect can be reversible or irreversible. Reversible electroporation is frequently used in combination with drugs to ensure efficient intracellular drug delivery, i.e., electrochemotherapy (Fig. 1.1).

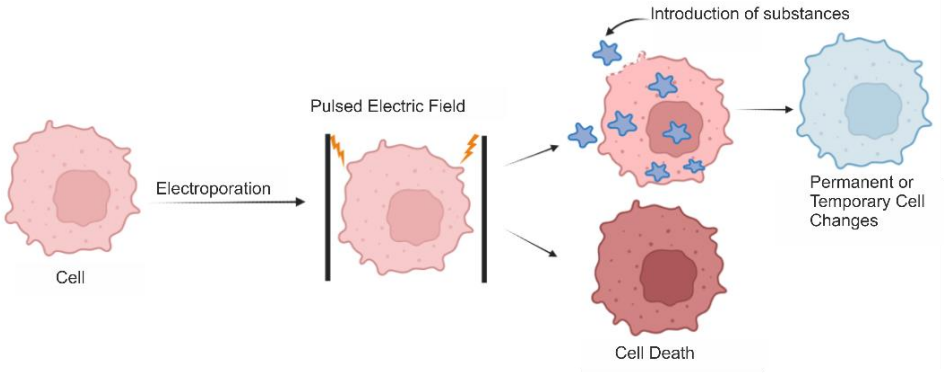

Fig. 1.1. Electroporation mechanism

In biological materials (when triggered by a specific PEF), permeabilisation is related to the formation of transient aqueous pores on the cell membrane, which create the pathways for external substances to enter the cell (Bö et al., n.d.; Freeman et al., 1994; Du et al., 2018). To create these pathways, cell transmembrane voltage has to reach an electroporation threshold (Kinosita and Tsong, 1977). Depending on PEF parameters (pulse duration, strength, repetition frequency, etc.), cells' response may vary (Szlasa et al., 2021; Vižintin et al., 2021). The defects on the membrane appear if transmembrane voltage exceeds the threshold value, but after a specific resealing time, the membrane integrity is restored, and the cell survives, indicating reversible electroporation (RE). Irreversible electroporation (IRE), on the contrary, refers to instantaneous cell death after PEF delivery.

Due to the high potential applicability of the described phenomena, electroporation is a multidisciplinary research field involving research in electronics and electrical engineering, biophysics, biomedicine, microbiology and food technology. Based on Clarivate Analytics Web of Science data, there are 17 179 papers featuring the "electroporation" keyword (Access date: 2022- 03- 01). A visual map of the most common keywords in electroporation papers is shown in Fig. 1.2. It can be seen that the applied aspects of the electroporation dominate the field; however, the inevitable interconnectivity with an electric field, electrodes, voltage and pulse characterisation is present (array of red circles).

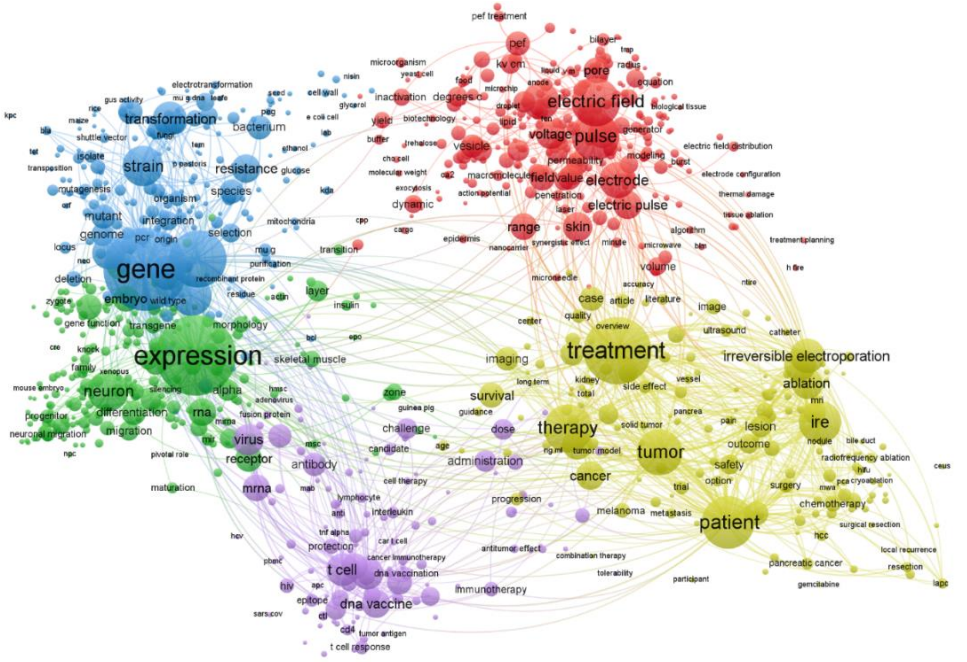

Fig. 1.2. Most common keywords used in electroporation studies. Visualised using the VOSviewer software, version 1.6.18 (Leiden University) (VOSviewer – visualising scientific landscapes, n.d.). A filter of at least 30 minimum occurrences of keywords has been used. A bigger circle size indicates a higher rate of occurrence of a specific keyword (Malyško-Ptašinskė et al., 2023)

The reversible electroporation, in combination with chemotherapeutic drugs, is a highly effective method for cancer treatment. However, if a significantly stronger PEF is applied, it may lead to irreversible electroporation (IRE) and cause cell death as well as ablation of the tissue (Sersa et al., 2008; Korohoda et al., 2013; Calvet and Mir, 2016; Cemazar and Sersa, 2019). Therefore, the desired outcome can be achieved by adjusting the PEF parameters.

A biological cell is considered a core-shell structure sphere, consisting of a very thin dielectric membrane surrounding the cytoplasm (intracellular medium (ICM)) and having an extracellular medium (ECM) outside the membrane (DeBruin and Krassowska, 1999).

Nearly all biological cells under normal conditions (without any external stimuli) uphold the electric potential difference between the intracellular and extracellular sides of their plasma membrane. Such potential difference is termed as resting transmembrane voltage (RTMV), which is typically in the range of millivolts.

Instantly after the exposure to PEF, the cell is polarised, and an additional voltage across the membrane is formed (ITMV), referred to as $\Delta\Psi_m$ (Kotnik et al., 2019). When TMP exceeds a specific threshold (typically referred to as 1 V), the cell membrane becomes permeable to exogenous molecules.

The ITMV can be found as a difference of potentials inside ($\Delta\Psi_{int}$) and outside ($\Delta\Psi_{ext}$) the membrane (Kotnik et al., 2010):

$$\Delta\Psi_m = \Delta\Psi_{int} - \Delta\Psi_{ext}. \tag{1.1}$$

The kinetics of electroporation after PEF application on a cellular level can be described in several stages: TMV exceeds the threshold value at the beginning of the electric pulse, TMV remains above the threshold when PEF is still present, as shown in Fig. 1.3., and TMV decreases as pulsing burst has ended (Hibino et al., 1993).

After the drop of TMV, the membrane starts to recover to an impermeable state. The process is termed resealing (Pucihar et al., 2008). Though, resealing is impossible in the case of irreversible electroporation, as the cell membrane fails to repair.

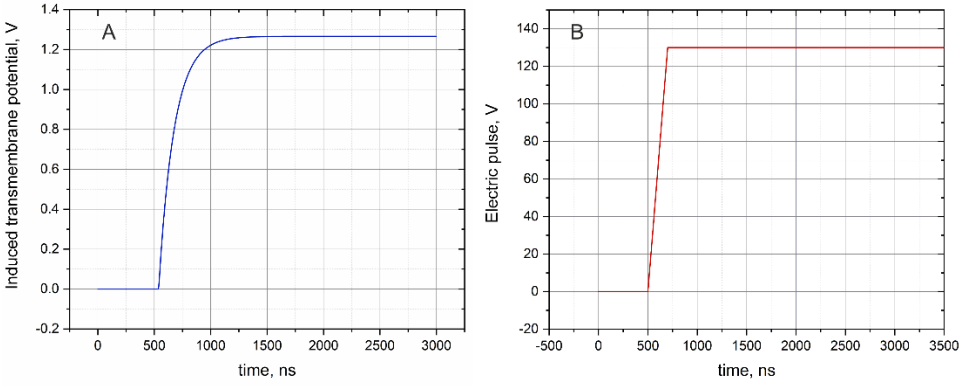

Fig. 1.3. Kinetics of electroporation after the PEF exposure:
(A) induced transmembrane potential; (B) applied 130 V electric pulse

Cell and its membrane from the electrical point of view can be analysed as an RC equivalent circuit as represented in Fig. 1.4. As a result, the cell membrane is described as a capacitor C_m with very high resistance (Weaver, 2000) and resistors R_{ICM} and R_{ECM}, respectively. When the membrane is polarised by PEF, the initial high resistance starts to decrease After the reversible electroporation cell resistances remain stable (Ye et al., 2020).

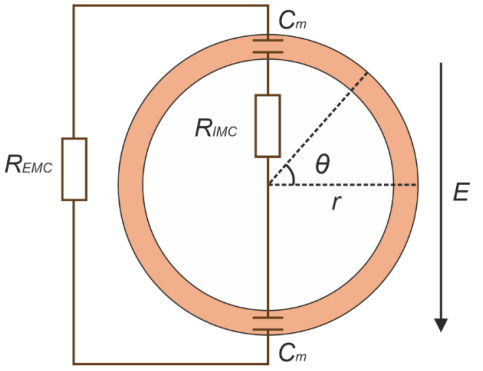

Fig 1.4. Equivalent cell membrane electrical circuit

The induced TMP for a spherical-shaped cell can be found using Schwan's equation, which considers the time constant τ_m needed to charge the capacitor C_m, referring to the cell membrane:

$$\Delta\Psi_m = \frac{3}{2} Er\theta \left(1 - \exp\left(-\frac{t}{\tau m}\right)\right). \quad (1.2)$$

In the equation above, *r*, *E*, θ and *t* correspond to the radius of the cell, the applied electric field, the angle between the surface and electric field direction and the time of PEF application, respectively. The expressed dependency also indicates the affinity of pulse strength and its duration. When electric pulses are shorter (e.g., nanosecond range), a much greater amplitude is required to polarise the cell to a threshold potential, while with the application of longer pulses (micro- or millisecond range), the electric field strength can be reduced (Pucihar et al., 2011).

1.2. Electrochemotherapy and Tissue Ablation

For decades, cancer has remained the main cause of mortality worldwide, despite the advances in cancer detection, types, prevention or treatment options. After the cancer diagnosis, patients usually have several treatment options, i.e., chemotherapy, radiation therapy or surgery (Litwin and Tan, 2017). The last-mentioned method is usually performed during the first cancer stages (without metastases); however, it does not guarantee full recovery as the tumour may regrow (Li et al., 2020).

Other well-established treatment methods, such as chemotherapy or radiation therapy, have significant side effects, reducing the overall quality of life. The

reasonable alternative to the traditional procedures is electroporation-based treatment, electrochemotherapy, which offers a safe and efficient approach for treating cancerous and subcutaneous nodules. ECT has been used in the treatment of subcutaneous and cutaneous lesions and metastases from tumours, with responses in the range of 75% to 99%. The method was applied to melanomas with metastases (Wichtowski and Murawa, 2018), carcinomas (Domanico et al., 2015), prostate (Blazevski et al., 2020), breast (Wichtowski et al., 2017), liver (Pavliha et al., 2012), pancreas (Casadei et al., 2020) and other types of cancer.

ECT is a local treatment that successfully combines the application of cell-membrane-permeabilising electric pulses and poorly permeant chemotherapeutic drugs, such as bleomycin or cisplatin (Sersa et al., 2008). During the clinical treatments, chemotherapeutic agents of the required concentration are injected intratumourally (Zimmermann et al., 2021) or intravenously (di Monta et al., 2017), followed by PEF exposure on the target of interest. This method enables localised tumour treatment, allowing for the minimisation of the side effects executed while applying chemotherapy alone (van den Boogaard et al., 2022). The effectiveness of ECT predominately depends on several factors, i.e., chemotherapeutic drugs and their concentration, molecular size and etc., tissue characteristics (composition, size, shape), dielectric properties of the tissue, PEF properties (amplitude, duration, repetition frequency and the number of pulses) and pulse applicators (electrodes).

To ensure effective molecular transport, chemotherapeutics must be spread in the cell-extracellular medium in sufficient concentration (Condello et al., 2022). Currently, bleomycin and cisplatin are the dominating drugs for ECT procedures (Probst et al., 2018; Ferioli et al., 2022). However, the field is rapidly growing; thus, the research is targeting alternative ECT drugs, such as doxorubicin (Rembiałkowska et al., 2022) or calcium ions (Gursoy et al., 2023).

The detection of PEF effects on cells *in vitro* stage is typically carried out using fluorophores or colour stain dyes. The most common fluorescent dyes are propidium iodide (PI), ethidium bromide (EtBr), ethidium homodimer 1 (EtH) and YO-PRO-1 Iodide, which uptake is monitored using flow cytometry. Colour stains, such as trypan blue, are used for viable cell counting using light microscopy (Batista Napotnik and Miklavčič, 2018; McKinnon, 2018).

In the case of *in vivo* applications on skin tissue, the pulsed electric field has to penetrate through specific skin layers; therefore, the skin structure and its electrical properties have to be well known. The skin has the main function of protecting the internal organs from environmental influence (Hayes et al., n.d.; Monteiro-Riviere and Riviere, 1999). Basically, it consists of the stratum corneum, epidermis, dermis, subcutaneous fat tissue and muscle tissue (Huclova et al., 2012; Ventrelli et al., 2015) (Fig. 1.5). The outer skin layer is the stratum corneum. It mostly consists of dead skin cells and, at the same time, has

the highest resistivity. For this reason, the skin is considered a barrier to successful electroporation applications when non-invasive electrodes are used. Epidermis and dermis are below the stratum corneum and have much lower resistivity; hence, there is a considerable voltage drop in the stratum corneum (Alkilani et al., 2015; Lu et al., 2018). Although, once the stratum corneum is permeabilised by forming electro pores (Gelker et al., 2018), deeper skin layers can be affected.

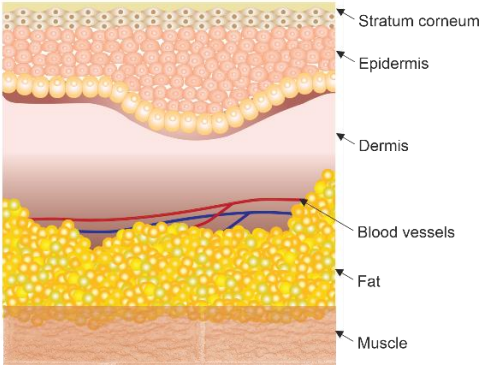

Fig. 1.5. Healthy skin (Malyško-Ptašinskė et al., 2023)

Electrochemotherapy procedures are applicable for various types of tumours in clinical trials (Li, 2008). Tumours may be grouped simply as cutaneous or subcutaneous lesions, which means the target is located on the skin surface, forming a visible lump (Fig. 1.6) or deep-seated (Fig. 1.7) in subcutaneous tissues, respectively.

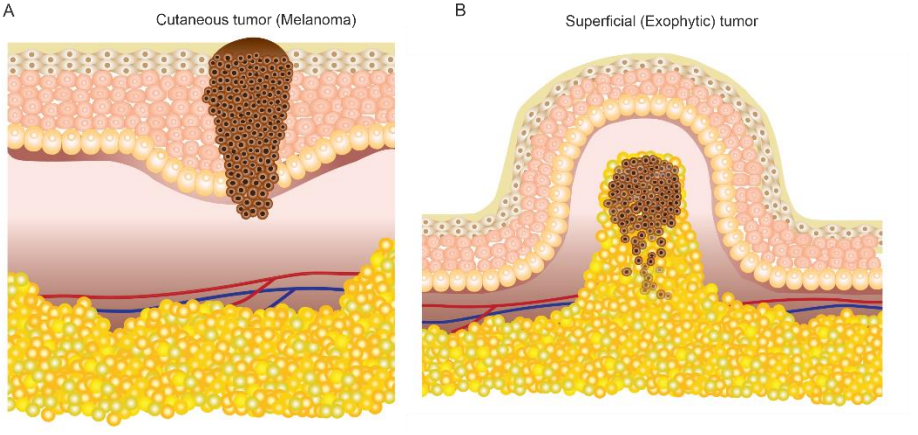

Fig. 1.6. Tumour types: (A) cutaneous tumour (Melanoma) and (B) superficial or exophytic tumour illustrations (Malyško-Ptašinskė et al., 2023)

Tissue electrical properties can be described using the concept of bioimpedance, which is a frequency-dependent parameter specific to tissue composition, including water content (Chumlea and Guo, 1994). Biological tissue is not considered a good conductor or insulator, but rather something in between, which allows the flow of specific value current. This is due to the influence of tissues being either aqueous, i.e., the muscle, or non-aqueous, i.e., bones or fat. In the low- and high-frequency ranges, the current density vectors vary, and the bioimpedance drops in the high-frequency range enabling a more homogeneous treatment (Raja et al., 2006). Therefore, the conductivity and permittivity changes in the tissue and their dependence on applied pulse frequency are considered for pretreatment planning through numerical modelling (Miklavčič et al., 2006; Zhang and He, 2010).

When a tumour is located on the skin or under the skin forming a lump (Fig. 1.6), electric pulses are delivered directly to the skin. In such a case, the electrical properties of this material are highly important for accurate analysis of electric field distribution. The specific conductivity σ, which is related to the formation of local transport regions after applying electric pulses (Pliquett et al., 1998), describes the ability of aqueous solutions to transfer electrical charges. The dependence of conductivities on frequency for different skin layers is summarised in Table 1.1.

Table 1.1. Skin's specific conductivity σ in low- and high-frequency ranges (Malyško-Ptašinskė et al., 2023)

Tissue	σ LF, Sm^{-1}	References	σ HF, Sm^{-1}	References
Skin (dry)	0.00565–0.25 0.0009 0.090–0.017 0.07	(Low Frequency (Conductivity), IT'IS Foundation, n.d.) (Gabriel et al., 1996) (Wake et al., 2016) (Hershkovich et al., 2019)	38.18 0.12	(Arab et al., 2020) (Hershkovich et al., 2019)
Skin (wet)	0.059	(Gabriel et al., 1996)	42.97	(Arab et al., 2020)
Stratum corneum	0.0002–0.002	(de Santis et al., 2015)	–	–
Epidermis	0.018 ± 0.008	(Wake et al., 2016)	~0.35	(Wake et al., 2016)
Dermis	0.434 ± 0.056	(Wake et al., 2016)	~0.45	(Wake et al., 2016)
Subcutaneous fat	0.024–0.215 0.147 ± 0.020 ~0.1	(Low Frequency (Conductivity), IT'IS Foundation, n.d.) (Wake et al., 2016) (Gabriel et al., 2009)	~0.15 ~0.22	(Wake et al., 2016) (Hershkovich et al., 2019)

End of Table 1.1

Tissue	σ LF, Sm^{-1}	References	σ HF, Sm^{-1}	References
Subcutaneous fat	~0.2	(Hershkovich et al., 2019)	~0.1	(Gabriel et al., 2009)
Muscle	0.1–0.726	(Low Frequency (Conductivity), IT'IS Foundation, n.d.)	–	–
longitudinal	~0.37	(Ahad et al., 2010)	~0.64	(Ahad et al., 2010)
	~0.4	(Nagy et al., 2019)	~0.6	(Nagy et al., 2019)
transverse	~0.15	(Ahad et al., 2010)	~0.46	(Ahad et al., 2010)
	~0.21	(Nagy et al., 2019)	~0.42	(Nagy et al., 2019)
Melanoma	0.00000265	(Glickman et al., 2003)	53.445	(Arab et al., 2020)
LF – up to 100 kHz frequency				
HF – 100 kHz and greater frequency				

The material capability to store charge is characterised as relative permittivity. The published values of permittivities for skin layers are presented in Table 1.2. According to other researchers, the subcutaneous tissue (fat) and dermis are considered to be composed of higher water content and have relatively low permittivity, hence the resistive nature. On the contrary, skin layers with lower water content and thickness, such as the stratum corneum and epidermis, are characterised by very low conductivity and much higher permittivity, thus, considered a capacitor (Hershkovich et al., 2019). Both of these properties, i.e., conductivity and permittivity, are vital for the numerical modelling of the tissue.

Table 1.2. Skin's relative permittivity ε_r in low- and high-frequency ranges (Malyško-Ptašinskė et al., 2023)

Tissue	ε_r, LF,	References	ε_r, HF,	References
Skin (dry)	1111 5340	(Gabriel et al., 1996) (Hershkovich et al., 2019)	6.565	(Arab et al., 2020)
Skin (wet)	1136	(Gabriel et al., 1996)	8.537	(Arab et al., 2020)
Epidermis	100 000–62 500	(Tsai et al., 2019)	62 500–50 000	(Tsai et al., 2019)

End of Table 1.2

Tissue	ε_r, LF,	References	ε_r, HF,	References
Stratum corneum	8000–700	(Birgersson et al., 2011) (Yamamoto and Yamamoto, 1976)	700–400	(Birgersson et al., 2011)
	1000 000–50 000	(Yamamoto and Yamamoto, 1976)	50 000–100	(Yamamoto and Yamamoto, 1976)
Dermis	1000 000–75 000	(Tsai et al., 2019)	75 000–50 000	(Tsai et al., 2019)
Subcutaneous fat	8648–617	(Gun et al., 2017)	175–58	(Gun et al., 2017)
Muscle				
longitudinal	~71 167	(Ahad et al., 2010)	~8700	(Ahad et al., 2010)
	~92 000	(Nagy et al., 2019)	~9500	(Nagy et al., 2019)
transverse	~53 467	(Ahad et al., 2010)	~11 867	(Ahad et al., 2010)
	~87 500	(Nagy et al., 2019)	~40 230	(Nagy et al., 2019)
Melanoma	–	–	9.631	(Arab et al., 2020)
LF – up to 100 kHz frequency				
HF – 100 kHz and greater frequency				

However, for deep-seated tumours (Fig. 1.7), such as the liver or pancreas, either invasive electrodes are used percutaneously, or the treatment is performed during open surgery (Granata et al., 2021); therefore, the skin has little to no effect on the electroporation procedure.

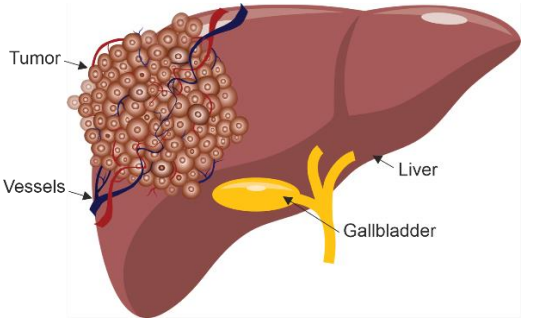

Fig. 1.7. Deep-seated liver tumour illustration

In most cases, deep-seated tumours are intact, with healthy organs of a living organism (Edhemovic et al., 2014) encapsulated into them (Ghossein, 2010) and surrounded by large blood vessels (Djokic et al., 2018).

The complexity of such a tumour composition influences the inhomogeneity of target tissue, which may result in non-uniform treatment. As a consequence, the electrical properties of such tumours and tissues in the vicinity may vary, therefore, must be considered. The specific conductivity and relative permittivity of various tissues, including the tumour, are summarised in Table 1.3 and 1.4, respectively.

Table 1.3. Other tissues' specific conductivity σ in low- and high-frequency ranges (Malyško-Ptašinskė et al., 2023)

Tissue	σ LF, Sm^{-1}	References	σ HF, Sm^{-1}	References
Tumour	0.22–0.40 0.00135 ± 0.19 0.166–0.222 0.411–0.461	(Miklavčič et al., 2006) (Ivorra et al., 2009) (Laufer et al., 2010) (Haemmerich et al., 2009a)	0.279–2.346 0.246–0.272 0.504–0.533	(Cheng and Fu, 2018) (Laufer et al., 2010) (Haemmerich et al., 2009a)
Liver	0.0636–0.43 0.03–0.091 0.075–0.179	(Low Frequency (Conductivity), IT'IS Foundation, n.d.) (Laufer et al., 2010) (Haemmerich et al., 2009b)	0.124–0.164 0.260–0.288 ~0.2	(Laufer et al., 2010) (Gun et al., 2017) (Gabriel et al., 2009)
	~0.075	(Gabriel et al., 2009)	–	–
Prostate	0.436–0.743 0.411–0783 0.238–0.901	(Low Frequency (Conductivity), IT'IS Foundation, n.d.) (Neal et al., 2014) (Santamaría et al., 2007)	0.916–1.06 0.290–1.149	(Neal et al., 2014) (Santamaría et al., 2007)
Lung	0.058–0.249 0.05–0.25	(Low Frequency (Conductivity), IT'IS Foundation, n.d.) (Wang et al., 2014)	0.151–0.309 0.16–0.57	(Yamazaki et al., 2013) (Wang et al., 2014)
inflated	~0.03	(Gabriel et al., 2009)	~0.06	(Gabriel et al., 2009)
deflated	~0.12	(Gabriel et al., 2009)	~0.2	(Gabriel et al., 2009)
LF – up to 100 kHz frequency				
HF – 100 kHz and greater frequency				

Table 1.4. Other tissues' relative permittivity ε_r in low- and high-frequency ranges

Tissue	ε_r, LF,	References	ε_r, HF,	References
Tumour	99 000–8600	(Laufer et al., 2010)	24.842–15.12 5100–3000	(Cheng and Fu, 2018) (Laufer et al., 2010)
Liver	82 000–11 000 82 306–18 899	(Laufer et al., 2010) (Gun et al., 2017)	6500–3400 1833–262	(Laufer et al., 2010) (Gun et al., 2017)
Prostate	90 200–449 000	(Santamaría et al., 2007)	13000–1160	(Santamaría et al., 2007)
Lung	~1000 000–~10 000	(Wang et al., 2014)	10000–100	(Wang et al., 2014)
LF – up to 100 kHz frequency				
HF – 100 kHz and greater frequency				

A similar tendency of conductivity changes is obtained with variations in the electric field. The conductivity can be expressed through the ratio – $\sigma = J/E$ (Pavšelj and Miklavčič, 2008a). From the expression, it can be seen that the tissue conductivity σ is the current density J and electric field E dependant property. Therefore, the variations in the electric field may also affect conductivity dynamics in the biological material; however, only if the electric field is between permeabilisation and ablation thresholds, E_{RE} and E_{IRE}, respectively (Guo et al., 2022). Therefore, when a high enough voltage is applied, the dynamics of the tissue conductivity must be considered (Fig 1.8).

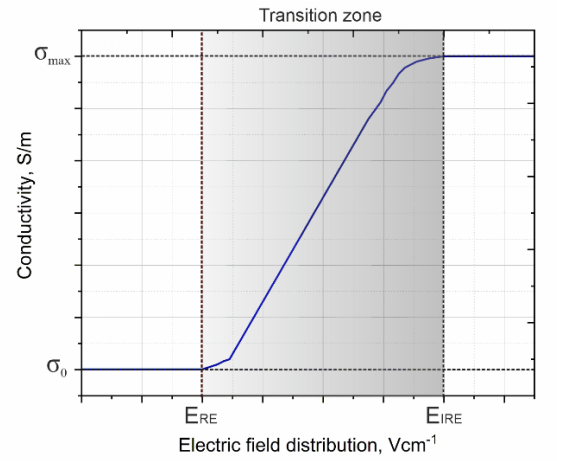

Fig. 1.8. Conductivity dynamics during PEF application

The precise calculation of conductivity increase from initial σ_0 to maximum σ_{max} can be found using the smoothed Heaviside function, which is widely used in describing conductivity dynamics versus the applied electric field or the Gompertz curve (Labarbera and Drapaca, 2017). The process is apparent in the transition zone between RE (E_{RE}) and IRE (E_{IRE}) electric field thresholds for all mammalian tissues. The conductivity increases and threshold values for different skin layers are summarised in Table 1.5.

Table 1.5. Skin layers and multilayers conductivity dynamics with respect to the applied electric field

Tissue	Initial σ, Sm^{-1}	Relative increase of σ	E_{RE}, Vcm^{-1}	E_{IRE}, V cm^{-1}	References
Stratum corneum	0.0005	1000	600	1200	(Pavšelj and Miklavčič, 2008b)
	0.0005	1000	–	–	(Pavšelj and Miklavčič, 2008a)
Skin	0.002	80	400	900	
Stratum corneum and epidermis	0.008	100	400	1200	(Corovic et al., 2013)
Epidermis and dermis	0.2	4	600	1200	(Pavšelj and Miklavčič, 2008b)
Dermis and fat	0.25	4	300	1200	(Corovic et al., 2013)
Subcutaneous fat	0.5	4	600	1200	(Pavšelj and Miklavčič, 2008b)
	0.03	3	_	_	(Pavšelj and Miklavčič, 2008a)
Connective tissue	0.03	3	300	–	(Pavšelj et al., 2005)
Muscle					
longitudinal	0.735 0.75	4 2.5	_ 80	_ 800	(Pavšelj and Miklavčič, 2008a) (Corovic et al., 2013)
transverse	0.11 0.135	4 2.5	_ 200	_ 800	(Pavšelj and Miklavčič, 2008a) (Corovic et al., 2013)
Tumour	0.3 0.3	2.7 2.5	_ 400	_ 800	(Pavšelj and Miklavčič, 2008a) (Pavšelj et al., 2005; Corovic et al., 2013)

The number of pulses also plays a role in conductivity dynamics when the delays between the pulses are decreased. With the increase in pulse quantity, σ_{max} has a very slight difference between the initial conductivity value σ; however, the transition zone expands (Sano et al., 2018). Though the process is likely to be

influenced by the temperature increase (Zhao et al., 2020). The temperature rise, known as Joule heating, can also play a role in cell death. The relevance of Joule heating can be neglected when appropriate pulse properties are selected (Davalos et al., 2005, 2015).

To summarise, the outcome of electrochemotherapy predominantly depends on various factors, including therapeutic substances, target tissue properties and location, PEF parameters and the structure of electrodes. Though from the perspective of electrical engineers, the therapy is considered successful when the whole tumour is covered by a sufficient electric field and the desired treatment volume is attained. The post-treatment effectiveness can be assessed by measuring the volume of the tumour. In the case of superficial tumours, it is measured with a digital clipper and calculated according to the formula – $v = \pi lw2/6$, where l is the length and w is the width of the tumour, or in the case of deep-seated tumours, monitored with magnetic resonance imaging (MRI), ultrasound or computed tomography (CT) (Granata et al., 2016).

1.3. Various Electrodes used in Electroporation

The electric pulses are delivered using pulse generators and electrodes, where the anode and the cathode of the electrode transfer the charge, and a pulsed electric field is induced in the biological material. Currently, various models and prototypes of electrodes are constantly proposed for electroporation-based cancer treatment or gene therapy (Dermol-Černe et al., 2020). The configuration of each electrode is frequently limited to a specific target tissue or the area of application. To generate an electric field, at least two electrode parts are used, i.e., positive (cathode) and negative (anode). Individual electrode types can have various configurations of anode/es and cathode/es; therefore, the outcome varies, including specific electric field distribution, strength and homogeneity.

For *in vivo* electroporation-based procedures, the electrodes are typically classified as invasive (involving the introduction of electrodes into the tissue), non-invasive, which do not require penetration into the tissue, instead delivering the pulses through contact with the object, or minimally invasive. Therefore, the configuration of electrodes has to complement the electroporation procedure and the target location. At the same time, the preferred electrode structure has to conform to the safety requirements, minimising the invasiveness of the methodology, preventing bacterial infections and ensuring better regeneration.

The electroporation effect on various tissues can be predicted and ensure precise electrode positioning using a wide spectrum of techniques (Neal II et al., 2012), including magnetic resonance (Figini et al., 2017; Boc et al., 2018). However, more frequently, numerical modelling is used for treatment planning as

a supplementary tool (Kranjc et al., 2017; Asadi et al., 2019). Such numerical models can serve as a successful method for an accurate prediction of the electroporation outcome and better pretreatment planning through the electric field distribution simulation (Miklavčič et al., 1998; Pavšelj and Miklavčič, 2008a).

This work compared different electrode types using numerical calculations in COMSOL Multiphysics, version 5.5 (COMSOL, Los Angeles, CA, USA), which is based on the finite element method (FEM). Each tumour or target tissue was modelled as a three-dimensional homogeneous tissue mass with constant specific conductivity and relative permittivity, σ is 1.5 S/m, and ε_r is 80, respectively. For the electric potential equation, the electrodes were represented by a fixed voltage (Dirichlet's boundary condition), with set positive ($V = V_{terminal}$) and zero ($V = 0$) potential/s, depending on each electrode configuration. The value of electric potential for each electrode configuration varied depending on previously published protocols; therefore, it was specified along with simulations. For an adequate comparison, several values of applied voltages were adjusted. The outer boundaries of the geometry were treated as electrically insulated according to Neumann's boundary condition, which refers to the calculation of a derivative applied on the specific boundary of the domain when a differential function is used (Sharawi et al., 2016). In the last step, the stationary analysis was computed to evaluate the spatial electric field distribution.

1.3.1. Invasive Electrodes

Invasive electrodes require penetration into the target; therefore, electrodes are usually needle-shaped, with a sharp tip. Most invasive electrodes deliver electric pulses through stainless-steel needles of different lengths. Currently, fixed position or adjustable position (Electrodes | IGEA Medical, n.d.; Electrodes for in vivo electroporation | BEX CO., LTD., n.d.) (Adjustable Electrodes – EPSA Series | IGEA Medical, n.d.) electrode pairs or arrays are commercially available. Fixed position electrodes are grouped as two-needle electrodes (Isobe et al., 2004; Chen et al., 2015; Langus et al., 2016; Zager et al., 2016; Yao et al., 2017), longitudinal or hexagonal electrode arrays.

The spatial electric field distribution for these electrodes is dependent on the number of needles (Adeyanju et al., 2012), length, gap distance and diameter (Davalos et al., 2005).

Fixed-position electrodes are beneficial in terms of non-parallelism minimisation. The spatial electric field distribution analysis of two needle-fixed electrodes with different lengths and gap distances is shown in Fig. 1.9 (A–F).

As shown, the field is non-homogeneous; thus, the gap between the needles and charging voltage should be adjusted accordingly to induce a high enough electric field for electroporation.

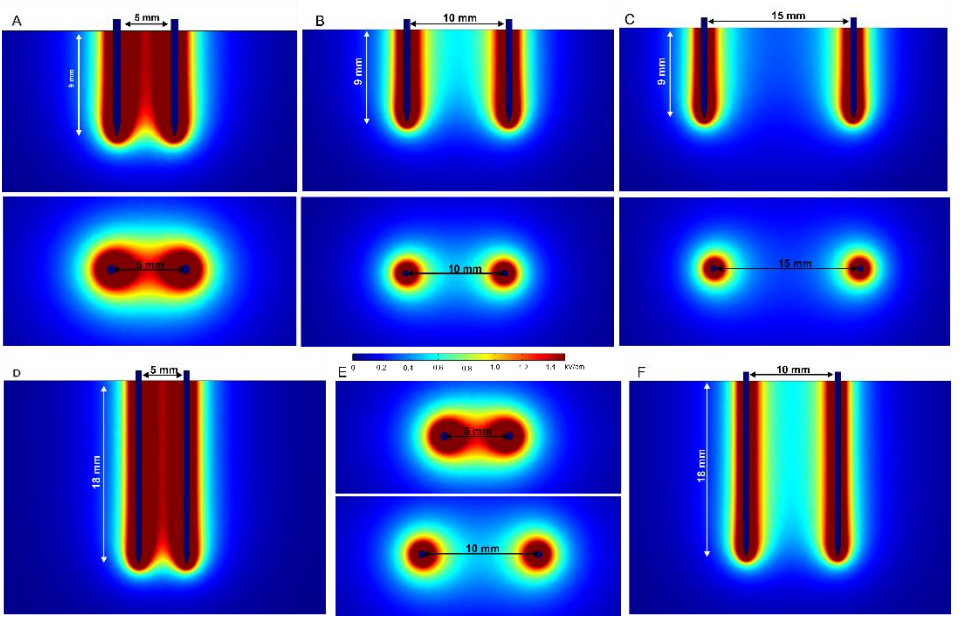

Fig. 1.9. Spatial electric field distribution of two-needle fixed-position electrodes with different lengths and gap sizes, using 500 V terminal voltage: (A) 5 mm gap between the electrodes; (B) 10 mm gap between the electrodes; (C) 15 mm gap between the electrodes; (D) 20 mm-length electrodes with a 5 mm gap; (E) 20 mm-length electrodes with 5 mm and 10 mm gaps, top view; (F) 20 mm-length electrodes with a 10 mm gap, side view (Malyško-Ptašinskė et al., 2023)

In the case of hexagonal shape electrodes (Fig. 1.10 (A–C)), the highest value of PEF is generated around a positively charged electrode. Therefore, when applied correctly, the central part of the tumour receives the highest intensity treatment, while healthy tissues around the tumour remain undamaged. These electrodes are suitable for ECT procedures with larger tumours (Pichi et al., 2018) as well as for gene therapy in different configurations (Gilbert et al., 1997).

Intradermal electrodes are used when the penetration of the surface skin layers, i.e., the stratum corneum, dermis and epidermis, is sufficient. To analyse the needle, 600 V was applied to 4-needle array electrodes. This induced a relatively homogenous 1.2 kV/cm electric field between the positive and negative 2- and 10-mm needle lengths electrode pairs (Fig. 1.10 (D–F)). Such electrodes

are commercially available and used for intradermal electroporation, featuring 2- and 10 mm electrode lengths (Fixed Electrodes – EPS Series | IGEA Medical, n.d.; Needle Array Electrodes for BTX AgilePulse In Vivo, n.d.).

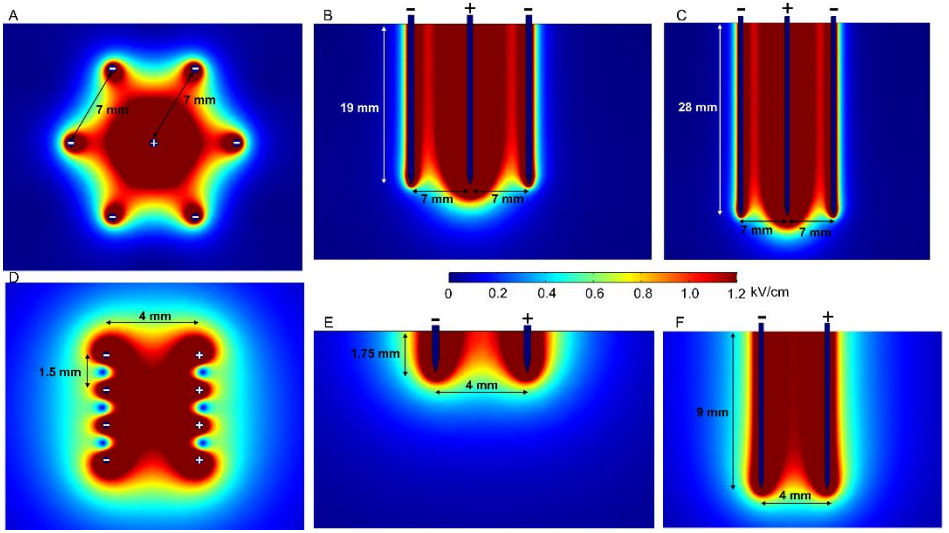

Fig. 1.10. Spatial electric field distribution generated by hexagonal shape and intradermal needle-type electrode arrays with 1500 V and 600 V terminal voltages, respectively, considering the different depth of penetration: (A) hexagonal shape electrodes, top view; (B) hexagonal shape 20 mm-length electrodes, side view; (C) hexagonal shape 30 mm-length electrodes, side view; (D) intradermal electrodes, top view; (E) intradermal 2-mm length electrodes, side view; (F) intradermal 10 mm-length electrodes, side view (Malyško-Ptašinskė et al., 2023)

There is a remarkable difference in the specific distribution of the electric field in the tissue; 10 mm needles produce a uniform electric field at a depth of about 7 mm; in contrast, 2-mm electrodes have a less homogeneous distribution of the electric field in the effective volume. Nevertheless, considering these limitations, the electrodes can be used successfully in practice (Roos et al., 2006, 2009; Lladser et al., 2010).

In summary, fixed-position electrodes are likely to produce a more uniform electric field because of the penetration into the tissue that can be controlled better. However, the fixed electrodes are only suitable for tumours of a certain size and are, therefore, less flexible for cancer treatment, especially when the tumour is significantly smaller or larger than the distance between the fixed electrodes. Intradermal electrodes are suitable for gene therapy, though the depth of penetration should be considered to ensure sufficient homogeneity of the electric field.

Single-needle electrode configuration would be a solution to minimise electrode positioning problems (Neal et al., 2010; Garcia et al., 2014). This type of electrode consists of an electrode body, a cathode, an insulator, and an anode at the sharp tip of the needle, each part having a specific length and width (Fig. 1.11 (A)). The results show that this design solves the problem of non-parallelism; however, the electric field distribution is relatively inhomogeneous. In addition, the diameter of this electrode is relatively large, making it suitable mainly for larger tumours.

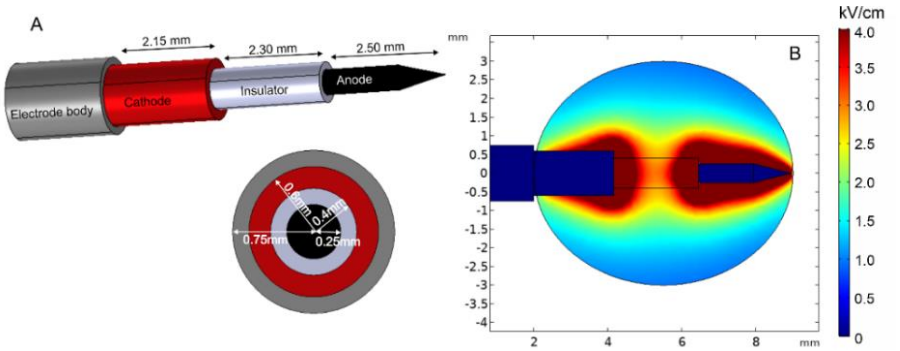

Fig. 1.11. Single-needle electrode model: (A) electrode structure; (B) spatial electric field distribution, with 1300 V terminal voltage (Malyško-Ptašinskė et al., 2023)

Alternatively, a new prototype of curved electrodes was proposed by Ritter et al. (Ritter et al., 2018). Curved electrodes consist of a penetrating central needle and four thin hollow expandable electrodes for pulse application and injection of the chemotherapeutics. For the simulation of such an electrode type, the terminal voltage was set to 1500 V. Further, electric field distribution analysis was performed and represented through the cut planes Cp1–Cp4 (Fig. 1.12). Cp1 shows the field strength on the surface of the penetration level is low.

As shown, electroporation may appear only around the central needle and at the positively charged satellite electrodes' tip. As a consequence, other areas will be electroporated insufficiently. However, penetration into deeper tissue layers gives a more homogeneous treatment (Cp2), creating a uniform triangular electric field. At the same time, results correspond to side views from Cp3 and Cp4. Clearly, the prototype with such a configuration could be improved if all satellite electrodes would act as cathodes. In such a case, the non-homogeneity between negative electrodes (Cp3) would be minimised. Such a shift of the polarities is already provided in this electrode composition. Moreover, the position of satellite needles can be adjusted with a movable part. This may increase the value of PEF around the tip of a central needle if the outer needles are dragged up.

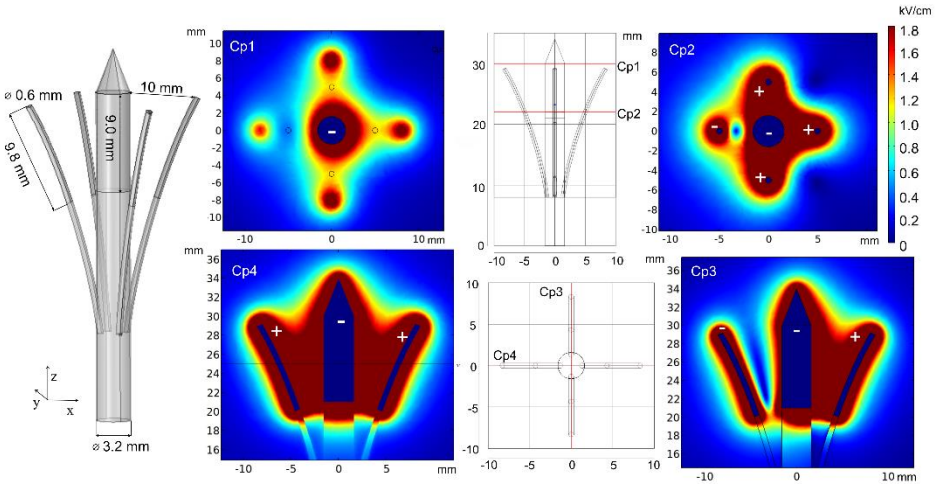

Fig. 1.12. Curved electrodes using 1500 V terminal voltage. *Cp represents cut planes for the electric field distribution analysis (Malyško-Ptašinskė et al., 2023)

When the target tissue or tumour is deep-seated, the electroporation procedure requires access to subcutaneous lesions with a limited incision in the skin. Such treatment is performed by laparoscopy with an open approach or by endoscopy transoral and transanal through the catheter (Li et al., 2021; 2019; 2021). Thus, the requirements for the electrode structure and placement become more complex. In the target, the electrodes must be strictly parallel to ensure a homogeneous PEF distribution, while the effective area must cover the entire tumour volume.

For the electroporation of the deep-seated tumour, needle arrays with adjustable position needles can be used to ensure a more homogeneous treatment. The placement of variable geometry needle electrodes is adapted to individual tumour size and shape. To obtain an above-the-threshold electric field covering the whole tumour volume, multiple needles at the tumour edges and/or into the tumour are inserted (Fig. 1.13 (A)). The number of needles should be limited to reduce treatment invasiveness and complexity.

Such an electroporation procedure requires very accurate pretreatment planning and PEF parameter evaluation (Miklavcic et al., 2010; Pavliha et al., 2012; Blazevski et al., 2020). This allows a more precise treatment that minimises the effects of tumour heterogeneity and also allows for the treatment of tumours that consist of multiple nodes (Fig. 1.13 (B)). However, non-parallelism may be a problem that is usually solved by radiographs during surgery after electrode positioning and fixation (Moreta-Martínez et al., 2022).

For deep-seated tumours, an electrode prototype was introduced by Izzo et al. (Izzo et al., 2020). Deployable and expandable 4-needle and 5-needle electrode configurations were tested for their effectiveness and suitability for the laparoscopic and endoscopic liver of Female *Sus Scrofa* using IRE.

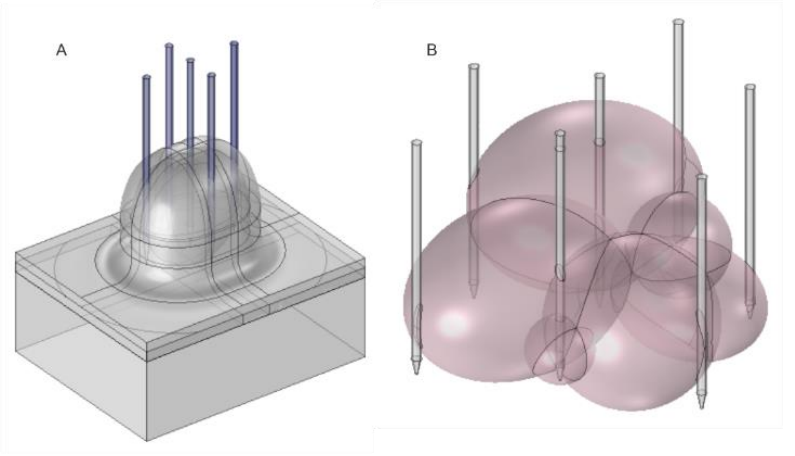

Fig. 1.13. The array of adjustable position needle electrodes for (A) corneous tumour; (B) deep-seated tumour (Malyško-Ptašinskė et al., 2023)

The model of such an electrode array is presented in Fig. 1.14 (A, B). Blue and red coloured needles represent negatively and positively charged electrode rods with a fixed length of 2 cm. The non-conductive electrode rods are adjustable to 2-, 3- or 4 mm lengths and 0°, 10°, 20° and 30° angles.

The spatial electric field distribution with 0°, 10° and 30° needle expansion angles are shown in Fig. 1.14 (C–F). Black arrows represent diagonal and semi-diagonal pairs for voltage application. As shown, changing the active electrode pairs provides flexibility to control the volume of the electroporated tissue. The entire volume of the tumour could be affected with high intensity due to the overlap of the PEF regions. The ability to increase the length of each needle independently also allows control of the depth of the electroporated volume. However, the problems of precise positioning of the needles remain.

To conclude, invasive electrodes are beneficial for deep-seated, intramuscular or intradermal targets. Fixed-position electrodes are easier to apply, but they are mostly suitable for specific size targets; otherwise, partial treatment will be assessed, or the healthy tissue will receive unnecessary pulsing. Multiple application fixed electrodes in such cases are needed. As a solution, manual needle repositioning or more accurate multiple needle applications along with a brachytherapy grid (van den Bos et al., 2016) may be considered. Such fixing

equipment, as well as non-conductive ring nuts or “stoppers”, helps to minimise non-parallelism after needle penetration.

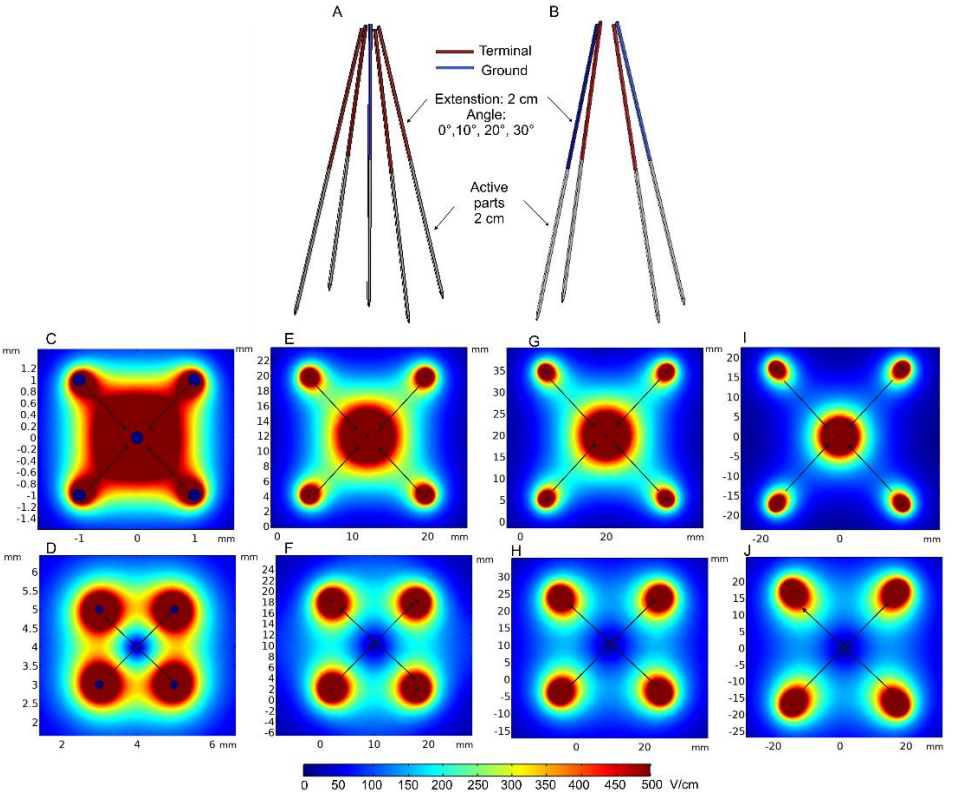

Fig. 1.14. Deployable expandable electrodes: (A) 5-needle electrode structure; (B) 4-needle electrode structure; (C) spatial electric field distribution of a 5 needle-electrode with an angle of 10° and a 2 cm extension; (D) spatial electric field distribution of a 4-needle electrode with an angle of 10° and a 2 cm extension; (E) spatial electric field distribution of a 5-needle electrode with the angle of 0° and a 2 cm extension; (F) spatial electric field distribution of a 4-needle electrode with the angle of 0° and a 2 cm extension. **The performed simulation includes single diagonal and semi-diagonal pulsing* (Malyško-Ptašinskė et al., 2023)

When a tumour is deep-seated, its boundaries are invisible without external imaging equipment, such as ultrasound (van den Bos et al., 2016; Hsiao and Huang, 2017) or fluoroscopy (Pavliha et al., 2012) guidance. The combination of invasive electrodes with different imaging methods gives the possibility for a more precise assessment of the target boundaries, minimising the possibility of repetitive pulsing on the same area of the tissue. Real-time imagining is also

advantageous when a tumour can be reached through the skin without incision (Lee et al., 2007).

1.3.2. Non-parallelism with Invasive Electrodes

The needles of invasive electrodes are relatively thin. Therefore, the distance between electrodes in deeper tissues may vary, leading to the inhomogeneous electric field distribution in the tissue. As shown in Fig. 1.15, the visible gap size in each case is the same, i.e., 5 mm; therefore, the top view is identical. Due to skin surface curvature and the "sandwich"-structured composition (Wei et al., 2017; Kopcewicz et al., 2020), non-parallelism in deeper tissues may become a concern, especially when longer needles are used. The process may attribute to the inhomogeneity of the electric field, as shown in Fig. 1.15. It is clearly seen that the tumour (represented by white dashed lines in Fig. 1.15) may be treated insufficiently, while the healthy tissue receives a dose of PEF.

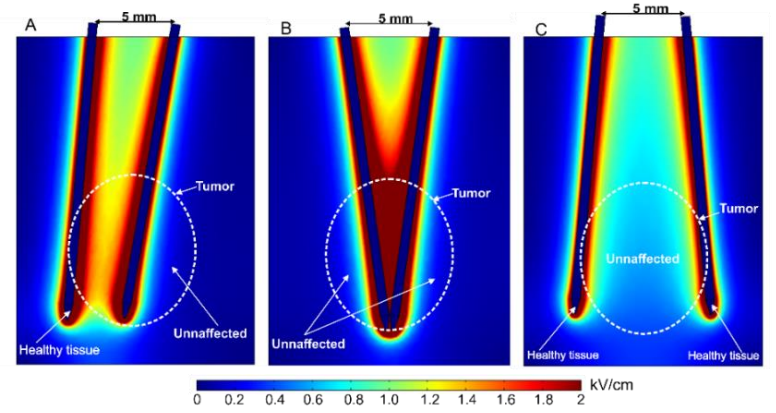

Fig. 1.15. Spatial electric field distribution of two-needle adjustable position electrodes with a 5 mm gap, using 500 V terminal voltage: (A) electrodes are rotated by 10° and 5°; (B) both electrodes are rotated by 8° and –8°; (C) both electrodes are rotated by –10° and 10° (Malyško-Ptašinskė et al., 2023)

The problem was analysed by Campana et al. using the potato model (Campana et al., 2019). Their study showed that when two needles are not perfectly parallel, i.e., placed aslant to one other by specific angles, as shown in Fig. 1.15, homogeneous distribution of the electric field is unfeasible. It was noticed that by increasing the angle, the electric field intensity and electroporation itself are lower and non-uniform. The case when both electrodes turn in the same direction (Fig. 1.15 (A)) or are spread from one another (Fig. 1.15 (C)) by specific angles was further analysed. In the first case (Fig. 1.15 (A)), PEF is insufficient

for successful electroporation of the whole tumour, while the adjacent non-target tissue is affected. Fig. 1.15 (C) shows that if electrodes in deeper tissues are spread apart, the tumour will not likely be electroporated.

A similar issue may also be present in the case of fixed-position needle arrays, which occur due to needle deflection (Andrade et al., 2022). After multiple electrode penetration into the tissue (especially the skin), needles experience mechanical stress, leading to needle deformation.

1.3.3. Minimally Invasive Electrodes

Currently, different minimally invasive (Choi et al., 2010; Yan et al., 2010; Xia et al., 2021) or non-invasive (Heller et al., 2010; Guo et al., 2011) microneedle array electrodes are introduced. Such electrodes are used for transdermal drug or gene delivery. The microneedles designed to affect outer skin layers with a sufficient electric field for RE are shown in Fig. 1.16 (A). A total of 900 (30 per row and 30 per column) 0.2 mm length microneedles placed at 0.1 mm distance between needle tips were analysed first. Positively and negatively charged electrode terminals are distributed in each row, as shown in Fig. 1.16 (A, D). The spatial electric field distribution estimation was performed using 100 V terminal voltage. The results of the electric field evaluation are illustrated in Fig. 1.16 (E, F).

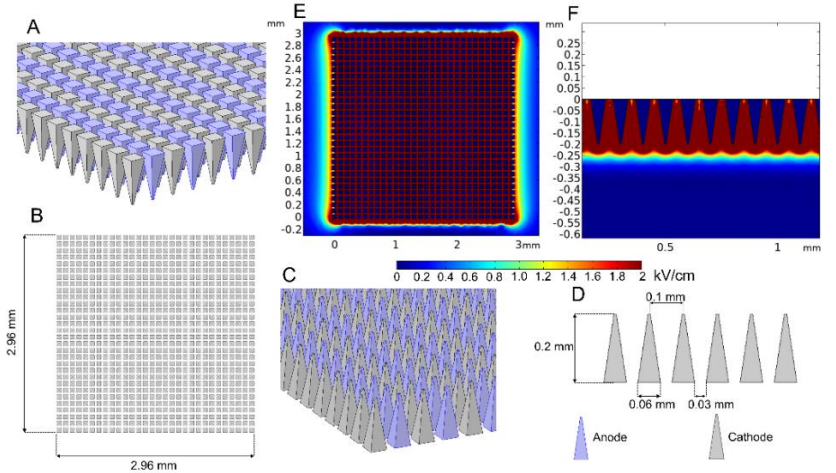

Fig. 1.16. Microneedle array applying 100 V voltage: (A–D) model; (E) spatial electric field distribution using 100 V terminal voltage, top view; (F) spatial electric field distribution using 100 V terminal voltage, side view (Malyško-Ptašinskė et al., 2023)

As demonstrated, the penetration depth of the high-intensity electric field is still sufficient for transdermal gene delivery. However, their effective area is relatively small. To increase the effective area of the minimally invasive electrodes, a rolling electrode can be used, as proposed by Yang et al. (2021). In Fig. 1.17 (A–C), the model of such an electrode with the expected electric field distribution is presented.

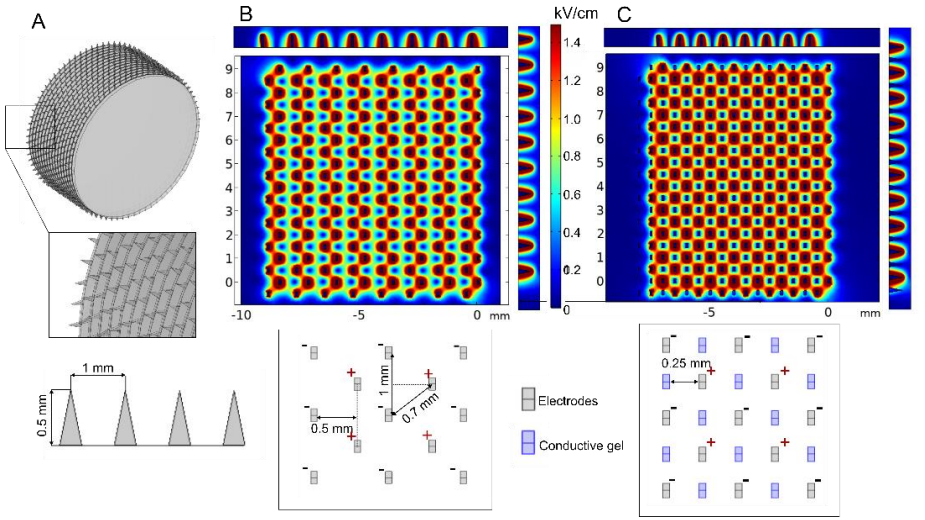

Fig. 1.17. Multi-needle roller electrode model when 100 V terminal voltage is used: (A) electrode structure; (B) spatial electric field distribution using 100 V terminal voltage, without conductive gel; (C) spatial electric field distribution using 100 V terminal voltage, with conductive gel channels (Malyško-Ptašinskė et al., 2023)

The results of the performed analysis show that the highest value of electric field strength is around the microneedle tips; however, it decreases significantly in the areas between the terminal and ground-representing needle pairs (Fig. 1.17 (B)). A similar electrode type was analysed by Huang et al. (2018). However, their study suggested implementing the structure with conductive gel microchannels formed by applying gel to the skin and rolling the needles on the skin before the application of PEF. For the analysis of such a technique, the additional microchannels of conductive gel were introduced, as shown in Fig. 1.17 (C). The results show that the conductive gel channels can improve the homogeneity of the electric field.

1.3.4. Non-invasive Electrodes

Non-invasive electrodes interact through the tissue interface; thus, they are incompatible with deep subcutaneous tumours but suitable for the treatment of exophytic tumours or melanoma, which appear on the skin surface. Several configurations of non-invasive electrodes are presented in this sub-section.

The L-shaped electrodes are mostly used for large cutaneous margins and are designed to treat skin tumours of all sizes. The model of such commercially available electrode arrangement is shown in Fig. 1.18 (A) (Accessories ElectroVet, LEROY Biotech, n.d.).

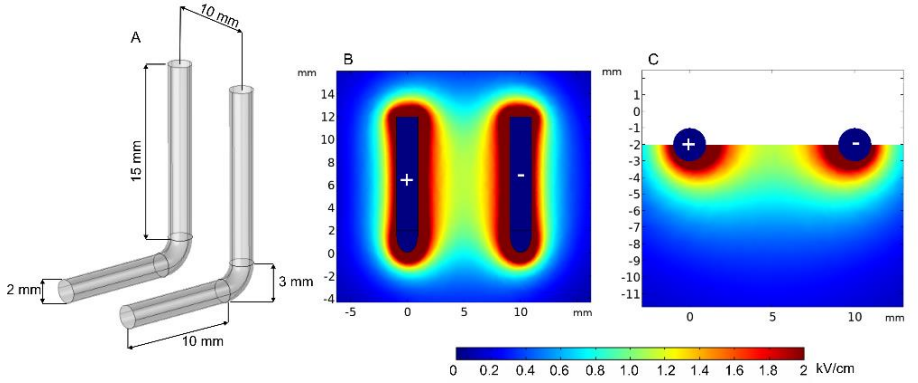

Fig. 1.18. L-shaped electrode using 1300 V terminal voltage: (A) electrode structure; (B) spatial electric field distribution, top view; (C) spatial electric field distribution, side view (Malyško-Ptašinskė et al., 2023)

For the simulation, the electrodes were placed on the tissue surface with slight pressure. The analysis was performed with the 1300 V terminal voltage. Fig. 1.18 (B, C) shows that the electric field generated by L-shaped electrodes is inhomogeneous. As demonstrated, the highest PEF intensity is expected at the skin surface, while deeper tissue layers and the gap between the electrodes are affected by significantly lower PEF. Similar electrode configurations were employed for *in vivo* electroporation for both GET and ECT by Mazères et al. (2008). For the treatment, the electrodes were repositioned by 90° after each pulse burst to ensure a more uniform electric field distribution. The treatment resulted in a 93% complete response in treated animals. The study highlighted that for the ECT procedure, the electrodes were more effective on tumours up to 5 cm in diameter. Despite the notable gene electrotransfer results, the ablation of the skin was observed.

While L-shaped electrodes are relatively popular, parallel plate electrodes are most commonly used as a non-invasive electrode type (Al-Sakere et al., 2007;

Sedlar et al., 2012; Novickij et al., 2021). These electrodes are composed of two rectangular-shaped plates with a fixed or adjustable gap (Caliper Electrodes for Electroporation Applications, n.d.; Wang et al., 2008) placed strictly in parallel and representing an anode and a cathode (Fixed Electrodes, EPS Series | IGEA Medical, n.d.). Fig. 1.19 (D–F) shows the plate electrode application for the skin (Fig. 1.19 (D)) and a superficial tumour (Fig. 1.19 (E)). It can be seen that in the case of skin electroporation, the distribution is similar to the L-shaped ones.

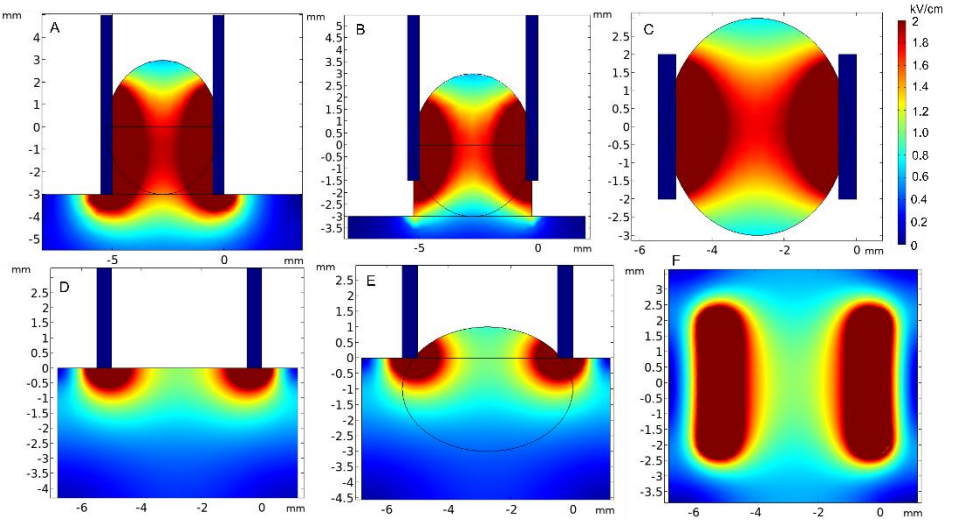

Fig. 1.19. Spatial electric field distribution of plate electrodes using 1000 V terminal voltage during (A) electroporation of superficial tumour, when plates embrace tumour sufficiently, side view; (B) electroporation of superficial tumour, when plates embrace tumour insufficiently, side view; (C) electroporation of superficial tumour, top view; (D) electroporation of the skin, side view; (E) electroporation of melanoma or a small superficial tumour; (F) electroporation of the skin or melanoma, top view (Malyško-Ptašinskė et al., 2023)

When a tumour is superficial, it is essential to have good contact between the electrodes and the tissue. As shown, when plate electrodes form a lump of the skin, the tissue of interest receives a higher dose of PEF. However, in all presented cases, the top and bottom of the tumour are covered by a significantly lower electric field. The same problem is present for the areas having no direct contact with electrodes.

Clipper- or tweezer-type electrodes are very similar to plate electrodes; however, they are more convenient if an adjustable gap is required. These electrodes can be either rectangular or round shaped. The round-shaped tweezer electrodes are commercially available (Tweezertrodes Electrodes for In Vivo and

In Utero Electroporation Applications, n.d.) with an adjustable 1–20 mm gap size. Round-shaped electrodes with a 5 mm diameter and a 4.5 mm gap have been used for the evaluation of the spatial electric field distribution within a tissue fold.

As expected, due to a reduced area of contact with electrodes, the electric field is inhomogeneous. Nevertheless, tweezer electrodes are beneficial due to their ease of use and compactness and are favourable for GET procedures (Maiorano and Mallamaci, 2009; Shi et al., 2010; Zhang et al., 2022). Other shapes of tweezer electrodes are available as well (Tweezertrodes Electrodes for In Vivo and In Utero Electroporation Applications, n.d.).

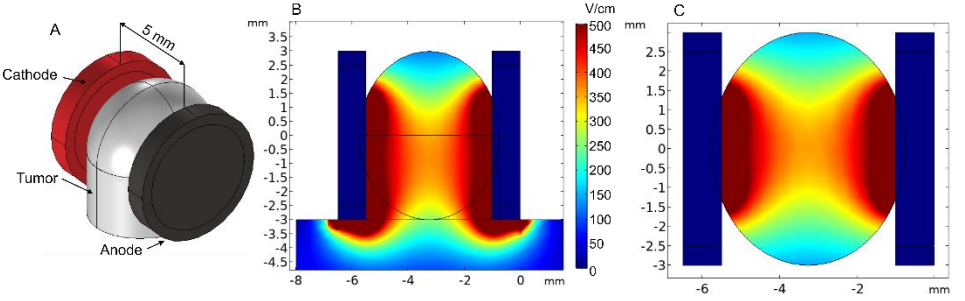

Fig. 1.20. Tweezer round-shaped electrodes using 1000V terminal voltage: (A) simulation model; (B) spatial electric field distribution, side view; (C) spatial electric field distribution, top view (Malyško-Ptašinskė et al., 2023)

The alternative for a non-invasive plate electrode is a 4-plate electrode (4PE), in which pulses are delivered by using two parallel pairs of electrodes instead of rotating them manually by 90 degrees. 4PE was originally developed for gene electrotransfer treatments by Heller et al. (2007). The electrodes are used in the following way: the metal plates are placed on the target, "gripping" the desired skin fold and tightening the non-conductive annular nut to achieve a fixed gap size.

The expected spatial electric field distribution was analysed with an 8° expansion and, without a plate, an expansion using two gap sizes, i.e., 8 mm and 6 mm, respectively (Fig. 1.21). The electric field generated by 4PE is similar to that of two plate electrodes; however, since pulsing is performed in two directions, the inhomogeneity of the treated volume during the second pulse train can be compensated.

According to the simulation results shown in Fig. 1.21, the value of the electric field decreases at the top and the bottom of the tissue. Although the expansion of the plates is beneficial, the target tissue is larger in size, and the mentioned issue becomes even more obvious when plates are turned at an angle (Fig. 1.21 (E, F)).

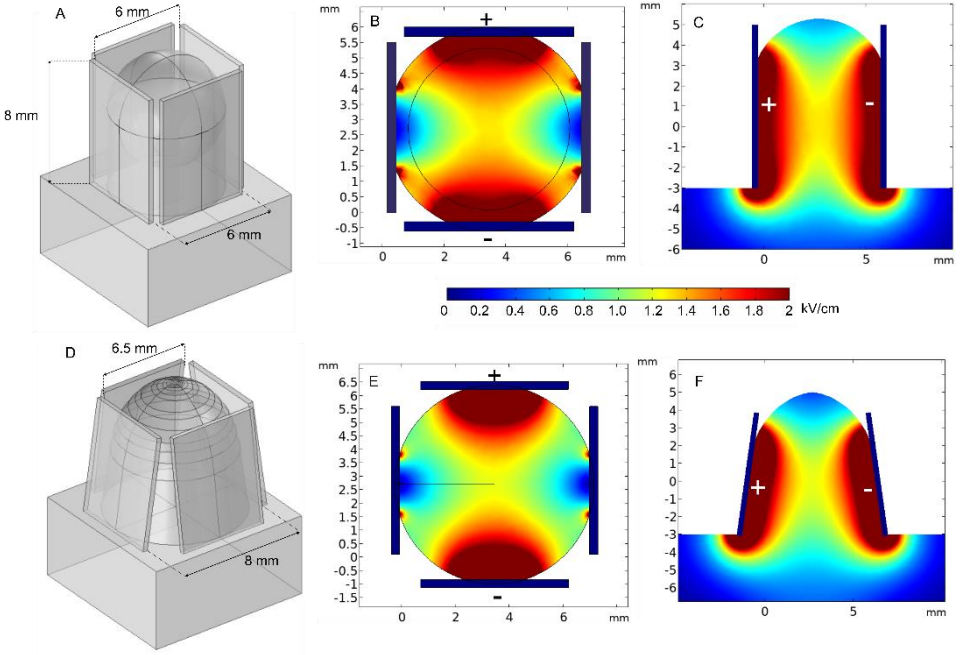

Fig. 1.21. 4-plate electrode applying 1300V terminal voltage: (A) electrode structure without plate expansion; (B) electrode structure with plate expansion by 8°; (C) spatial electric field distribution without plate expansion, top view; (D) spatial electric field distribution without plate expansion, side view; (E) spatial electric field distribution with plates expansion by 8°; top view; (F) spatial electric field distribution without plate expansion by 8°, side view

In the case of superficial treatment, flexible patch-shaped electrodes may be considered. The electrodes are designed to adapt to the tissue surface and ensure good contact. Fig. 1.22 illustrates the pliable electroporation patch (ep-Patch) golden rectangular-shaped electrode for gene introduction presented by Wei et al. (2015).

This electrode is composed of a comb-shaped anode and cathode with 0.2 mm width and 0.5 mm spacings, as shown in Fig. 1.22 (A). For the evaluation of electric field distribution, a 50 V terminal voltage was selected. The results of FEM analysis indicate that the electrodes are capable of ensuring a transdermal electric field distribution. Due to reduced penetration of the electric field and pliability, the electrodes can be successfully employed for the delivery of DNA into a tissue.

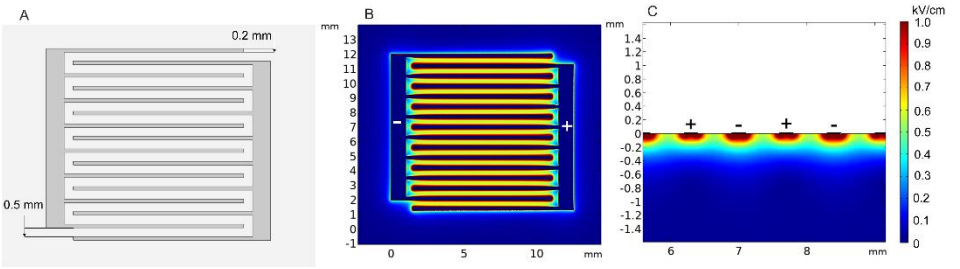

Fig. 1.22. Planar golden ep-Patch electrode using 50 V terminal voltage: (A) electrode structure; (B) spatial electric field distribution, top view; (C) spatial electric field distribution, side view

The survey of non-invasive electroporation electrodes showed that most electrodes have some limitations, i.e., non-uniform electric field distribution, inconvenient operation, limited active area or adaptability for different targets, etc.

1.3.5. Other Types of Electrodes

Commercially available plate-and-fork-type electrodes (Electrodes for in vivo electroporation | BEX CO., LTD., n.d.) could be considered an alternative to invasive and non-invasive electrodes.

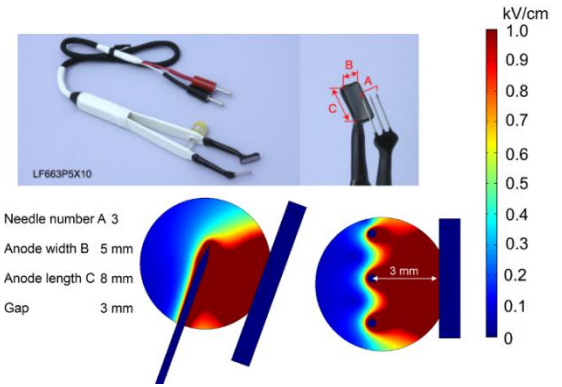

Fig. 1.23. Plate-and-fork-type electrodes using 500 V terminal voltage: (A) commercially available electrodes; (B) electrode structure; (C) spatial electric field distribution, side view; (D) spatial electric field distribution, top view

The electrode consists of a series of three invasive 3-mm stainless steel needles, namely, the fork and a 5 x 8-mm non-invasive plate (Fig. 1.23). The analysis of the spatial distribution of the electric field using plate-and-fork-type electrodes was performed with a spherical shape tumour. The fork with needles is

inserted into the tissue, and at the same time, a rectangular plate surrounds the target tissue. This electrode also contains a fixation part to keep the gap size between the fork and the plate stable during the application of the pulses. This way, the target tissue can be captured closely and accurately. Considering the obtained results of FEM analysis, the applicators form a homogeneous electric field on the target tissue (Fig. 1.23 (C, D). The effectiveness of these electrodes has been demonstrated for gene therapy (Maruyama et al., 2001).

1.3.6. Effects of Conductive Gel on Electric Field Distribution

It is clear that non-invasive electrodes have limitations in terms of spatial electric field distribution when the skin fold is forming a curve. Such electrodes are less capable of ensuring the sufficient value of an electric field within the tumour volume, especially when its shape is irregular. The issue could be partially improved with a sufficient amount of the conductive gel. The conductive gel is typically used to fill the spaces between plate electrodes and the tissue. The considerable implementation by means of electric field homogeneity with previously presented plate electrodes is shown in Fig. 1.24.

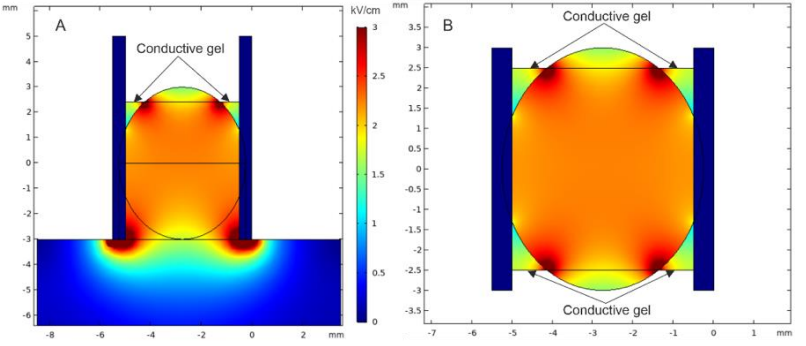

Fig. 1.24. Spatial electric field distribution using plate electrodes and conductive gel: (A) side view; (B) top view

In other studies, the conductivity of the material is reported to be appropriate in the range of 0.5–1 S/m (Ivorra et al., 2008). For the simulation, the maximum 1 S/m conductivity has been selected.

As demonstrated, the layer of conductive gel plays a role in diminishing the areas covered by below-threshold electric field values. However, depending on the amount of conductive gel, the top part of the tissue can still receive a much lower PEF dose (light green area in Fig. 1.24 (A)) than the central part. Thus, a greater amount of gel could be used to fully cover the skin fold. Though, when

there is a considerable difference in conductivities between materials, the current is likely to flow through a more conductive material. In such an instance, the conductive gel may shunt the tumour, leading to a decreased electric field within the tissue.

Conductive gel may also affect the electric field distributions for electroporation-based procedures with invasive needle electrodes (Suzuki et al., 2016). In this case, the conductivity of conductive gel is considered to be much lower, 0.05–0.2 S/m, respectively (Lopes et al., 2021). The efficacy of this technique has been evaluated with a 4 × 4 10 mm length needle array electrode on a superficial tumour covered with 0.1 S/m conductive gel, as shown in Fig. 1.25 (A). As shown, conductive gel improves the electric field distribution significantly if compared to the same model without conductive gel (Fig. 1.25 (B)).

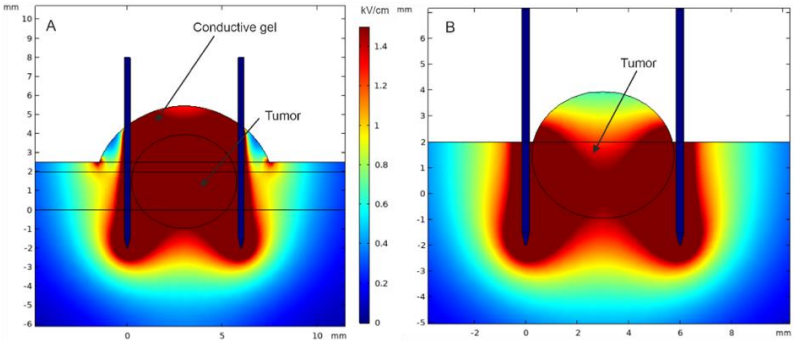

Fig. 1.25. Spatial electric field distribution using needle electrode: (A) with conductive gel; (B) without conductive gel

The optimal amount of conductive gel during an electroporation-based procedure may be hard to define sometimes. Thus, the electric properties and the gel influence on the whole treatment should be properly modelled during the treatment planning step.

1.4. Electric Pulse Parameters used for Electroporation-Based Ablation, Drug and Gene Delivery

The electroporation outcome heavily depends on the pulse parameters. Optimal pulsing parameters have to be selected and adjusted to electrode structure and electric tissue properties to enhance treatment efficacy.

A typical square-shaped unipolar electric waveform is presented in Fig. 1.26. Pulse generators are usually capable of generating amplitudes up to tens of kilovolts while minimising the distortion of the signal, namely, overshoot $V_{overshoot}$ and undershoot $V_{undershoot}$. The plateau region with the effective voltage, V_p, characterises the voltage applied to the biological load. The rise and fall times of the signal, t_{rise} and t_{fall}, respectively, are expected to be in the sub-microsecond range. At the same time, pulse width t_w is characterised as the time range at which the signal reaches half of its effective amplitude and goes below this value (Miklavčič, 2017). The full duration of a single pulse (from the pulse initiation to the beginning of the following pulse) is termed a period T.

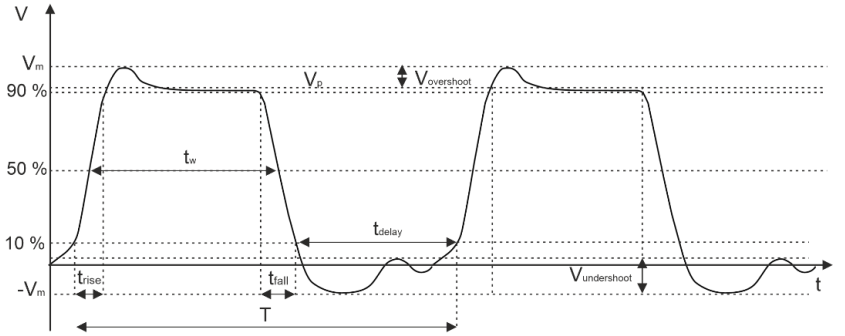

Fig. 1.26. Typical unipolar electric pulses with main characteristics

The determination of optimal PEF parameters is an essential step in electroporation-based procedures. Currently, a wide range of parametric protocols has been introduced and used; however, they vary significantly between the treatments. The summary of the exemplary pulsing protocols used with the electrodes presented in sub-section 1.3 is shown in Tables 1.6–1.8.

Table 1.6. Parametric protocols for ECT with various electrode types (Malyško-Ptašinskė et al., 2023)

Electrode	Tumour/target type	Protocols	References
Needle pair	C3H strain mice Dunn murine osteosarcoma	75 ms, 100 V/cm; 8p, 8 Hz	(Isobe et al., 2004)
	Lung cancer and colorectal cancer	ESOPE	(Tremble et al., 2019)
Needle array	Feline nasal planum squamous cell carcinoma	ESOPE	(Tellado et al., 2022)
Needle array with reposition	Mice spine (Sp2/0)	ESOPE; 800 ns, 3.5 kV/cm, 250p	(Novickij et al., 2020a)

End of Table 1.6

Electrode	Tumour/target type	Protocols	References
Needle array with reposition	Mice SA-1 tumour	100 µs, 530 V, 8px2, 100 Hz	(Reberšek et al., 2008)
Hexagonal shape	Human head and neck malignancies	ESOPE	(Pichi et al., 2018)
L-shaped	Horse sarcoid	*Gap 9 mm:* 100 µs, 1170 V, 8px2, 1Hz	(Mazères et al., 2008)
Curved	Malignant skin lesions	ESOPE	(Ritter et al., 2018)
	Rat liver	100 µs 360 kV/cm, 8p, 1Hz	(Ritter et al., 2018)
Plate	Mice SA-1 tumour	100 µs, 1300 V/cm, (2 sets changing polarity each 4p), 1 Hz	(Sedlar et al., 2012)
	Mice murine sarcoma	ESOPE	(Cemazar et al., 2001)
	Mice oesophageal adenocarcinoma, prostate adenocarcinoma, breast adenocarcinoma	*Gap 6 mm:* ESOPE	(Larkin et al., 2007)
Clipper plate	BALB/c nude mice melanoma	300ns, 20kV/cm, 1000p, 1Hz	(Guo et al., 2014)

As shown in Table 1.6, the ESOPE-established protocols are dominant in the context of electrochemotherapy. For GET treatments, longer pulses (millisecond range) with a reduced amplitude are more favourable in this field of application due to a more profound electrophoretic component of the treatment. Nevertheless, recent studies have shown an interest in more complex waveforms, including bipolar sequences. As demonstrated by Potočnik et al., the successful use of short high-frequency bipolar pulses in the context of gene delivery *in vitro* (Potočnik et al., 2021). The data of PEF protocols for GET procedures are shown in Table 1.7.

Table 1.7. Parametric protocols for GET with various electrode types (Malyško-Ptašinskė et al., 2023)

Electrode	Tumour/target type	Protocols	References
Needle array	Female C57Bl/6 or Balb/c mice skin	Gap 4 mm: 100 µs,1750 V/cm, 6p, ~8 Hz 50 µs, 1125 V/cm, 2p, ~3.3 Hz 10 ms, 275 V/cm, 8p, ~3.2 Hz 50 µs, 1125 V/cm, 2p, ~2 Hz + 10 ms, 275 V/cm, 8p, ~1.96 Hz	(Roos et al., 2006)
Intradermal	C57BL/6 mice melanoma)	50 µs, 1,125 V/cm, 2p; 10 ms, 275 V/cm, 8p	(Roos et al., 2009)

End of Table 1.7

Electrode	Tumour/target type	Protocols	References
Micro needle array	Human skin (hand)	53, 108, 173 V; 1p – τ=0.5ms and τ=1ms; 3p – τ=0.5ms, 20 s delay	(Choi et al., 2010)
	Rat skin	200 V, 10ms, 10p	(Yan et al., 2010)
	Porcine skin (*ex vivo)*	296±25 V and -313±20 V (bipolar) ~10 μs (oscillations up to ~60 μs) 32.1±0.2 V 52.2±4.4 ms or 99±5 V 50.1±2.7ms (unipolar)	(Xia et al., 2021)
Multi-needle roller	C57BL/6 mice and	10 ms (10-1-10ms), 10 p, 50 V or 70 V	(Huang et al., 2018)
Multi-electrode array	Guinea pig, Sprague Dawley rat skin	150ms, 250 V/cm, 150ms delay, 72p (trough each pair)	(Heller et al., 2010; Guo et al., 2011)
L-shaped	Mice skin surface	*Gap 6 mm:* 20ms, 60–240 V, 8x2p, 1Hz	(Mazères et al., 2008)
4-plate	Skin surface	25–800 V/cm, 1–200ms, 1 Hz, 8p; 700–2000 V/cm, 10–1000ms, 1 Hz, 8p	(Heller et al., 2007)
Round tweezers	Mice uterus	*Gap 7 mm:* 50 ms, 40 mV, 1 Hz, 4p	(Maiorano and Mallamaci, 2009)
	Male mice testis	50ms, 40 V, 1 Hz, 8p	(Shi et al., 2010)
	Mice embryos	*Gap 2 mm:* 50ms, 36–39 mV, 1 Hz, 5p	(Zhang et al., 2022)
Plate	Mice SA-1 tumour and IL-12 gen	100 μs, 600 V/cm, 1p, 1 Hz + [1s delay] + 100 ms, 80 V/cm, 4p, 1 Hz	(Sedlar et al., 2012)
Clipper	Rabbit skin Mice skin	100 V, 60ms and 60 Hz 50 V, 60ms and 60 Hz	(Wang et al., 2008)
Planar golden	BALB/c nude mice skin	20ms, 40 V, 5p, 2s delay	(Wei et al., 2015)
Plate-and-fork-type	mouse/rat/human skin	50 ms, 18 V, 4p + 4 inversed	(Maruyama et al., 2001)

Irreversible electronation procedures, on the contrary, employ greater pulse amplitudes, and more flexibility is observed in the applied research. Nanosecond range exposures are already heavily used for non-thermal tissue ablation procedures. Short pulses with a high pulse repetition frequency have already been introduced for the treatment of pancreatic and liver cancers (O'Brien et al., 2019; Partridge et al., 2020). Examples of parametric protocols for IRE with various electrode types are summarised in Table 1.8.

Table 1.8. Parametric protocols for IRE with various electrode types (Malyško-Ptašinskė et al., 2023)

Electrode	Tumour/target type	Protocols	References
Needle pair	Sprague–Dawley rats myocardial decellularisation	*Gap 10 mm*: 50 V, 100 µs, 1 Hz, 10p 250 V, 100 µs, 1 Hz, 10p 500 V, 100 µs, 1 Hz, 10p (significant) 500 V, 70 µs, 1, 2 or 4 Hz, 10p and 20p	(Zager et al., 2016)
	Porcine livers	3000 V, 70 µs, 20 A, 90p	(Chen et al., 2015)
	Swine liver and liver hilum	100 µs, 2500–3000 V/cm, 90p (10p with 250 ms delay each)	(Charpentier et al. , 2011)
	Beef liver tissue (*ex vivo*)	*Gap 10 mm*: 500 V, 100 and 1000 µs, 1 and 4762 Hz, 8p 750 V, 100 µs, 1 and 4762 Hz, 8p 1000 V, 100 and 100 µs, 1 and 4762 Hz, 8p	(Langus et al., 2016)
	Rabbit livers	*Gap 10 mm*: (bipolar) 2–50 µs, 1000–2000 V, 2 µs delay, 100 µs on-time per burst, 2 – 50 p/burst, 90p 100 µs, 1000–1500 V, 100 µs on-time per burst, 1 p/burst, 90p	(Yao et al., 2017)
Needle array with reposition	Prostate	70–100 µs, 1500 V/cm, 90p	(Blazevski et al., 2020)
Curved	Rat liver	100 µs 640 kV/cm, 8p, 1Hz	(Ritter et al., 2018)
Single needle	Female Nu/Nu mice; human breast carcinoma cells	100 µs (4 sets changing polarity each 25p), 1300 V, 3 µs delay, ~9,7 kHz	(Neal et al., 2010)
	Pancreas	2250 V, (1-5-1, 2-5-2, and 5-5-5 µs) (energised time 100 µs, 300p) H-FIRE	(O'Brien et al., 2019)
	Liver	2250 V, 2-5-2 µs, (energised time 100 µs) H-FIRE	(Partridge et al., 2020)
Deployable expandable	Female Sus Scrofa liver	100 µs x 5 kHz	(Izzo et al., 2020)
5 needles		*0°:* V_{side} 186 V + $V_{d/2}$ 118 V x 80p *20°, 20 mm:* V_{side} 1200 V + $V_{d/2}$ 900 V x 120p *20°, 30 mm:* V_{side} 1700 V + $V_{d/2}$ 1100 V x 120p	

End of Table 1.8

Electrode	Tumour/target type	Protocols	References
4 needles		*10°, 20 mm:* V_{side} 1100 V + $V_{d/2}$ 1700 V x 80p *10°, 30 mm:* V_{side} 1500 V + $V_{d/2}$ 2200 V x 80p *20°, 40 mm:* V_{side} 1900 V + $V_{d/2}$ 2700 V x 80p	
Plate	C57Bl/ 6 female mice LPB cell line	*Gap ~4 mm:* 100 µs, 2500 V/cm, 80p, 0.3 Hz	(Al-Sakere et al., 2007)

It should be noted that the collected data on PEF protocols and their use with a specific electrode structure cannot be treated as a rule. Depending on the flexibility of the generator, any electrode type can be used as a load.

1.5. Conclusions of the First Chapter and Formulation of the Dissertation Tasks

Electroporation-based techniques have a great potential for cancer treatment by means of tissue ablation, chemotherapeutic drugs or gene delivery into the cells. In applied research and clinical trials, the optimisation of the electric pulse parameters and electrode structures is, though, required.

The outcome of an electroporation-based procedure depends on spatial electric field distribution in the material, and its composition, dielectric properties and response to PEF should also be contemplated. For a more accurate evaluation of electric field distribution and pretreatment planning, a realistic numerical model of skin tissue and superficial tumour considering the dielectric properties and its dynamics triggered by PEF must be developed. The analysis of the spatial electric field distribution, the effects of conductivity and tissue heterogeneity using simulations based on FEM can significantly improve the efficiency of the whole treatment.

The justified concern of non-uniform electric field distribution causes non-invasive electrodes, such as L, tweezer, round, or plate electrodes. The analysis showed that these applicators are less able to reach deeper tissues with sufficient PEF value. A larger pulse amplitude or higher pulse intensity with these electrodes would increase the ablation. The layer of conductive gel between the electrodes and the tissue fold would increase the efficiency of PEF distribution.

Invasive needle electrodes are more efficient for deep-seated tissues. The fixed-position needle arrays presented so far show good performance in generating a homogeneous electric field. However, electrodes of this type have a fixed gap size and are, therefore, suitable for targets of a certain size. Otherwise,

the healthy lesion will be unnecessarily (or harmfully) affected by PEF. On the other hand, if the target is larger than the gap between the electrodes, multiple penetrations are required. Therefore, the manual repositioning of the needles can be considered.

Minimally invasive or ep-Patch electrodes are advantageous for electroporation-based gene electrotransfer treatments. The electrodes are capable of affecting only the surface of the tissue, typically the skin. Therefore, they are inadequate for most ECT procedures.

The electrochemotherapy treatment is typically performed using conventual ESOPE-established pulsed electric field properties. Despite the efficacy offered, the treatment using microsecond PEF is associated with negative factors. The application of shorter pulses can significantly reduce the adverse effects while maintaining the high efficacy of the treatment. Therefore, novel sub-microsecond PEF parametric protocols efficiency-wise equivalent to or better than the standard clinical ESOPE procedures are currently in demand.

Based on the literature survey, the following tasks have to be solved:

- Develop the realistic numerical model of skin tissue and superficial tumour considering the conductivity dependency on PEF for evaluation of spatial electric field distribution.
- Propose the electrode capable of creating a more homogeneous spatial electric field distribution for application in electrochemotherapy *in vivo.*
- To perform parametric drug transport *in vitro* analysis and propose new sub-microsecond protocols for applied electrochemotherapy research.
- Research the suitability of developed electrode structure in electrochemotherapy experiments *in vivo.*

The applicability and efficacy of research findings must be further assessed through numerical methods as well as *in vitro* and *in vivo* research.

2

Development of Tissue Electroporation Models for Treatment Prediction

This Chapter covers the development of superficial tumour and skin models used to estimate spatial electric field distribution. The model is first tested with invasive two-needle and non-invasive plate electrodes. Considering the inhomogeneity of the generated electric field in the skin, a needle electrode composition with a repositioning strategy and a passive needle plate electrode was proposed. The analysis of the influence of conductive gel on the spatial distribution of the electric field was performed. Superficial electroporation using a skin model was also analysed. Three scientific publications on the topic of the Second Chapter were published (Novickij et al., 2020, Novickij et al., 2021, Perminaitė et al., 2023).

2.1. Superficial Tumour Model for Estimation of Electric Field Distribution

The properties of separate skin layers determine the current pathways and densities and, therefore, the outcome of electroporation-based treatments. Each

skin layer has different dielectric parameters and thicknesses, which subsequently influence the electric field distribution. The three-dimensional model of the tumour has been developed in COMSOL Multiphysics (COMSOL, Stockholm, Sweden) (Fig. 2.1).

The skin model involves inhomogeneity of the tissue structure considering skin layers, such as the stratum corneum, epidermis, dermis, fat, muscle and a subcutaneous tumour. Since not all of the layers are electrically characterised in literature, the stratum corneum was combined with the epidermis, and the dermis was combined with fat.

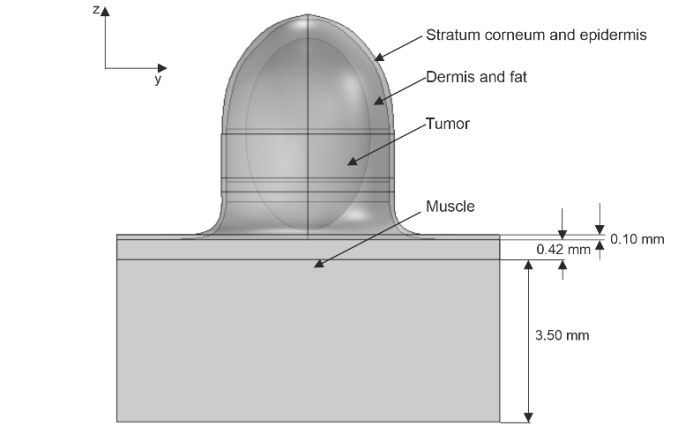

Fig. 2.1. FEM model of the superficial tumour for the estimation of spatial electric field distribution (Novickij et al., 2021)

Each layer has a specific conductivity, but based on previous studies, the conductivity can be treated as a constant value when the applied voltage is sufficiently low and does not exceed the threshold value. In *in vivo* ECT treatments, the dynamics of tissue conductivity (relative increase of σ) must be considered. The corresponding modelled tissue conductivities are summarised in Table 2.1.

Table 2.1. Skin layers and multilayers conductivity dynamics with respect to applied electric field (Novickij et al., 2021)

Tissue	Initial σ, Sm^1	Relative increase of σ	E_{RE}, Vcm^{-1}	E_{IRE}, $V\ cm^{-1}$
Stratum corneum and epidermis	0.003	800	600	1200
Dermis and fat	0.4	6	600	1200
Tumour	0.5	2.5	400	900
Muscle	0.5	2.5	400	1200

The values have been selected based on experimental data by measuring the resultant current and voltage drop on the tumour. The experimental setup is shown in Fig. 2.2.

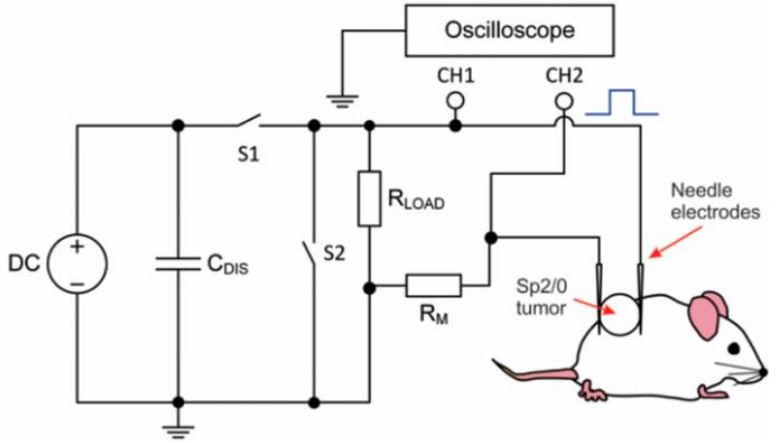

Fig. 2.2. Experimental setup for measurement of voltage and current in the superficial tumour (Novickij et al., 2021)

During the treatment, an ESOPE protocol was employed (1.4 kV/cm × 100 μs × 8), and the current increase indicating electroporation was measured. The waveform is presented in Fig. 2.3.

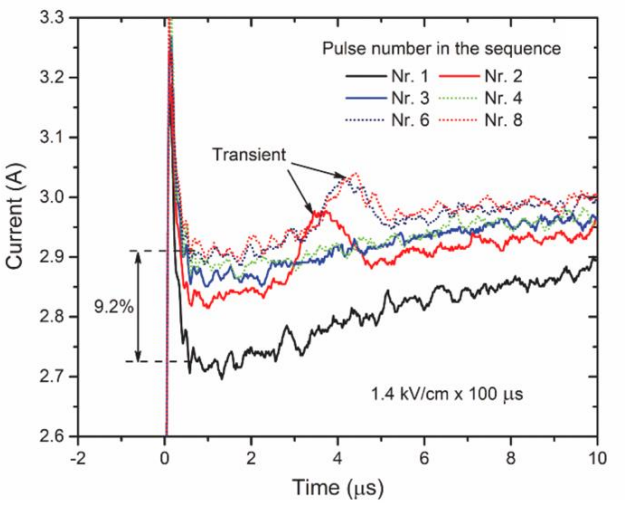

Fig. 2.3. Increase in the current during 8 electroporation pulses (Novickij et al., 2020)

Pulses were filtered to reduce transients, and the impedance of the load between the electrodes was then calculated using Ohm's law. The adjustments of conductivity values and electric field threshold in the simulation model were performed until the deviation between experimental and calculated data (measured and computed current) did not exceed 10%. The model was also checked with parallel plate electrodes (Novickij et al., 2021), and thus, the parameters presented in Table 2.1 were derived.

The developed model is further employed for the analysis of spatial electric field distribution using different electrode structures suitable for ECT treatment of superficial tumours. The model allows for the analysis of the electrode limitations, testing the feasible options for improvement, selecting optimal pulse properties, and designing new electrode structures.

2.1.1. Invasive Needle Electrodes with Multiple Reposition

The simulation of spatial electric field distribution inside a superficial tumour was carried out with an invasive needle electrode composed of two stainless steel needles placed in a 4 mm gap distance. Both applicators are injected into the most distant edges of the tumour in ~4.3 mm depth (Fig. 2.4). For the spatial electric field distribution analysis, 800 V terminal voltage was selected.

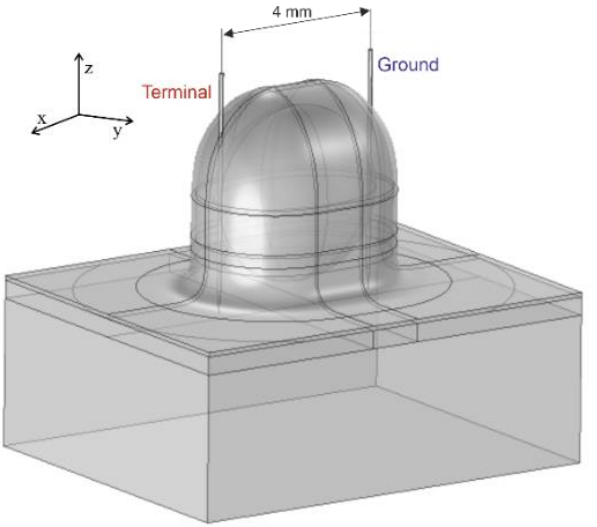

Fig. 2.4. Model of a superficial tumour with invasive needle electrodes

Needle pair electrodes, capable of reducing ablation, are used on the skin surface; however, they are relatively inefficient in terms of uniform electric field

generation. An array composed of two needle electrodes cannot ensure sufficient PEF covering the whole tumour volume. As shown in Fig. 2.5, the highest PEF is located around the needles, though it decreases notably at perpendicular edges and the central part of the tumour. This may result in non-uniform treatment and potential tumour regrowth.

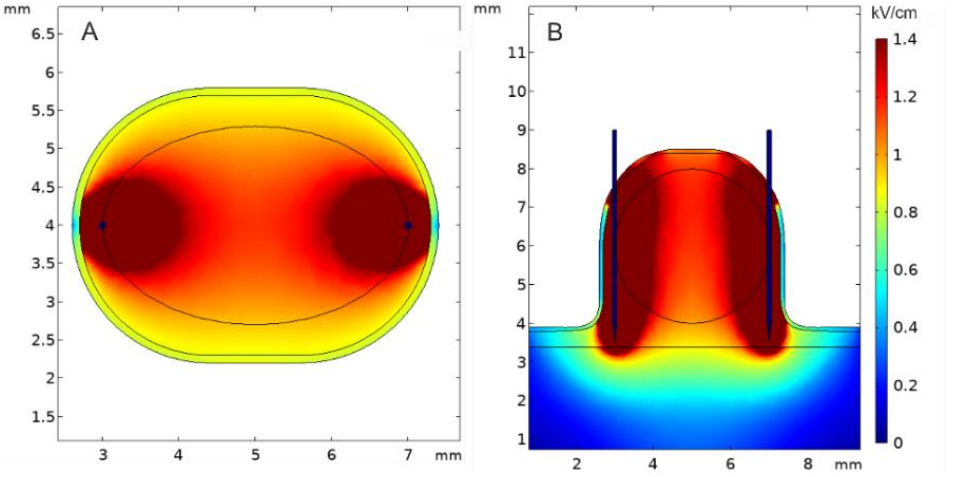

Fig. 2.5. Results of FEM simulation of the superficial tumour with two-needle electrodes, where: (A) spatial electric field distribution, YX axis; (B) spatial electric field distribution, ZX axis

Implementation of multiple needles or needle repositioning would be a reasonable option for solving the problem. Needle repositioning allows for more precise targeting of nodule edges independent of tumour size or shape. At the same time, a variation of the positioning option may offer a sufficient electric field covering the central part of the target tissue. Therefore, the needles should be injected into the tumour to subject the central part to the highest PEF dose. The proposed electrode setup operates as follows: a pair of needle electrodes was injected in the centre, and at the edge of the tumour, the edge electrode was then repositioned four times every 90 degrees, PEF was generated at each needle position, and the amplitude is adjusted depending on the tissue impedance and needle spacing. The study supports the hypothesis that the central part of the tumour is exposed to the highest value of electric field (Fig. 2.6).

The proposed electrode reposition technique may offer more efficient ECT treatment with additional necrosis in the central part of the tumour and better tumour coverage at the edges.

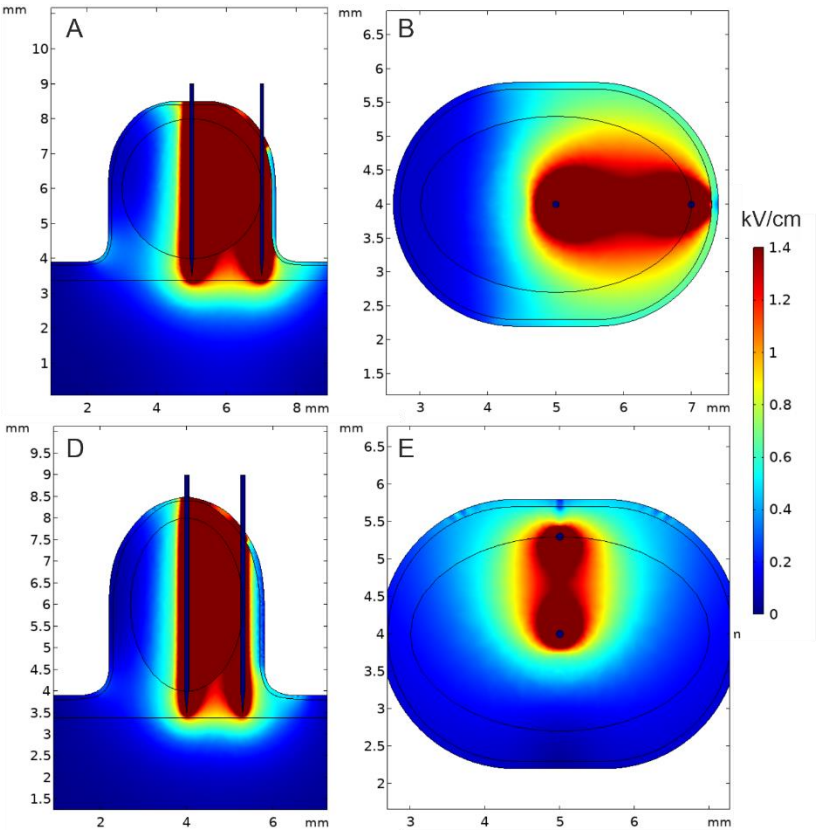

Fig. 2.6. Results of the FEM simulation (1.4 kV/cm pulse), where: (A, D) spatial distribution of electric field, side view; (B, E) spatial distribution of electric field, top view. *Terminal voltages 500 V and 270 V were applied with respect to the electrode gap distance*

As a drawback, the invasiveness of the method can be highlighted. Also, the applicability of the technique in the case of small tumours is limited, i.e., the healthy tissue will be affected.

2.1.2. Non-invasive Plate Electrodes

Non-invasive electrodes are more frequently used with superficial tumours. For the computation, needle electrodes were replaced with plate electrodes, slightly squeezing the superficial lesion (Fig. 2.7). Squeezing is advantageous in terms of increased contact between the target and the electrode surface. The voltage

(500 V) was applied between positively and negatively charged plates placed at a ~4 mm distance.

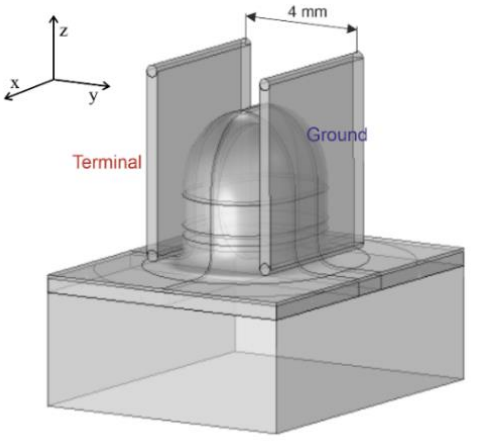

Fig. 2.7. The model of a superficial tumour with non-invasive plate electrodes

The computation confirmed the assumption of plate electrode field inhomogeneity. As shown in Fig. 2.8, the tumour will not be covered by a uniform electric field. The areas of tissue which do not have direct contact with electrodes receive an approximately 2-fold lower dose of the pulsed electric field.

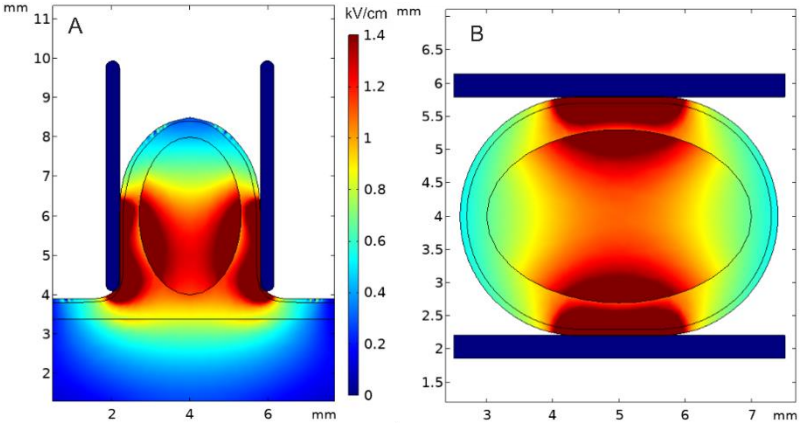

Fig. 2.8. Results of FEM simulation superficial tumour with plate electrodes, where: (A) spatial electric field distribution, side view; (B) spatial electric field distribution, top view

To improve the treatment, the modification of the PEF parameters could be performed. Namely, increasing the pulse intensity could be considered to expose the entire tumour to a higher electric field value. However, this option would potentially result in a large ablation area at the skin surface or thermal damage. Another option is to compensate for the non-homogeneity with a layer of conductive gel. The effects of conductive gel in the context of the developed mode were, therefore, investigated in the next sub-section.

2.1.3. Implementation of the Conductive Gel

It was shown that the specific amount of conductive gel drastically affects the electric field distribution in tissues. Therefore, the model with plate electrodes was supplemented with conductive gel. The empty spaces between the electrodes and the tumour were filled with conductive gel (conductivity of 1.1 S/m), as shown in Fig. 2.9. Terminal voltage value remained the same, i.e., 500 V.

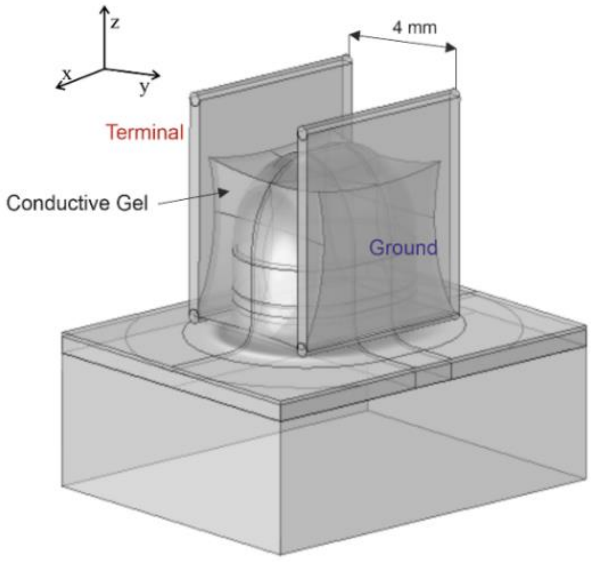

Fig. 2.9. FEM model of the superficial tumour positioned between two parallel plate electrodes with conductive gel

To minimise the possibility of shunting the tumour with conductive gel, a layer of conductive gel was placed so that the top part of the superficial tumour stayed uncovered. Fig. 2.10 shows spatial electric field distribution using plate electrodes with conductive gel.

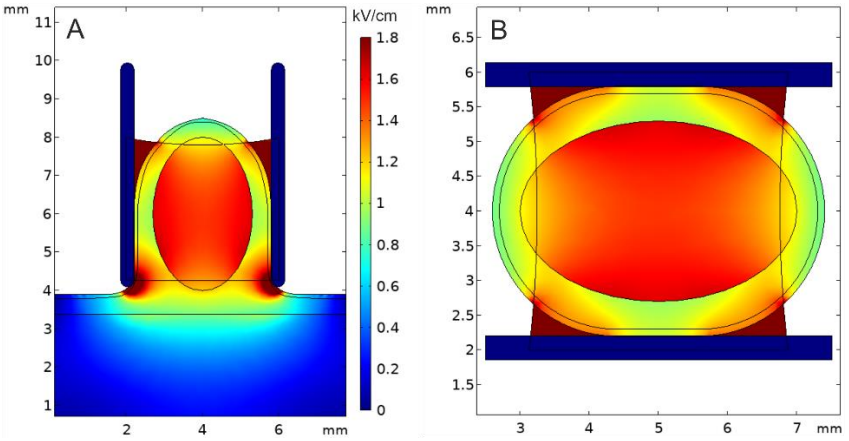

Fig. 2.10. Results of FEM simulation superficial tumour with plate electrodes and conductive gel, where: (A) spatial electric field distribution, side view; (B) spatial electric field distribution, top view

As demonstrated, the conductive gel can improve spatial electric field distribution homogeneity within the tumour. Nevertheless, the lowest and highest parts of the tumour experience a drop in the electric field value. To compensate for this, a passive centre needle electrode was proposed in this work.

2.1.4. Non-invasive Plate Electrodes with Passive Needle Electrode

A typical electrochemotherapy treatment is performed with a single localised injection of chemotherapeutic agents intratumourally *via* a sterile syringe prior to PEF exposure. The studies suggest combining the drug and PEF delivery using the electrode with hollow needles for the drug (Ritter et al., 2018) or gene introduction (Liu and Huang, 2002). Such an electrode composition strategy is advantageous for the facilitation of treatment, simultaneously reducing the treatment time. Moreover, the strategy preserves the leaking of chemotherapeutics after the needle is pulled out.

The detachable needle of the syringe could potentially enhance the electric field in the tumour because of the relatively high conductivity of the stainless-steel needle (Online Materials Information Resource, MatWeb, n.d.). To verify the hypothesis, the FEM model of the plate electrode and passive syringe needle was created (Fig. 2.11).

To spread the drug throughout the tumour in the most efficient way, the syringe needle is gradually pushed straight down into the tumour, followed by

intermittent drug injections, until the needle reaches the most distant tumour boundary.

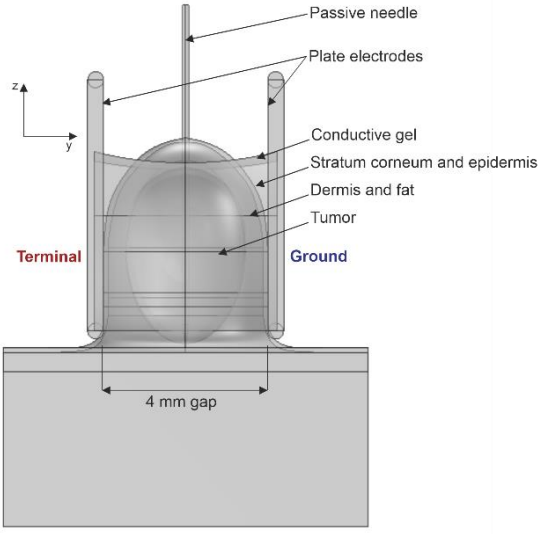

Fig. 2.11. The model of a superficial tumour with non-invasive plate electrodes and a passive needle

After the drug injection, the needle is not removed from the tumour to serve as a passive central electrode. The effects of such a strategy on the spatial electric field distribution are shown in Fig. 2.12.

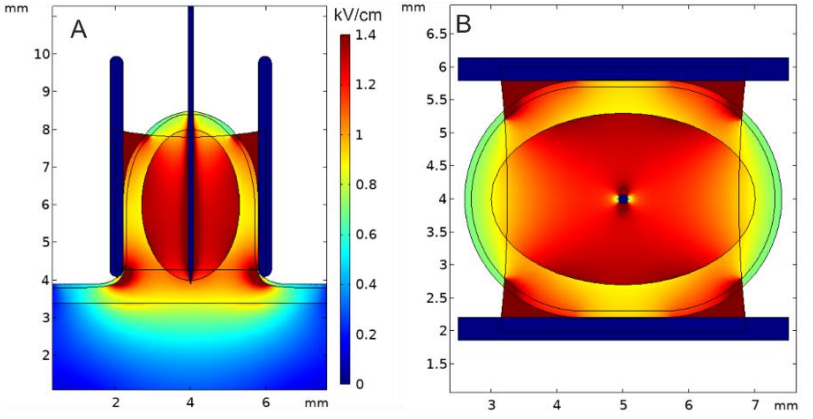

Fig. 2.12. Results of FEM simulation superficial tumour with plate electrodes and a passive needle, where: (A) spatial electric field distribution, side view ZY axis; (B) spatial electric field distribution, top view YX axis

Spatial electric field distribution analysis was performed with a terminal voltage of 420 V and conductivity of the inactive needle of 4×10^6 S/m, keeping the other model properties consistent. The obtained simulation results confirm the provided speculation of electric field amplification within the tumour. Based on Fig. 2.13, using lower terminal voltage, the superficial tumour is covered by the equivalent electric field when compared with the results of the spatial electric field distribution for which no passive needle was provided (Fig. 2.10). Such an approach allows inducing a more homogeneous spatial electric field distribution at the top and bottom parts of the tumour. The passive needle plays a role in increasing the electric field in the lower and upper parts of the tumour.

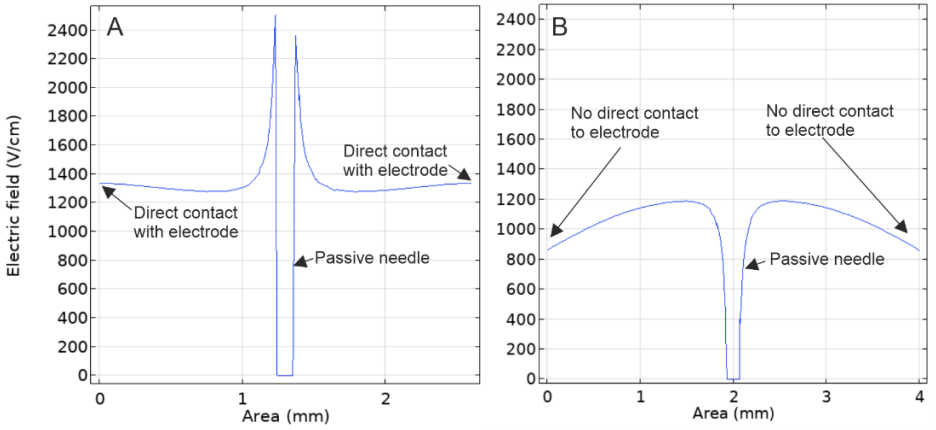

Fig. 2.13. Linear electric field values at the central part of the tumour, where: (A) YZ axis; (B) XZ axis

The proposed electrode configuration is beneficial in terms of spatial electric field distribution. However, according to Fig. 2.13, the electrode composition does not solve the issue of the tumour areas having no direct contact with electrodes. At these boundaries, the electric field strength hardly reaches 0.9 kV/cm and thus, a higher input voltage needs to be applied. However, a better solution is to reposition the plate electrodes by 90 degrees or use the electrodes composed of two plate pairs.

2.2. Electroporation-based Treatment of Superficial Infections *in vivo*

Electroporation-based treatment can also be used for the treatment of wounds. In this context, only the upper layers of the skin should be covered by high-intensity

PEF without significant effects on deeper layers, such as muscle. The experimental procedures, which do not require access to deep-seated tissues, i.e., ECT of superficial tumours (Tozon et al., 2014; Kranjc et al., 2016), intramuscular or skin GET (Ursic et al., 2021), wound sterilisation (Wu et al., 2021), etc., are typically performed through the skin. However, most of the available studies deal with a skin-fold to support the feasibility of electroporation-based wound sterilisation. This dissertation proposes an alternative approach using tweezer electrodes with a very small electrode gap (1.2 mm). The developed model (Fig. 2.14) can be further used for *in vivo* experiments on the skin and adjusted to the actual treatment.

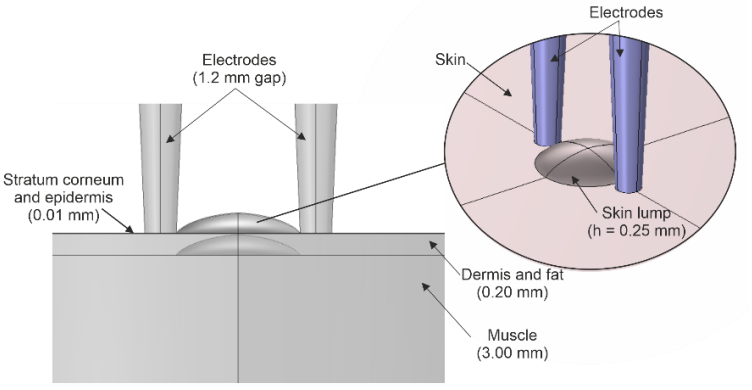

Fig. 2.14. FEM model of the hairless mice skin model positioned between sharp-tip (cone-shaped) tweezer electrodes

Table 2.2. Mice skin multilayer's thicknesses, conductivity values and simulation properties (Perminaitė et al., 2023)

Parameter	Value	Reference
Stratum corneum & epidermis conductivity	0.008 S/m; 1 S/m[a]	(Pavšelj et al., 2007; Čorović et al., 2012; Corovic et al., 2013)
Stratum corneum & epidermis thickness	10 μm	(Guo et al., 2016)
Dermis and fat conductivity	0.2–0.4 S/m; 1 S/m[a]	(Wake et al., 2016)
Dermis and fat thickness	200 μm	(Guo et al., 2016)
Muscle conductivity	0.62 S/m; 1.5 S/m[a]	(Corovic et al., 2013; Yu et al., 2016)
Muscle thickness	3 mm	–
Electrode conductivity	1.4×10^6 S/m[a]	(Callister and Rethwisch, 2007)
Terminal voltage	3000 V	–
[a] modelled change in conductivity due to the application of electric field pulses		

The model was composed of two multilayers, i.e., the stratum corneum and epidermis, dermis and fat, and muscle, considering initial tissue conductivity and conductivity changes due to applied electric field pulses. The corresponding values of tissue thicknesses and conductivities are summarised in Table 2.2.

For the evaluation of spatial PEF distribution, cone-shaped tweezer electrodes are placed at a 1.2 mm distance on the skin with minimal press, forming a small skin lump without penetration. A 0.25 mm lump height was modelled. Spatial electric field distribution was generated considering initial multilayer conductivities at the permeabilisation threshold (Fig. 2.15 (A)), and the conductivity rise when cells are permeabilised irreversibly due to PEF (Fig. 2.15 (B)) using a 3 kV terminal voltage.

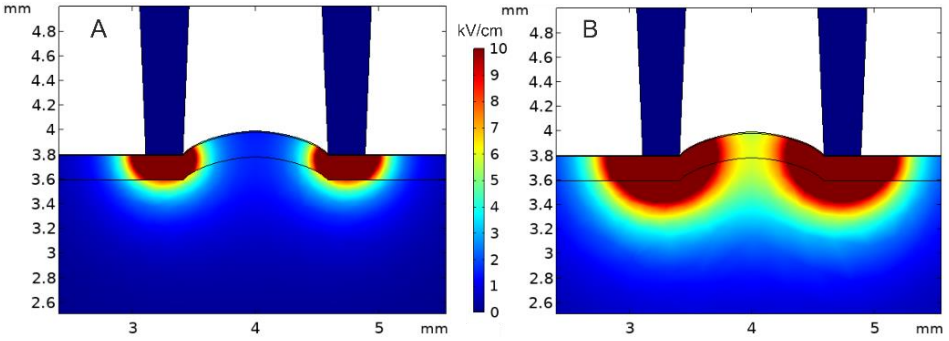

Fig. 2.15. Spatial distribution of the electric field during pulsed electric field treatment, where (A) tissue conductivities are nominal and not affected by PEF; (B) tissue electrical conductivities are increased due to permeabilisation triggered by PEF

Based on Fig. 2.15 (A), the highest electric field is concentrated in the region of the electrode-tissue contact. However, after the exposure to the electric pulse burst, the tissue would be electroporated irreversibly, indicating that conductivity increases. Therefore, Fig. 2.15 (B) illustrates the actual spatial electric field distribution when a relatively high PEF is applied. The penetration depth of the electric field can be manipulated by adjusting the electrode distance. The simulation results indicate that the small gap between the electrodes without penetration enables the superficial permeabilisation of the cells with no effect on the subcutaneous tissues, such as muscle.

2.3. Conclusions of the Second Chapter

1. The developed superficial tumour model enables a precise evaluation of spatial electric field distribution using various electrodes with a ±10%

deviation. It was found that spatial electric field distribution strongly depended upon the conductivity dynamics of separate skin layers during the electric pulse delivery.

2. The typical composition of two needle electrodes placed at the edges of the tumour cannot guarantee a sufficient electric field within the tumour volume. A repositioning strategy allows compensating for this limitation.
3. The parallel plate electrodes are incapable of producing a homogeneous electric field at the tumour areas perpendicular to electrodes as well as the top and bottom parts; however, the homogeneity of the field can be improved with conductive gel.
4. To amplify the electric field strength within the tumour, parallel plate electrodes with an additional passive needle were proposed. The results have shown that such an electrode composition is capable of improving electric field homogeneity in the top and bottom parts of the tumour; however, it cannot solve the reduction of the electric field in areas perpendicular to electrodes. Two parallel pairs of electrodes, such as 4PE, with a passive needle, could be used to minimise this issue.
5. The proposed non-penetrating tweezer small-gap (1.2 mm) electrodes allow to affect only the upper layers of the skin without damage to the deeper tissue and, thus, are applicable for the treatment of superficial skin infections. The operating area of such an electrode is relatively small; therefore, multiple applications may be needed to treat the whole tissue. For more efficient and streamlined treatment, a multi-needle electrode array with a small gap between positively and negatively charged electrode pairs can be considered.

3

Applied Electrochemotherapy with Microsecond and Sub-microsecond Pulsed Electric Fields

This Chapter presents the experimental results with the proposed electrode structures. It characterises the feasibility of proposed electrode structures and pulsed electric field parametric protocols according to the obtained results. It is shown that sub-microsecond range electric field pulses result in a successful ECT procedure both *in vitro* and *in vivo*. Furthermore, the applicability of small-gap tweezer electrodes with a repositioning technique is experimentally evaluated for the treatment of superficial infections.

Four scientific publications were published on the Third Chapter topic (Novickij et al., 2020a, 2020b, 2021; Perminaitė et al., 2023).

3.1. Application of Sub-microsecond Pulses for Permeabilisation of Cell Membrane

To derive novel and efficacy-wise efficient electroporation protocols, firstly, the research has been performed *in vitro* using mice luminescent myeloma SP2/0 cells (SP2/0-Luc). The experiment tested 0.1–5 μs × 250 and 100 μs × 1–8 pulsing

protocols in the 1–2.5 kV/cm PEF range. The electric pulses were delivered to a 1 mm gap cuvette with aluminium electrodes. Changes in cell morphology, permeabilisation and membrane resealing were then evaluated. Cell morphological changes and uptake of fluorescent dye (Propidium iodide) are shown in Fig. 3.1.

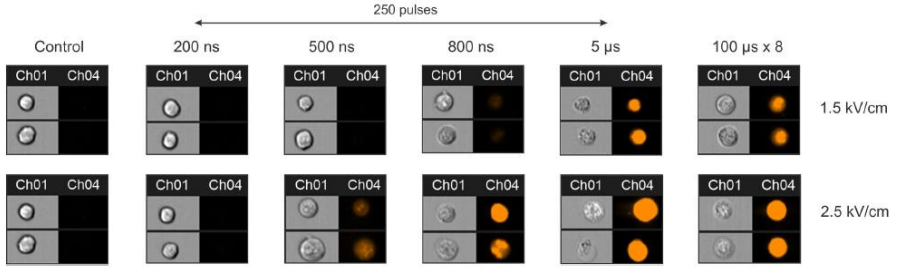

Fig. 3.1. Changes of cell morphology depending on the PEF treatment intensity, where Ch01 – brightfield image; Ch04 – fluorescence image using the bandpass filter of 610–630 nm (Novickij et al., 2020b)

Unaffected cells are shown (control) as a reference. According to the data, PEF of 1.5 and 2.5 kV/cm does not trigger detectable permeabilisation with 200 ns pulses when delivered in a kHz burst. However, for a more accurate definition of an electroporation threshold, the dependence of the cell permeabilisation rate on applied pulsing protocols was studied using flow cytometry. The results are shown in Fig. 3.2.

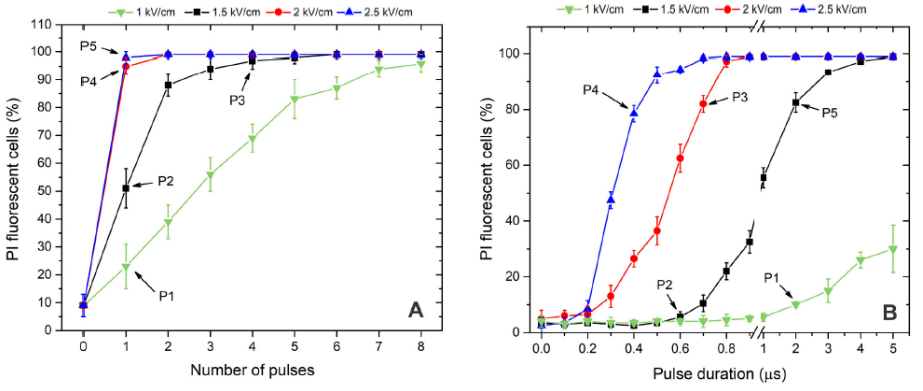

Fig. 3.2. Dependence of cell permeabilisation rate on applied PEF parameters, where (A) – microsecond range ESOPE pulses and (B) – short pulses. P1–P5 correspond to specific protocols triggering different rates of permeabilisation for comparison purposes with the resealing and viability data (Novickij et al., 2020b)

It can be seen that electroporation is a threshold-type phenomenon. In the case of microsecond pulses, the 1 kV/cm is sufficient to permeabilise all the cells only after 8 pulses; however, if the amplitude is increased, the saturated permeabilisation is reached already after 1–2 pulses. In the case of nanosecond bursts, only 2 and 2.5 kV/cm electric field pulses are effective. For example, equivalent permeabilisation (~80%) is reached with 700 ns and 300 ns × 250 pulses if 2 and 2.5 kV/cm PEF is used, respectively. The results were further supported by the resealing data, which was acquired 1-h post-treatment and are summarised in Fig. 3.3.

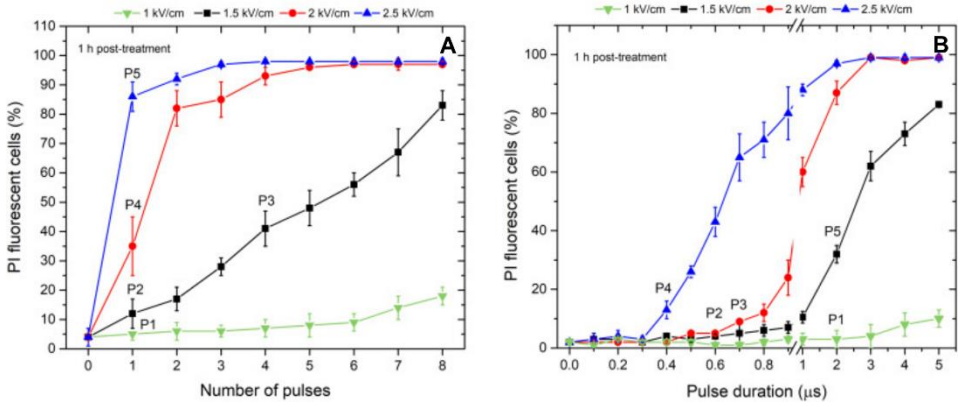

Fig. 3.3. Dose-dependent response of cell membrane resealing after electric field treatment, where (A) long 100 μs pulses, and (B) short pulses (Novickij et al., 2020b)

As shown, depending on the number of pulses and the PEF amplitude, the electroporation can be irreversible both with ESOPE and short microsecond and sub-microsecond pulses. A trade-off between the pulse amplitude, duration and the number of pulses should always be made. All of the sub-microsecond protocols used in the study had no significant influence on the resealing of the cell membrane, which indicated reversible electroporation. With the increase in duration (e.g., 2 μs), the number of cells unable to reseal was almost 40% (P5 in Fig. 3.3 (B)). The ESOPE pulses with 1 kV/cm amplitude trigger reversible permeabilisation in the whole 1–8 pulses range. With the increase of PEF amplitude, the number of irreversibly permeabilised cells increases, which is an expected result.

Finally, the cell line was used in pilot *in vivo* experiments for the establishment of tumours and testing the applicability of bleomycin-based electrochemotherapy. Electric pulses (1.2 kV/cm × 100 μs × 8) were delivered

administering bleomycin. Parallel plate non-invasive electrodes have been used. The images of the luminescent tumour before and after the treatment were captured and are shown in Fig. 3.4. The detailed experimental methodology can be found in the publication by Novickij et al. (2020b).

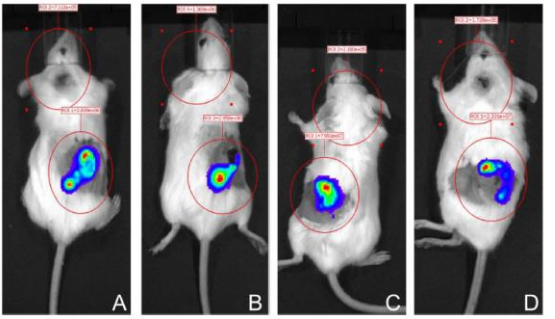

Fig. 3.4. Luminescence of the Sp2/0 tumours, where (A, B) mouse before and after the treatment using PEF only; (C, D) mouse before and after ECT with bleomycin (Novickij et al., 2020b)

To compare luminescence and volumetric data, the measurement was repeated after three days. The decrease of luminescence was noticed in the case where ECT (PEF + BL) indicated a tumour response to the treatment (Fig. 3.5). The volumetric analysis failed to show significant differences since a necrotic scab formed, preventing accurate measurements; therefore, luminescence was a more accurate tool to evaluate tumour growth dynamics in the first days after the treatment.

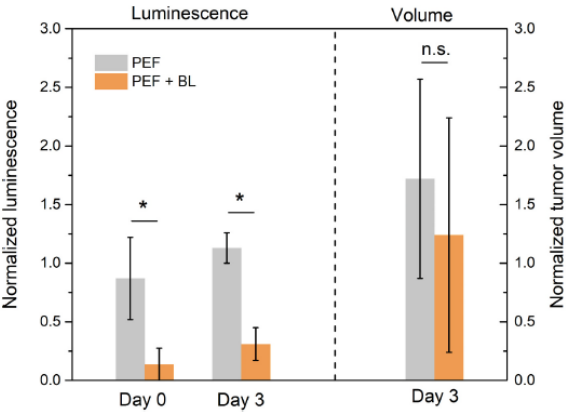

Fig. 3.5. Luminescence of the Sp2/0 tumours, where (A, B) mouse before and after the treatment using PEF only; (C, D) mouse before and after ECT with bleomycin (Novickij et al., 2020b)

All experimental protocols were approved by the Lithuanian State Food and Veterinary Service (approval of 2020-04-14 No. G2-145), and the study was performed strictly according to the recommendations in the Guide for the Care and Use of Laboratory Animals.

Further, the pilot experiments with doxorubicin and needle electrodes were performed. The repositioning technique described in the second chapter of this dissertation was used. The experiment used nsPEF (3.5 kV/cm × 800 ns × 250) and ESOPE-like (1.4 kV/cm × 100 μs × 8) electric pulses. The photographs of mice after the treatment are shown in Fig. 3.6.

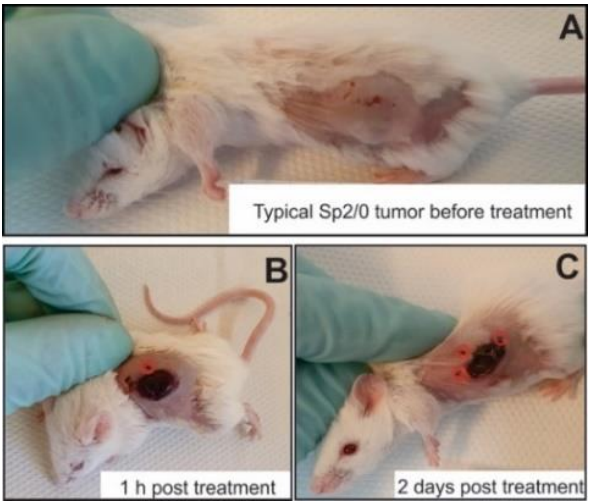

Fig. 3.6. Representative photographs of mice before (A) and after 1-hour (B) and two days (C) post-treatment (3.5 kV/cm × 800 ns × 250 pulses with doxorubicin). Red circles (B, C) represent visible electrode injection points (Novickij et al., 2020a)

The *in vivo* experiment used 12 animals with SP2/0 tumours ~150–500 mm^3 in size in total. For ECT, 12 mg/kg of doxorubicin was injected 15–20 min before the treatment, followed by the delivery of nsPEF and μsPEF pulsing protocols. The necrosis of cancerous lesions was detected after two days post-treatment. The mice were observed for 30 days, and the dynamics of tumour growth were determined. The results are summarised in Fig. 3.7.

The sub-microsecond electrochemotherapy with needle electrodes and the positioning technique showed the best treatment outcome. The survival of mice was doubled if compared to the untreated control. In the case of ESOPE protocols, a significant delay in tumour growth was also detectable; however, the efficacy was inferior to the sub-microsecond protocols.

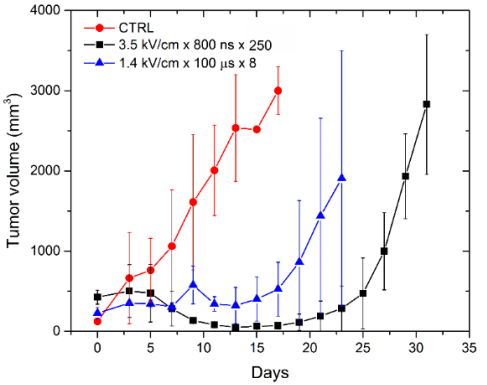

Fig. 3.7. Dynamics of tumour growth after treatment with pulsed electric fields and doxorubicin, where CTRL – untreated control (Novickij et al., 2020a)

The detailed methodology can be found in the publication by Novickij et al., 2020a. With the pilot data showing tumour response towards the treatment, a full-scale electrochemotherapy experiment was planned. Also, it was decided to determine the effects of pulse repetition frequency on the treatment outcome.

3.2. Sub-microsecond Electrochemotherapy in High Pulse Repetition Frequency Range

Sub-microsecond ECT was performed using unipolar high repetition frequency (1 kHz and 1 MHz) pulses and bleomycin on the Lewis lung carcinoma (LLC1) cell line. The summary of the applied electric field parameters is presented in Table 3.1.

Table 3.1. Electroporation protocols (Novickij et al., 2021)

Name	Protocol parameters
CTRL	Untreated
nsPEF1	3.5 kV/cm × 200 ns × 200, 1 kHz
nsPEF2	3.5 kV/cm × 200 ns × 200, 1 MHz
nsPEF3	3.5 kV/cm × 700 ns × 200, 1 kHz
nsPEF4	3.5 kV/cm × 700 ns × 200, 1 MHz
µsPEF	1.3 kV/cm × 100 µs × 8, 1 Hz (ESOPE)

It is crucial to ensure high permeabilisation of the cells to trigger high-efficiency ECT; therefore, the permeabilisation of the cells *in vitro* was analysed using a fluorescent YO-PRO-1 dye. The results are summarised in Fig. 3.8.

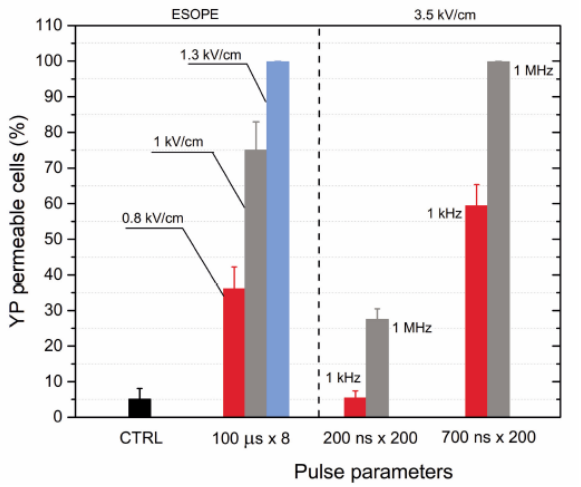

Fig. 3.8. Effects of pulsed electric field on membrane permeability to YP (Novickij et al., 2021)

As demonstrated, 700 ns duration pulses delivered at 1 MHz frequency trigger saturated permeabilisation similar to ESOPE pulses at 1.3 kV/cm. Increasing the delay between nanosecond pulses (1 kHz) significantly reduces the efficacy of the treatment. The 200 ns pulses trigger low permeabilisation of the cell membrane; however, a frequency dependency is also present.

Finally, the tumours have been established in mice (C57BL). The treatment was performed with intertumoural injection of bleomycin (50 µL of 1500 IU solution) and nanosecond (3.5 kV/cm, 200 and 700 ns duration pulses were delivered in a burst of 200 at repetition frequencies of 1 kHz and 1 MHz). Microsecond ESOPE protocol (1.3 kV/cm) was also performed for comparison.

Non-invasive parallel plate electrodes were used for the treatment. Treatment planning was performed by simulation of the spatial electric field distribution according to established simulation models. The computation was performed considering skin layers, i.e., the stratum corneum, epidermis, dermis, fat, muscle and a subcutaneous tumour. Electric pulses were delivered with plate electrodes placed at a 4 mm distance between slightly squeezing tumour tissue and increasing the contact area. The empty space between the electrodes was filled with conductive gel (conductivity of 1.1 S/m) to reduce inhomogeneity and achieve better overall treatment. Treated tumour skin layers and thicknesses were selected using the data from mice skin measurements (Hew et al., 2016; Wei et al., 2017). The boundary conditions were selected using Dirichlet's and Neumann boundary conditions, where one of the electrodes stands as ground with zero potential, while the second electrode transfers the applied voltage amplitude value (3.5 kV/cm and

1.3 kV/cm for nano and microsecond protocols, respectively), surface boundaries were electrically insulated. In this computation, stationary analysis was performed using the finite element method. The spatial electric field distribution for microsecond and sub-microsecond pulsing protocols is shown in Fig. 3.9.

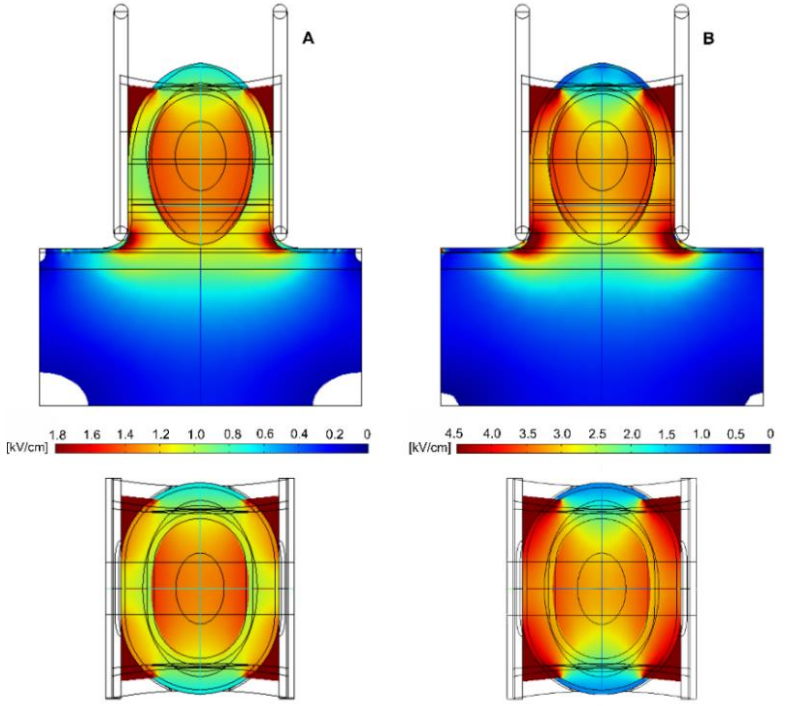

Fig. 3.9. Spatial distribution of an electric field during electrochemotherapy, where (A) 1.3 kV/cm 100 μs protocol; (B) 3.5 kV/cm nanosecond protocol (Novickij et al., 2021)

To evaluate conductivity dynamics, the conductivity step function (smoothed Heaviside function) from the initial E1 (150–400 V) up to irreversible E2 (800–1200 V) values for all skin layers was included. For adequate result evaluation and verification of conductivity dynamics, the current was also measured for microsecond and nanosecond pulses. The obtained results indicate good scaling with Ohms law (only with up to 5–20% differences in load impedance, in some cases, the differences were barely distinguishable). Thus, the resulting impedances of the tumours were similar for all protocols.

The spatial distribution of the electric field for both cases confirmed that the top and the bottom parts of the tumour received the lowest dose of PEF, while the stratum corneum, which was in contact with the electrodes, was treated

irreversibly and, therefore, skin necrosis of was expected. The fraction of volume of the tumour receiving PEF of different amplitude was evaluated and is presented in Fig. 3.10.

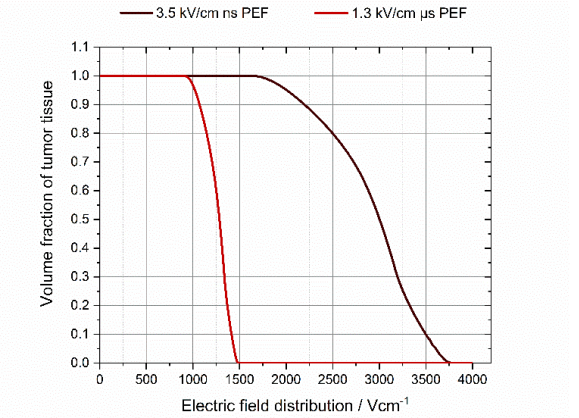

Fig. 3.10. Fraction of tumour volume affected by the pulsed electric field due to field non-homogeneity (Novickij et al., 2021)

As shown, due to the limitations of plate electrodes, the amplitude of the PEF within the tumour may scale more than 30%. The dynamics of the tumour growth after various treatments were evaluated and are presented in Fig. 3.11.

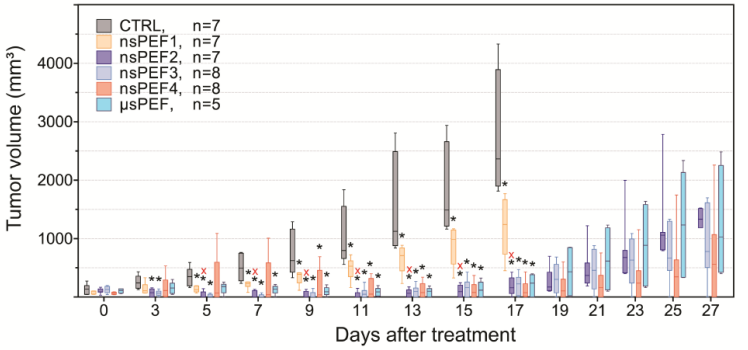

Fig. 3.11. Volumetric changes of the tumours after bleomycin electrochemotherapy; CTRL – untreated control. Asterisk (*) indicates a statistically significant (P<0.05) difference versus CTRL; (X) – indicates a statistically significant (P<0.05) difference versus nsPEF1. Whiskers extend to maximum or minimum data values from the median of the dataset (Novickij et al., 2021)

The partial or full response to the treatment was observed in all the treated groups, including ESOPE. Three of all 16 mice treated with different pulsing conditions showed full recovery. These tumours were exposed to 3.5 kV/cm × 700 ns × 200 pulses delivered at 1 MHz repetition frequency. It was shown that the proposed sub-microsecond electrochemotherapy protocols are more effective than standard ESOPE procedures. The detailed methodology can be found in the publication by Novickij et al. (2021).

All experimental protocols were approved by the Lithuanian State Food and Veterinary Service (2020-04-14, No. G2-145), and the study was performed strictly according to the recommendations in the Guide for the Care and Use of Laboratory Animals.

3.3. Amplification of Electric Field using Passive Needle Electrode

The plate electrode with the passive needle described in the Second Chapter was tested in the electrochemotherapy treatment of murine melanoma (B16) *in vivo*. The tumours were treated using ESOPE pulsing protocol (1.3 kV/cm × 100 µs × 8 (1 Hz)) with calcium chloride ($CaCl_2$) (CaPEF + EL group). To evaluate the efficacy of the proposed electrode composition, a reference treatment without a passive needle was performed (CaPEF group). Untreated mice are represented as the CTRL group. The survival rate of each group was evaluated, as shown in Fig. 3.12.

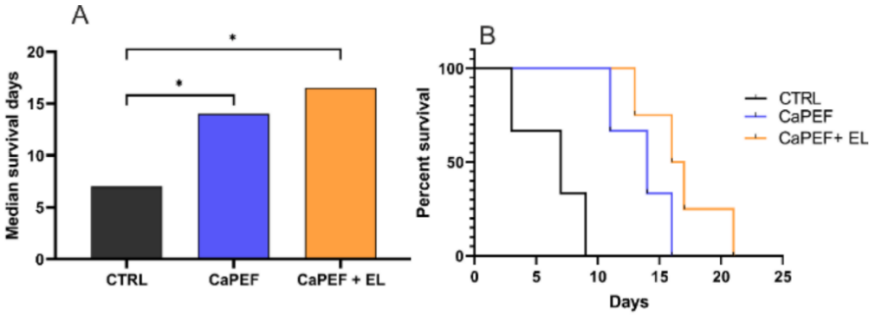

Fig. 3.12. Mice with melanoma tumours treated with electroporation (PEF; 1.3 kV/cm × 100 µs × 8 (1 Hz)) combined with or without central electrode (EL) and calcium chloride; CTRL – not treated tumour bearing mice. (A) Kaplan-Meier survival curves and (B) median survival days. Statistical analysis using Log-rank (Mantel-Cox) test for trend was performed to demonstrate the significance ($P < 0.05$) between control and treated groups

The results indicate that the overall treatment using calcium chloride was better than the untreated CTRL group, as the median survival days were, on average, two-fold higher. As demonstrated in Fig. 3.12, the developed electrode structure with a passive electrode was, on average, better if compared with the CaPEF group, which is in agreement with the simulation presented in the Second Chapter.

3.4. Electroporation for Bacterial Killing on the Skin Surface

This Chapter introduces the pulsed electric field (15- and 25- kV/cm × 750 ns × 1000 pulses with 15 kHz repetition frequency) in combination with (1%) acetic acid of low concentration to inactivate P. *aeruginosa*. An *in vivo* mouse wound model (BALB/C) was developed using a luminescent strain of P. *aeruginosa*. For the pretreatment planning, the mice skin model with 1.2 mm tweezer electrode spacing was used, as described in the Second Chapter

The animals were anaesthetised using intraperitoneal 80 mg/kg ketamine injection and 10 mg/kg of xylazine, followed by the transfer of bacteria in phosphate-buffered saline (PBS) on ~10 mm diameter irritated skin surface (scratched with a sharp tweezer tip). The bioluminescence signal was considered to be proportional to the number of contaminating live bacteria. The PEF treatment with 1% (100 μL) acetic acid and acetic acid alone was then applied to animals. The bacterial contamination analysis was performed for each mice group on days 0, 3, 5 and 7 (Fig. 3.13).

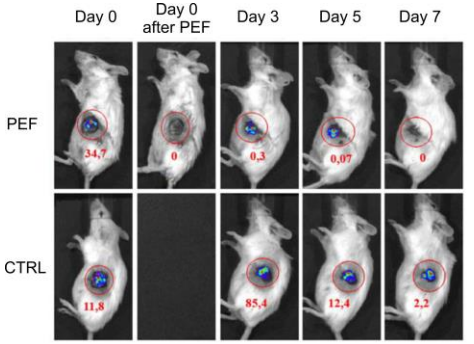

Fig. 3.13. Mice with just the acetic acid (1%) treatment (CTRL) and treated with PEF (3 kV voltage is applied between 1.2 mm gap electrodes) and 1% acetic acid treatment. The red circle indicates the region of interest (ROI) where the luminescence signal was quantified. The number indicates the intensity of luminescence in the ROI (Perminaitė et al., 2023)

A total of ~14 repositioning of the electrodes was required to cover the entire treatment area. The treatment of PEF and acetic acid group results in effective bacterial decontamination of the area. The quantified results are summarised in Fig. 3.14.

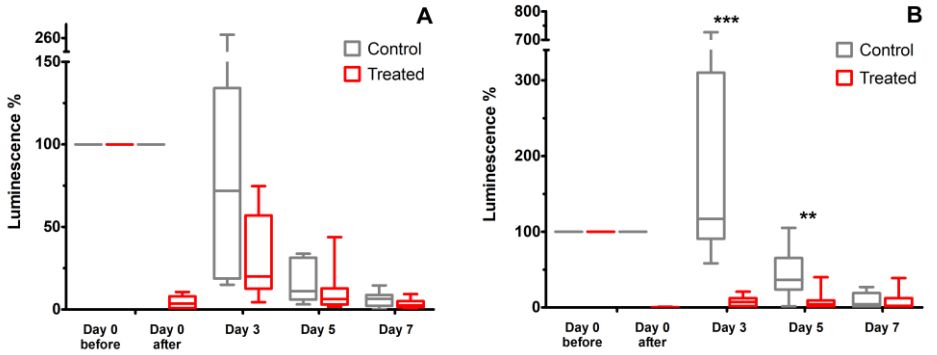

Fig. 3.14. Luminescence of the ROI after the treatment using 1.8 kV protocol (A) and 3 kV protocol (B). All the data were normalised to the CTRL group. The asterisk ** $p \leq 0.01$; *** $p \leq 0.001$ (Perminaitė et al., 2023)

The experiment has shown that an electric field of up to 25 kV/cm in combination with acetic acid has a bacteriostatic effect that prevents further infection within seven days post-treatment when compared with the CTRL group (Fig. 3.14).

The study has proved that the proposed small-gap tweezer electrodes with the repositioning technique can generate a sufficient electric field to inactivate bacteria when combined with low concentrations of acetic acid. In summary, PEF treatment using nanosecond pulses is a viable option for wound treatment but needs further optimisation in terms of pulse parameters and the optimal concentration of acetic acid.

The protocol was approved by the State Food and Veterinary Service (License No. G2-48). The detailed methodology can be found in the publication by Perminaite et al. (2023).

3.4. Conclusions of the Third Chapter

1. The efficacy and suitability of sub-microsecond pulsed electric fields were demonstrated *in vitro* and *in vivo*. The proposed parametric protocols are able to trigger efficiency-wise ESOPE-equivalent or better treatment. The outcome of the electroporation-based biomedical

procedures could be further manipulated by adjusting the pulse amplitude, duration, the number of pulses or pulse repetition frequency. However, this requires the development of pulsed systems capable of delivering electrical pulses with higher parameter flexibility.

2. The developed needle electrode with reposition technique has been successfully applied in the electrochemotherapy experiment *in vivo*. According to the obtained results, the methodology offers good treatment localisation and improvement of field homogeneity.
3. Sub-microsecond electric pulses compressed into high-frequency (MHz) bursts resulted in significantly reduced tumour regrowth in the treated animals compared to the conventional microsecond pulses. The obtained results suggest researching the efficacy of sub-microsecond pulses delivered at above 1 MHz repetition frequency.
4. The proposed small-gap tweezer electrodes with a repositioning technique are suitable for wound decontamination when used in combination with acetic acid. The wounds of different diameters were treated using multiple repositioning of the electrodes, which is inconvenient from a time perspective and may be harmful due to the potential risk of repetitive PEF application. To reduce the time required for the procedure, electrodes with a wider operating area would be more appropriate.

General Conclusions

1. The developed numerical model of the superficial tumour was developed based on the finite element method. The model enables accurate (±10% results uncertainty) electrochemotherapy pretreatment planning considering the conductivity dynamics of separate skin layers. The model is suitable for the evaluation of the spatial electric field distribution within the superficial tumour using different electrode configurations.
2. The proposed invasive needle electrodes with a repositioning technique can be successfully employed for electrochemotherapy treatments. The electrodes are capable of producing a sufficient effect on the tumour while concentrating the highest dose of PEF at the central part of the tumour, improving treatment localisation.
3. High-frequency (MHz) nanosecond pulses have been applied *in vivo*, showing significantly better efficacy than ESOPE protocols, ensuring slower tumour growth or complete recovery.
4. The proposed small-gap tweezer electrodes with a repositioning technique are suitable for wound decontamination when used in combination with acetic acid ensuring predominantly superficial treatment.

Recommendations

1. It is recommended to further compress the electric pulses (>MHz) as it could potentially allow to achieve more significant treatment efficacy. However, the approach requires the development of novel electroporation devices.
2. To facilitate the treatment of wound decontamination with acetic acid and PEF, it is recommended to replace tweezer electrodes with an array of multiple needles.

References

Adeyanju, O. O., Al-Angari, H. M., & Sahakian, A. V. (2012). The optimization of needle electrode number and placement for irreversible electroporation of hepatocellular carcinoma. *Radiol Oncol, 46*, 126–135. https://doi.org.10.2478/v10019-012-0026-y.

Adjustable Electrodes – EPSA Series | IGEA Medical (n. d.). https://www.igeamedical.com/en/electrochemotherapy/products/electrodes/adjustable-epsa-series

Ahad, M. A., Narayanaswami, P., Kasselman, L. J., & Rutkove, S. B. (2010). The effect of subacute denervation on the electrical anisotropy of skeletal muscle: Implications for clinical diagnostic testing. *Clinical Neurophysiology, 121*, 882–886. https://doi.org.10.1016/j.clinph.2010.01.017

Alkilani, A. Z., McCrudden, M. T. C., & Donnelly, R. F. (2015). Transdermal drug delivery: Innovative pharmaceutical developments based on disruption of the barrier properties of the stratum corneum. *Pharmaceutics, 7*, 438–470. https://doi.org.10.3390/pharmaceutics7040438

Al-Sakere, B., André, F., Bernat, C., Connault, E., Opolon, P., Davalos, R. V., et al. (2007). Tumor ablation with irreversible electroporation. *PLoS One, 2*, 1–8. https://doi.org.10.1371/journal.pone.0001135

Andrade, D. L. L. S., Guedert, R., Pintarelli, G. B., Rangel, M. M. M., Oliveira, K. D., Quadros, P. G., et al. (2022). Electrochemotherapy treatment safety under parallel needle deflection. *Sci Rep*, *12*, 1–10. https://doi.org.10.1038/s41598-022-06747-x

Arab, H., Chioukh, L., Dashti Ardakani, M., Dufour, S., & Tatu, S. O. (2020). Early-stage detection of melanoma skin cancer using contactless millimeter-wave sensors. *IEEE Sens J*, *20*, 7310–7317. https://doi.org.10.1109/JSEN.2020.2969414

Asadi, M., Beik, J., Hashemian, R., Laurent, S., Farashahi, A., Mobini, M., et al. (2019). MRI-based numerical modeling strategy for simulation and treatment planning of nanoparticle-assisted photothermal therapy. *Physica Medica*, *66*, 124–132. https://doi.org.10.1016/j.ejmp.2019.10.002

Batista Napotnik, T., & Miklavčič, D. (2018). In vitro electroporation detection methods – An overview. *Bioelectrochemistry*, *120*, 166–182. https://doi.org.10.1016/j.bioelechem.2017.12.005

BEX CO., LTD. (n. d.). *Electrodes for in vivo electroporation.* https://www.bexnet.co.jp/english/product/device/in-vivo/2.html

Birgersson, U., Birgersson, E., Åberg, P., Nicander, I., & Ollmar, S. (2011). Non-invasive bioimpedance of intact skin: Mathematical modeling and experiments. *Physiol Meas*, *32*, 1–18. https://doi.org.10.1088/0967-3334/32/1/001

Blazevski, A., Scheltema, M. J., Amin, A., Thompson, J. E., Lawrentschuk, N., & Stricker, P. D. (2020). Irreversible electroporation (IRE): a narrative review of the development of IRE from the laboratory to a prostate cancer treatment. *BJU Int*, *125*, 369–378. https://doi.org.10.1111/bju.14951

Böckmann, R. A., de Groot, B. L., Kakorin, S., Neumann, E., & Grubmü, H. (n.d.). Kinetics, statistics, and energetics of lipid membrane electroporation studied by molecular dynamics simulations. *Biophysical Journal*, 6076701. https://doi.org.10.1529/biophysj.108.129437

Boc, N., Edhemovic, I., Kos, B., Music, M. M., Brecelj, E., Trotovsek, B., et al. (2018). Ultrasonographic changes in the liver tumors as indicators of adequate tumor coverage with electric field for effective electrochemotherapy. *Radiol Oncol*, *52*, 383–391. https://doi.org.10.2478/raon-2018-0041

Caliper Electrodes for Electroporation Applications. (n.d.). https://www.btxonline.com/caliper-electrodes.html

Callister, W. D., & Rethwisch, D. G. (2007). *Materials science and engineering: An Introduction.* Wiley.

Calvet, C. Y., & Mir, L. M. (2016). The promising alliance of anti-cancer electrochemotherapy with immunotherapy. *Cancer and Metastasis Reviews*, *35*, 165–177. https://doi.org.10.1007/s10555-016-9615-3

Campana, L. G., di Barba, P., Dughiero, F., Forzan, M., Mognaschi, M. E., Rizzo, R., et al. (2019). Non-parallellism of needles in electroporation: 3D computational model and experimental analysis. *COMPEL - The International Journal for Computation and Mathematics in Electrical and Electronic Engineering*, *38*, 348–361. https://doi.org.10.1108/COMPEL-04-2018-0189

Casadei, R., Ricci, C., Ingaldi, C., Alberici, L., di Marco, M., Guido, A., et al. (2020). Intraoperative electrochemotherapy in locally advanced pancreatic cancer: indications, techniques and results—a single-center experience. *Updates Surg*, *72*, 1089–1096. https://doi.org.10.1007/s13304-020-00782-x

Cemazar, M., Miklavcic, D., Mir, L. M., Belehradek, J., Bonnay, M., Fourcault, D., et al. (2001). Electrochemotherapy of tumours resistant to cisplatin: A study in a murine tumour model. *Eur J Cancer*, *37*, 1166–1172. https://doi.org.10.1016/S0959-8049(01)00091-0

Cemazar, M., and Sersa, G. (2019). Recent advances in electrochemotherapy. *Bioelectricity*, *1*, 204–213. https://doi.org.10.1089/bioe.2019.0028

Charpentier, K. P., Wolf, F., Noble, L., Winn, B., Resnick, M., & Dupuy, D. E. (2011). Irreversible electroporation of the liver and liver hilum in swine. *Hpb*, *13*, 168–173. https://doi.org.10.1111/j.1477-2574.2010.00261.x

Chen, X., Ren, Z., Zhu, T., Zhang, X., Peng, Z., Xie, H., et al. (2015). electric ablation with irreversible electroporation (IRE) in Vital hepatic structures and follow-up investigation. *Sci Rep*, *5*, 1–9. https://doi.org.10.1038/srep16233

Cheng, Y., & Fu, M. (2018). Dielectric properties for non-invasive detection of normal, benign, and malignant breast tissues using microwave theories. *Thorac Cancer*, *9*, 459–465. https://doi.org.10.1111/1759-7714.12605

Choi, S. O., Kim, Y. C., Park, J. H., Hutcheson, J., Gill, H. S., Yoon, Y. K., et al. (2010). An electrically active microneedle array for electroporation. *Biomed Microdevices*, 12, 263–273. https://doi.org.10.1007/s10544-009-9381-x

Chumlea, W. C., & Guo, S. S. (1994). Bioelectrical impedance and body composition: Present status and future directions. *Nutr Rev*, *52*, 123–131. https://doi.org.10.1111/j.1753-4887.1994.tb01404.x

Condello, M., D'Avack, G., Spugnini, E. P., & Meschini, S. (2022). Electrochemotherapy: An alternative strategy for improving therapy in drug-resistant SOLID tumors. *Cancers (Basel)*, *14*, 1–16. doi: 10.3390/cancers14174341

Corovic, S., Lackovic, I., Sustaric, P., Sustar, T., Rodic, T., &Miklavcic, D. (2013). Modeling of electric field distribution in tissues during electroporation. *Biomed Eng Online*, *12*, 1–27. https://doi.org.10.1186/1475-925X-12-16

Čorović, S., Mir, L. M., & Miklavčič, D. (2012). In vivo muscle electroporation threshold determination: Realistic numerical models and in vivo experiments. *Journal of Membrane Biology*, *245*, 509–520. https://doi.org.10.1007/s00232-012-9432-8

Davalos, R. v., Bhonsle, S., &Neal, R. E. (2015). Implications and considerations of thermal effects when applying irreversible electroporation tissue ablation therapy. *Prostate*, *75*, 1114–1118. https://doi.org.10.1002/pros.22986

Davalos, R. v., Mir, L. M., and Rubinsky, B. (2005). Tissue ablation with irreversible electroporation. *Ann Biomed Eng*, 33, 223–231. https://doi.org.10.1007/s10439-005-8981-8

de Santis, V., Chen, X. L., Laakso, I., & Hirata, A. (2015). An equivalent skin conductivity model for low-frequency magnetic field dosimetry. *Biomed Phys Eng Express*, *1*. https://doi.org.10.1088/2057-1976/1/1/015201

DeBruin, K. A., & Krassowska, W. (1999). Modeling electroporation in a single cell. I. Effects of field strength and rest potential. *Biophys J*, 77, 1213–1224. https://doi.org.10.1016/S0006-3495(99)76973-0

Dermol-Černe, J., Pirc, E., & Miklavčič, D. (2020). Mechanistic view of skin electroporation–models and dosimetry for successful applications: an expert review. *Expert Opin Drug Deliv*, *17*, 689–704. https://doi.org.10.1080/17425247.2020.1745772

di Monta, G., Caracò, C., Simeone, E., Grimaldi, A. M., Marone, U., di Marzo, M., et al. (2017). Electrochemotherapy efficacy evaluation for treatment of locally advanced stage III cutaneous squamous cell carcinoma: A 22-cases retrospective analysis. *J Transl Med*, *15*, 1–8. https://doi.org.10.1186/s12967-017-1186-8

Djokic, M., Cemazar, M., Popovic, P., Kos, B., Dezman, R., Bosnjak, M., et al. (2018). Electrochemotherapy as treatment option for hepatocellular carcinoma, a prospective pilot study. *European Journal of Surgical Oncology*, *44*, 651–657. https://doi.org.10.1016/j.ejso.2018.01.090

Domanico, R., Trapasso, S., Santoro, M., Pingitore, D., and Allegra, E. (2015). Electrochemotherapy in combination with chemoradiotherapy in the treatment of oral carcinomas in advanced stages of disease: Efficacy, safety, and clinical outcomes in a small number of selected cases. *Drug Des Devel Ther*, *9*, 1185–1191. https://doi.org.10.2147/DDDT.S75752

Du, X., Wang, J., Zhou, Q., Zhang, L., Wang, S., Zhang, Z., et al. (2018). Advanced physical techniques for gene delivery based on membrane perforation. *Drug Deliv*, *25*, 1516–1525. https://doi.org.10.1080/10717544.2018.1480674

Edhemovic, I., Brecelj, E., Gasljevic, G., Marolt Music, M., Gorjup, V., Mali, B., et al. (2014). Intraoperative electrochemotherapy of colorectal liver metastases. *J Surg Oncol*, *110*, 320–327. https://doi.org.10.1002/jso.23625

Ferioli, M., Lancellotta, V., Perrone, A. M., Arcelli, A., Galuppi, A., Strigari, L., et al. (2022). Electrochemotherapy of skin metastases from malignant melanoma: a PRISMA-compliant systematic review. *Clin Exp Metastasis*, *39*, 743–755. https://doi.org.10.1007/s10585-022-10180-9

Figini, M., Wang, X., Lyu, T., Su, Z., Procissi, D., Yaghmai, V., et al. (2017). Preclinical and clinical evaluation of the liver tumor irreversible electroporation by magnetic resonance imaging. *Am J Transl Res*, *9*, 580–590.

Freeman, S. A., Wang, M. A., & Weavert, J. C. (1994). Theory of electroporation of planar bilayer membranes: Predictions of the aqueous area, change in capacitance, and pore-pore separation. *Biophys J*, *67*, 42–56.

Gabriel, C., Peyman, A., & Grant, E. H. (2009). Electrical conductivity of tissue at frequencies below 1 MHz. *Phys Med Biol*, *54*, 4863–4878. https://doi.org.10.1088/0031-9155/54/16/002

Gabriel, S., Lau, R. W., & Gabriel, C. (1996). The dielectric properties of biological tissues: III. Parametric models for the dielectric spectrum of tissues. *Phys Med Biol*, *41*, 2271–2293. https://doi.org.10.1088/0031-9155/41/11/003

Garcia, P. A., Davalos, R. v., & Miklavcic, D. (2014). A numerical investigation of the electric and thermal cell kill distributions in electroporation-based therapies in tissue. *PLoS One*, *9*(8): e103083. https://doi.org.10.1371/journal.pone.0103083

Gelker, M., Müller-Goymann, C. C., & Viöl, W. (2018). Permeabilization of human stratum corneum and full-thickness skin samples by a direct dielectric barrier discharge. *Clin Plasma Med*, *9*, 34–40. https://doi.org.10.1016/j.cpme.2018.02.001

Ghossein, R. (2010). Encapsulated malignant follicular cell-derived thyroid tumors. *Endocr Pathol*, *21*, 212–218. https://doi.org.10.1007/s12022-010-9141-8

Gilbert, R. A., Jaroszeski, M. J., & Heller, R. (1997). Novel electrode designs for electrochemotherapy. *Biochim Biophys Acta Gen Subj*, *1334*, 9–14. https://doi.org.10.1016/S0304-4165(96)00119-5

Glickman, Y. A., Filo, O., David, M., Yayon, A., Topaz, M., Zamir, B., et al. (2003). Electrical impedance scanning: A new approach to skin cancer diagnosis. *Skin Research and Technology*, *9*, 262–268. https://doi.org.10.1034/j.1600-0846.2003.00022.x

Granata, V., de Lutio di Castelguidone, E., Fusco, R., Catalano, O., Piccirillo, M., Palaia, R., et al. (2016). Irreversible electroporation of hepatocellular carcinoma: preliminary report on the diagnostic accuracy of magnetic resonance, computer tomography, and contrast-enhanced ultrasound in evaluation of the ablated area. *Radiologia Medica*, *121*, 122–131. https://doi.org.10.1007/s11547-015-0582-5

Granata, V., Fusco, R., D'alessio, V., Giannini, A., Venanzio Setola, S., Belli, A., et al. (2021). Electroporation-based treatments in minimally invasive percutaneous, laparoscopy and endoscopy procedures for treatment of deep-seated tumors. *Eur Rev Med Pharmacol Sci*, *25*, 3536–3545. https://doi.org.10.26355/eurrev_202105_25836

Gun, L., Ning, D., & Liang, Z. (2017). Effective Permittivity of Biological Tissue: Comparison of Theoretical Model and Experiment. *Math Probl Eng*, 2017. https://doi.org.10.1155/2017/7249672

Guo, F., Deng, H., Qian, K., & Li, X. (2022). Characterization of dispersion and anisotropic-conductivity in tissue model during electroporation pulses. *Bioelectrochemistry, 144*, 108029. https://doi.org.10.1016/j.bioelechem.2021.108029

Guo, F., Yao, C., Li, C., Mi, Y., Peng, Q., & Tang, J. (2014). In vivo evidences of nanosecond pulsed electric fields for melanoma malignancy treatment on tumor-bearing BALB/c nude mice. *Technol Cancer Res Treat, 13*, 337–344. https://doi.org.10.7785/tcrt.2012.500385

Guo, S., Donate, A., Basu, G., Lundberg, C., Heller, L., and Heller, R. (2011). Electro-gene transfer to skin using a noninvasive multielectrode array. *Journal of Controlled Release, 151*, 256–262. https://doi.org.10.1016/j.jconrel.2011.01.014

Guo, Y., Dreier, J. R., Cao, J., Du, H., Granter, S. R., & Kwiatkowski, D. J. (2016). Analysis of a mouse skin model of tuberous sclerosis complex. *PLoS One, 11*, 1–13. https://doi.org.10.1371/journal.pone.0167384

Gursoy, G., Esmekaya, M. A., & Cicek, Z. (2023). Treatment of cervical cancer by electrochemotherapy with bleomycin, cisplatin, and calcium: an in vitro experimental study. *Medical Oncology, 40*, 1–16. https://doi.org.10.1007/s12032-022-01921-7

Haemmerich, D., Schutt, D. J., Wright, A. W., Webster, J. G., & Mahvi, D. M. (2009). Electrical conductivity measurement of excised human metastatic liver tumours before and after thermal ablation. *Physiol Meas, 30*, 459–466. https://doi.org.10.1088/0967-3334/30/5/003

Hayes, A. W., Thomas, J. A., & Gardner, D. E. (n. d.). *Series Editors Toxicology of the*.

Heller, L. C., Jaroszeski, M. J., Coppola, D., Mccray, A. N., Hickey, J., & Heller, R. (2007). Optimization of cutaneous electrically mediated plasmid DNA delivery using novel electrode. *Gene Ther, 14*, 275–280. https://doi.org.10.1038/sj.gt.3302867

Heller, R., Cruz, Y., Heller, L. C., Gilbert, R. A., & Jaroszeski, M. J. (2010). Electrically mediated delivery of plasmid DNA to the skin, using a multielectrode array. *Hum Gene Ther, 21*, 357–362. https://doi.org. 10.1089/hum.2009.065

Hershkovich, H. S., Urman, N., Yesharim, O., Naveh, A., & Bomzon, Z. (2019). The dielectric properties of skin and their influence on the delivery of tumor treating fields to the torso: A study combining in vivo measurements with numerical simulations. *Phys Med Biol, 64*(18). https://doi.org.10.1088/1361-6560/ab33c6

Hew, J., Solon-Biet, S. M., McMahon, A. C., Ruohonen, K., Raubenheimer, D., Ballard, J. W. O., et al. (2016). The effects of dietary macronutrient balance on skin structure in aging male and female mice. *PLoS One, 11*, 1–15. https://doi.org.10.1371/journal.pone.0166175

Hibino, M., Itoh, H., & Kinosita, K. (1993). Time courses of cell electroporation as revealed by submicrosecond imaging of transmembrane potential. *Biophys J, 64*, 1789–1800. https://doi.org.10.1016/S0006-3495(93)81550-9

Hsiao, C. Y., & Huang, K. W. (2017). Irreversible Electroporation: A Novel Ultrasound-guided Modality for Non-thermal Tumor Ablation. *J Med Ultrasound*, *25*, 195–200. https://doi.org.10.1016/j.jmu.2017.08.003

Huang, D., Zhao, D., Wang, X., Li, C., Yang, T., Du, L., et al. (2018). Efficient delivery of nucleic acid molecules into skin by combined use of microneedle roller and flexible interdigitated electroporation array. *Theranostics*, *8*, 2361–2376. https://doi.org.10.7150/thno.23438

Huclova, S., Erni, D., & Fröhlich, J. (2012). Modelling and validation of dielectric properties of human skin in the MHz region focusing on skin layer morphology and material composition. *J Phys D Appl Phys*, *45*. https://doi.org.10.1088/0022-3727/45/2/025301

IGEA Medical. (n. d.). *Electrodes.* https://www.igeamedical.com/en/electrochemotherapy/products/electrodes

IGEA Medical. (n. d.). *Fixed Electrodes – EPS Series.* https://www.igeamedical.com/en/electrochemotherapy/products/electrodes/fixed-eps-series

Isobe, K., Shimizu, T., Nikaido, T., & Takaoka, K. (2004). Low-voltage electrochemotherapy with low-dose methotrexate enhances survival in mice with osteosarcoma. *Clin Orthop Relat Res*, *426*, 226–231. https://doi.org.10.1097/01.blo.0000138962.42433.db

Ivorra, A., Al-Sakere, B., Rubinsky, B., & Mir, L. M. (2008). Use of conductive gels for electric field homogenization increases the antitumor efficacy of electroporation therapies. *Phys Med Biol*, *53*, 6605–6618. https://doi.org.10.1088/0031-9155/53/22/020

Ivorra, A., Al-Sakere, B., Rubinsky, B., & Mir, L. M. (2009). In vivo electrical conductivity measurements during and after tumor electroporation: Conductivity changes reflect the treatment outcome. *Phys Med Biol*, *54*, 5949–5963. https://doi.org.10.1088/0031-9155/54/19/019

Izzo, F., Ionna, F., Granata, V., Albino, V., Patrone, R., Longo, F., et al. (2020). New deployable expandable electrodes in the electroporation treatment in a pig model: A feasibility and usability preliminary study. *Cancers (Basel)*, *12*. https://doi.org.10.3390/cancers12020515

Kinosita, K., & Tsong, Y. (1977). Voltage-induced pore formation and hemolysis of human erythrocytes. *Biochim Biophys Acta*, *471*, 227–242.

Korohoda, W., Grys, M., & Madeja, Z. (2013). Reversible and irreversible electroporation of cell suspensions flowing through a localized DC electric field. *Cell Mol Biol Lett*, *18*, 102–119. https://doi.org.10.2478/s11658-012-0042-3

Kotnik, T., Pucihar, G., & Miklavčič, D. (2010). Induced transmembrane voltage and its correlation with electroporation- mediated molecular transport. *Journal of Membrane Biology*, *236*, 3–13. https://doi.org.10.1007/s00232-010-9279-9

Kotnik, T., Rems, L., Tarek, M., & Miklavcic, D. (2019). Membrane Electroporation and Electropermeabilization: Mechanisms and Models. *Annu Rev Biophys*, *48*, 63–91. https://doi.org.10.1146/annurev-biophys-052118-115451

Kranjc, M., Kranjc, S., Bajd, F., Serša, G., Serša, I., & Miklavčič, D. (2017). Predicting irreversible electroporation-induced tissue damage by means of magnetic resonance electrical impedance tomography. *Sci Rep*, *7*, 1–10. https://doi.org.10.1038/s41598-017-10846-5

Kranjc, S., Kranjc, M., Scancar, J., Jelenc, J., Sersa, G., & Miklavcic, D. (2016). Electrochemotherapy by pulsed electromagnetic field treatment (PEMF) in mouse melanoma B16F10 in vivo. *Radiol Oncol*, *50*, 39–48. https://doi.org.10.1515/raon-2016-0014

Labarbera, N., and Drapaca, C. (2017). Anistropically varying conductivity in irreversible electroporation simulations. *Theor Biol Med Model*, *14*, 1–12. https://doi.org.10.1186/s12976-017-0065-6

Langus, J., Kranjc, M., Kos, B., Šuštar, T., & Miklavčič, D. (2016). Dynamic finite-element model for efficient modelling of electric currents in electroporated tissue. *Sci Rep*, 6. https://doi.org.10.1038/srep26409

Larkin, J. O., Collins, C. G., Aarons, S., Tangney, M., Whelan, M., O'Reily, S., et al. (2007). Electrochemotherapy: Aspects of preclinical development and early clinical experience. *Ann Surg*, *245*, 469–479. https://doi.org.10.1097/01.sla.0000250419.36053.33

Laufer, S., Ivorra, A., Reuter, V. E., Rubinsky, B., & Solomon, S. B. (2010). Electrical impedance characterization of normal and cancerous human hepatic tissue. *Physiol Meas*, *31*, 995–1009. https://doi.org.10.1088/0967-3334/31/7/009

Lee, E. W., Loh, C. T., & Kee, S. T. (2007). Imaging guided percutaneous irreversible electroporation: Ultrasound and immunohistological correlation. *Technol Cancer Res Treat*, *6*, 287–293. https://doi.org.10.1177/153303460700600404

Lee, J. M., Choi, H. S., Chun, H. J., Kim, E. S., Keum, B., Seo, Y. S., et al. (2019). EUS-guided irreversible electroporation using endoscopic needle-electrode in porcine pancreas. *Surg Endosc*, *33*, 658–662. https://doi.org.10.1007/s00464-018-6425-4

LEROY Biotech. (n.d.). *Accessories ElectroVet*. https://www.leroybiotech.com/electrovet-ez/accessories/

Li, C., Zhu, H., Zong, X., Wang, X., Gui, S., Zhao, P., et al. (2020). Experience of trans-nasal endoscopic surgery for pituitary tumors in a single center in China: Surgical results

in a cohort of 2032 patients, operated between 2006 and 2018. *Clin Neurol Neurosurg*, *197*, 106176. https://doi.org.10.1016/j.clineuro.2020.106176

Li, Q., Gao, X., Zhang, Y., Han, X., Li, Z., Zhang, Y., et al. (2021). Magnetic anchoring and guidance-assisted endoscopic irreversible electroporation for gastric mucosal ablation: a preclinical study in canine model. *Surg Endosc*, *35*, 5665–5674. https://doi.org.10.1007/s00464-020-08245-5

Li, S. (2008). *Electroporation Protocols*.

Litwin, M. S., and Tan, H. J. (2017). The diagnosis and treatment of prostate cancer: A review. *JAMA - Journal of the American Medical Association*, *317*, 2532–2542. https://doi.org.10.1001/jama.2017.7248

Liu, F., and Huang, L. (2002). A syringe electrode device for simultaneous injection of DNA and electrotransfer. *Molecular Therapy*, *5*, 323–328. https://doi.org.10.1006/mthe.2002.0540

Lladser, A., Ljungberg, K., Tufvesson, H., Tazzari, M., Roos, A. K., Quest, A. F. G., et al. (2010). Intradermal DNA electroporation induces survivin-specific CTLs, suppresses angiogenesis and confers protection against mouse melanoma. *Cancer Immunology, Immunotherapy*, *59*, 81–92. https://doi.org.10.1007/s00262-009-0725-4

Lopes, L. B., Pintarelli, G. B., dos Santos, C. S. F., & Suzuki, D. O. H. (2021). Computer optimization of conductive gels for electrochemotherapy. *Med Eng Phys*, *98*, 133–139. https://doi.org.10.1016/j.medengphy.2021.10.011

IT'IS Foundation. (n.d.). *Low Frequency (Conductivity)*. https://itis.swiss/virtual-population/tissue-properties/database/low-frequency-conductivity/

Lu, F., Wang, C., Zhao, R., Du, L., Fang, Z., Guo, X., et al. (2018). Review of stratum corneum impedance measurement in non-invasive penetration application. *Biosensors (Basel)*, *8*. https://doi.org.10.3390/bios8020031

Maiorano, N. A., & Mallamaci, A. (2009). Promotion of embryonic cortico-cerebral neuronogenesis by miR-124. *Neural Development*, *4*, 40. https://doi.org.10.1186/1749-8104-4-40

Maruyama, H., Ataka, K., Higuchi, N., Sakamoto, F., Gejyo, F., & Miyazaki, J. (2001). Skin-targeted gene transfer using in vivo electroporation. *Gene Ther*, *8*, 1808–1812. www.nature.com/gt

Mazères, S., Sel, D., Golzio, M., Pucihar, G., Tamzali, Y., Miklavcic, D., et al. (2008). Non invasive contact electrodes for in vivo localized cutaneous electropulsation and associated drug and nucleic acid delivery. *J Control Release*, *134*(2), 125–131. https://doi.org.10.1016/j.jconrel.2008.11.003

McKinnon, K. M. (2018). Flow cytometry: An overview. *Curr Protoc Immunol*, 5.1.1–5.1.11. https://doi.org.10.1002/cpim.40

Miklavčič, D. (2017). Handbook of Electroporation. *Handbook of Electroporation*, 1–4, 1–2998. https://doi.org.10.1007/978-3-319-32886-7

Miklavčič, D., Beravs, K., Šemrov, D., Čemažar, M., Demšar, F., and Serša, G. (1998). The importance of electric field distribution for effective in vivo electroporation of tissues. *Biophys J*, *74*, 2152–2158. https://doi.org.10.1016/S0006-3495(98)77924-X

Miklavčič, D., Pavšelj, N., & Hart, F. X. (2006). Electric Properties of Tissues. *Wiley Encyclopedia of Biomedical Engineering*, 1–12. https://doi.org.10.1002/9780471740360.ebs0403

Miklavcic, D., Snoj, M., Zupanic, A., Kos, B., Cemazar, M., Kropivnik, M., et al. (2010). Towards treatment planning and treatment of deep-seated solid tumors by electrochemotherapy. *BioMedical Engineering OnLine*, *9*, 10. http://www.biomedical-engineering-online.com/content/9/1/10

Monteiro-Riviere, N. A., & Riviere, J. E. (1999). Chapter 18 - Skin. *Toxicology*, 439–457. https://doi.org/10.1016/B978-012473270-4/50077-8

Moreta-Martínez, R., Rubio-Pérez, I., García-Sevilla, M., García-Elcano, L., & Pascau, J. (2022). Evaluation of optical tracking and augmented reality for needle navigation in sacral nerve stimulation. *Comput Methods Programs Biomed*, *224*. https://doi:10.1016/j.cmpb.2022.106991

Nagy, J. A., DiDonato, C. J., Rutkove, S. B., & Sanchez, B. (2019). Permittivity of ex vivo healthy and diseased murine skeletal muscle from 10 kHz to 1 MHz. *Sci Data*, *6*. https://doi.org.10.1038/s41597-019-0045-2

Neal II, R. E., Cheung, W., Kavnoudias, H., & Thomson, K. R. (2012). Spectrum of imaging and characteristics for liver tumors treated with irreversible electroporation. *J Biomed Sci Eng*, *05*, 813–818. https://doi.org.10.4236/jbise.2012.512a102

Neal, R. E., Millar, J. L., Kavnoudias, H., Royce, P., Rosenfeldt, F., Pham, A., et al. (2014). In vivo characterization and numerical simulation of prostate properties for non-thermal irreversible electroporation ablation. *Prostate*, *74*, 458–468. https://doi.org.10.1002/pros.22760

Neal, R. E., Singh, R., Hatcher, H. C., Kock, N. D., Torti, S. V., & Davalos, R. V. (2010). Treatment of breast cancer through the application of irreversible electroporation using a novel minimally invasive single needle electrode. *Breast Cancer Res Treat*, *123*, 295–301. https://doi.org.10.1007/s10549-010-0803-5

Needle Array Electrodes for BTX AgilePulse In Vivo (n. d.). https://www.btxonline.com/needle-array-electrodes-for-agilepulse-in-vivo.html

O'Brien, T. J., Passeri, M., Lorenzo, M. F., Sulzer, J. K., Lyman, W. B., Swet, J. H., et al. (2019). Experimental high-frequency irreversible electroporation using a single-needle delivery approach for nonthermal pancreatic ablation in vivo. *Journal of Vascular and Interventional Radiology*, *30*, 854-862.e7. https://doi.org.10.1016/j.jvir.2019.01.032.

Online Materials Information Resource - MatWeb (n. d.). https://www.matweb.com/index.aspx

Partridge, B. R., O'Brien, T. J., Lorenzo, M. F., Coutermarsh-Ott, S. L., Barry, S. L., Stadler, K., et al. (2020). High-Frequency Irreversible Electroporation for Treatment of Primary Liver Cancer: A Proof-of-Principle Study in Canine Hepatocellular Carcinoma. *Journal of Vascular and Interventional Radiology, 31,* 482–491.e4. https://doi.org.10.1016/j.jvir.2019.10.015

Pavliha, D., Kos, B., Županič, A., Marčan, M., Serša, G., & Miklavčič, D. (2012). Patient-specific treatment planning of electrochemotherapy: Procedure design and possible pitfalls. *Bioelectrochemistry, 87,* 265–273. https://doi.org.10.1016/j.bioelechem.2012.01.007

Pavšelj, N., Bregar, Z., Cukjati, D., Batiuskaite, D., Mir, L. M., & Miklavčič, D. (2005). The course of tissue permeabilization studied on a mathematical model of a subcutaneous tumor in small animals. *IEEE Trans Biomed Eng, 52,* 1373–1381. https://doi.org.10.1109/TBME.2005.851524.

Pavšelj, N., and Miklavčič, D. (2008a). Numerical modeling in electroporation-based biomedical applications. *Radiol Oncol, 42,* 159–168. https://doi.org.10.2478/v10019-008-0008-2

Pavšelj, N., and Miklavčič, D. (2008b). Numerical models of skin electropermeabilization taking into account conductivity changes and the presence of local transport regions. *IEEE Transactions on Plasma Science, 36,* 1650–1658. https://doi.org.10.1109/TPS.2008.928715

Pavšelj, N., Préat, V., & Miklavčič, D. (2007). A numerical model of skin electropermeabilization based on in vivo experiments. *Ann Biomed Eng, 35,* 2138–2144. https://doi.org.10.1007/s10439-007-9378-7

Pichi, B., Pellini, R., de Virgilio, A., & Spriano, G. (2018). Electrochemotherapy: A well-accepted palliative treatment by patients with head and neck tumours. *Acta Otorhinolaryngologica Italica, 38,* 181–187. https://doi.org.10.14639/0392-100X-1262

Pliquett, U. F., Vanbever, R., Preat, V., & Weaver, J. C. (1998). Local transport regions (LTRs) in human stratum corneum due to long and short "high voltage" pulses. *Bioelectrochemistry and Bioenergetics, 47,* 151–161. https://doi.org.10.1016/S0302-4598(98)00180-9

Potočnik, T., Miklavčič, D., & Maček Lebar, A. (2021). Gene transfer by electroporation with high frequency bipolar pulses in vitro. *Bioelectrochemistry, 140,* 34–36. https://doi.org.10.1016/j.bioelechem.2021.107803

Probst, U., Fuhrmann, I., Beyer, L., and Wiggermann, P. (2018). Electrochemotherapy as a new modality in interventional oncology: A review. *Technol Cancer Res Treat, 17,* 1–12. https://doi.org.10.1177/1533033818785329

Pucihar, G., Kotnik, T., Miklavčič, D., & Teissié, J. (2008). Kinetics of transmembrane transport of small molecules into electropermeabilized cells. *Biophys J, 95*, 2837–2848. https://doi.org.10.1529/biophysj.108.135541

Pucihar, G., Krmelj, J., Reberˇ, M., Napotnik, T. B., & Miklavčič, D. (2011). Equivalent pulse parameters for electroporation. *IEEE Transactions onBiomedical Engineering*, *58*(11), 3279–3288

Raja, M. K., Raymer, G. H., Moran, G. R., Marsh, G., & Thompson, R. T. (2006). Changes in tissue water content measured with multiple-frequency bioimpedance and metabolism measured with31P-MRS during progressive forearm exercise. *J Appl Physiol, 101*, 1070–1075. https://doi.org.10.1152/japplphysiol.01322.2005.Reberšek, M., Čorović, S., Serša, G., and Miklavčič, D. (2008). Electrode commutation sequence for honeycomb arrangement of electrodes in electrochemotherapy and corresponding electric field distribution. *Bioelectrochemistry, 74*, 26–31. https://doi.org.10.1016/j.bioelechem.2008.03.001

Rembiałkowska, N., Novickij, V., Baczyńska, D., Dubińska-Magiera, M., Saczko, J., Rudno-Rudzińska, J., et al. (2022). Micro-and Nanosecond Pulses Used in Doxorubicin Electrochemotherapy in Human Breast and Colon Cancer Cells with Drug Resistance. *Molecules, 27*. https://doi.org.10.3390/molecules27072052

Ritter, A., Bruners, P., Isfort, P., Barabasch, A., Pfeffer, J., Schmitz, J., et al. (2018). Electroporation of the Liver: More Than 2 Concurrently Active, Curved Electrodes Allow New Concepts for Irreversible Electroporation and Electrochemotherapy. *Technol Cancer Res Treat, 17*, 1–8. https://doi.org.10.1177/1533033818809994

Roos, A. K., Eriksson, F., Walters, D. C., Pisa, P., & King, A. D. (2009). Optimization of skin electroporation in mice to increase tolerability of DNA vaccine delivery to patients. *Molecular Therapy, 17*, 1637–1642. https://doi.org.10.1038/mt.2009.120

Roos, A. K., Moreno, S., Leder, C., Pavlenko, M., King, A., & Pisa, P. (2006). Enhancement of cellular immune response to a prostate cancer DNA vaccine by intradermal electroporation. *Molecular Therapy, 13*, 320–327. https://doi.org.10.1016/j.ymthe.2005.08.005

Sano, M. B., DeWitt, M. R., Teeter, S. D., & Xing, L. (2018). Optimization of a single insertion electrode array for the creation of clinically relevant ablations using high-frequency irreversible electroporation. *Comput Biol Med, 95*, 107–117. https://doi.org.10.1016/j.compbiomed.2018.02.009

Santamaría, L., Alonso, L., Ingelmo, I., Pozuelo, J. M., & Rodriguez, R. (2007). The human prostate. *Adv Anat Embryol Cell Biol, 194*, 2–11. https://doi.org.10.1007/978-3-540-69816-6_2

Sedlar, A., Dolinsek, T., Markelc, B., Prosen, L., Kranjc, S., Bosnjak, M., et al. (2012). Potentiation of electrochemotherapy by intramuscular IL-12 gene electrotransfer in murine sarcoma and carcinoma with different immunogenicity. *Radiol Oncol, 46*, 302–311. https://doi.org..2478/v10019-012-0044-9

Sersa, G., Miklavcic, D., Cemazar, M., Rudolf, Z., Pucihar, G., & Snoj, M. (2008). Electrochemotherapy in treatment of tumours. *European Journal of Surgical Oncology, 34*, 232–240. https://doi.org.10.1016/j.ejso.2007.05.016

Sharawi, A. A., Hamoda, E. A., & Karrar, A. A. (2016). Evaluation of a numerical model using COMSOL multi-physics package. In *Proceedings - 2015 5th International Conference on e-Learning, ECONF 2015* (pp. 42–46). https://doi.org.10.1109/ECONF.2015.62

Shi, W., Shi, T., Chen, Z., Lin, J., Jia, X., Wang, J., et al. (2010). Generation of sp3111 transgenic RNAi mice via permanent integration of small hairpin RNAs in repopulating spermatogonial cells in vivo. *Acta Biochim Biophys Sin (Shanghai), 42*, 116–121. https://doi.org.10.1093/abbs/gmp110

Suzuki, D. O. H., Marques, C. M. G., & Rangel, M. M. M. (2016). Conductive Gel Increases the Small Tumor Treatment With Electrochemotherapy Using Needle Electrodes. *Artif Organs, 40*, 705–711. https://doi.org.10.1111/aor.12631

Szlasa, W., Kiełbik, A., Szewczyk, A., Novickij, V., Tarek, M., Łapińska, Z., et al. (2021). Atorvastatin modulates the efficacy of electroporation and calcium electrochemotherapy. *Int J Mol Sci, 22*. https://doi.org.10.3390/IJMS222011245

Tellado, M., Michinski, S., Impellizeri, J., Marshall, G., Signori, E., & Maglietti, F. (2022). Electrochemotherapy using thin-needle electrode improves recovery in feline nasal planum squamous cell carcinoma - a translational model. *Cancer Drug Resistance, 5*, 595–611. https://doi.org.10.20517/cdr.2022.24

Tozon, N., Pavlin, D., Sersa, G., Dolinsek, T., & Cemazar, M. (2014). Electrochemotherapy with intravenous bleomycin injection: An observational study in superficial squamous cell carcinoma in cats. *J Feline Med Surg, 16*, 291–299. https://doi.org.10.1177/1098612X13507071

Tremble, L. F., O'Brien, M. A., Soden, D. M., & Forde, P. F. (2019). Electrochemotherapy with cisplatin increases survival and induces immunogenic responses in murine models of lung cancer and colorectal cancer. *Cancer Lett, 442*, 475–482. https://doi.org.10.1016/j.canlet.2018.11.015

Tsai, B., Xue, H., Birgersson, E., Ollmar, S., & Birgersson, U. (2019). Dielectrical properties of living epidermis and dermis in the frequency range from 1 kHz to 1 MHz. *J Electr Bioimpedance, 10*, 14–23. https://doi.org.10.2478/joeb-2019-0003.

Tweezertrodes Electrodes for In Vivo and In Utero Electroporation Applications. (n.d.). https://www.btxonline.com/tweezertrodes-electrodes.html

Ursic, K., Kos, S., Kamensek, U., Cemazar, M., Miceska, S., Markelc, B., et al. (2021). Potentiation of electrochemotherapy effectiveness by immunostimulation with IL-12 gene electrotransfer in mice is dependent on tumor immune status. *Journal of Controlled Release, 332*, 623–635. https://doi.org.10.1016/j.jconrel.2021.03.009

van den Boogaard, W. M. C., Komninos, D. S. J., & Vermeij, W. P. (2022). Chemotherapy Side-Effects: Not All DNA Damage Is Equal. *Cancers (Basel), 14*, 1–27. https://doi.org.10.3390/cancers14030627

van den Bos, W., de Bruin, D. M., Jurhill, R. R., Savci-Heijink, C. D., Muller, B. G., Varkarakis, I. M., et al. (2016). The correlation between the electrode configuration and histopathology of irreversible electroporation ablations in prostate cancer patients. *World J Urol, 34*, 657–664. https://doi.org.10.1007/s00345-015-1661-x

Ventrelli, L., Marsilio Strambini, L., & Barillaro, G. (2015). Microneedles for Transdermal Biosensing: Current Picture and Future Direction. *Adv Healthc Mater, 4*, 2606–2640. https://doi.org.10.1002/adhm.201500450

Vižintin, A., Marković, S., Ščančar, J., & Miklavčič, D. (2021). Electroporation with nanosecond pulses and bleomycin or cisplatin results in efficient cell kill and low metal release from electrodes. *Bioelectrochemistry, 140*. https://doi.org.10.1016/j.bioelechem.2021.107798

VOSviewer. (n. d.). *Visualizing scientific landscapes*. https://www.vosviewer.com/

Wake, K., Sasaki, K., & Watanabe, S. (2016). Conductivities of epidermis, dermis, and subcutaneous tissue at intermediate frequencies. *Phys Med Biol, 61*, 4376–4389. https://doi.org.1088/0031-9155/61/12/4376

Wang, J. R., Sun, B. Y., Wang, H. X., Pang, S., Xu, X., & Sun, Q. (2014). Experimental study of dielectric properties of human lung tissue in vitro. *J Med Biol Eng, 34*, 598–604. https://doi.org.10.5405/jmbe.1774

Wang, S., Zhang, C., Zhang, L., Li, J., Huang, Z., & Lu, S. (2008). The relative immunogenicity of DNA vaccines delivered by the intramuscular needle injection, electroporation and gene gun methods. *Vaccine, 26*, 2100–2110. https://doi.org.10.1016/j.vaccine.2008.02.033

Weaver, J. C. (2000). Electroporation of cells and tissues. *IEEE Transactions on Plasma Science, 28*, 24–33. https://doi.org.10.1109/27.842820

Wei, J. C. J., Edwards, G. A., Martin, D. J., Huang, H., Crichton, M. L., & Kendall, M. A. F. (2017). Allometric scaling of skin thickness, elasticity, viscoelasticity to mass for micro-medical device translation: From mice, rats, rabbits, pigs to humans. *Sci Rep, 7*, 1–17. https://doi.org.10.1038/s41598-017-15830-7

Wei, Z., Huang, Y., Zhao, D., Hu, Z., Li, Z., & Liang, Z. (2015). A Pliable Electroporation Patch (ep-Patch) for Efficient Delivery of Nucleic Acid Molecules into Animal Tissues with Irregular Surface Shapes. *Sci Rep, 5*, 1–9. https://doi.org.10.1038/srep07618

Wichtowski, M., & Murawa, D. (2018). Electrochemotherapy in the treatment of melanoma. *Wspolczesna Onkologia, 22*, 8–13. https://doi.org.10.5114/wo.2018.74387

Wichtowski, M., Murawa, D., Kulcenty, K., & Zaleska, K. (2017). Electrochemotherapy in Breast Cancer-Discussion of the Method and Literature Review. *Breast Care, 12*, 409–414. https://doi.org.10.1159/000479954

Wu, M., Rubin, A. E., Dai, T., Schloss, R., Usta, O. B., Golberg, A., et al. (2021). High-Voltage, Pulsed Electric Fields Eliminate Pseudomonas aeruginosa Stable Infection in a Mouse Burn Model. *Adv Wound Care (New Rochelle), 10*, 477–489. https://doi.org.10.1089/wound.2019.1147

Xia, D., Jin, R., Byagathvalli, G., Yu, H., Ye, L., Lu, C. Y., et al. (2021). An ultra-low-cost electroporator with microneedle electrodes (ePatch) for SARS-CoV-2 vaccination. *Proc Natl Acad Sci U S A, 118*. https://doi.org.10.1073/pnas.2110817118

Yamamoto, T., and Yamamoto, Y. (1976). Dielectric constant and resistivity of epidermal stratum corneum. *Med Biol Eng, 14*, 494–500. https://doi.org.10.1007/BF02478045

Yamazaki, N., Watanabe, H., Lu, X., Isobe, Y., Kobayashi, Y., Miyashita, T., et al. (2013). The relation between temperature distribution for lung RFA and electromagnetic wave frequency dependence of electrical conductivity with changing a lung's internal air volumes. In *Proceedings of the Annual International Conference of the IEEE Engineering in Medicine and Biology Society, EMBS* (pp. 386–391). https://doi.org.10.1109/EMBC.2013.6609518

Yan, K., Todo, H., & Sugibayashi, K. (2010). Transdermal drug delivery by in-skin electroporation using a microneedle array. *Int J Pharm, 397*, 77–83. https://doi.org.10.1016/j.ijpharm.2010.06.052

Yang, T., Huang, D., Li, C., Zhao, D., Li, J., Zhang, M., et al. (2021). Rolling microneedle electrode array (RoMEA) empowered nucleic acid delivery and cancer immunotherapy. *Nano Today, 36*, 101017. https://doi.org.10.1016/j.nantod.2020.101017

Yao, C., Dong, S., Zhao, Y., Lv, Y., Liu, H., Gong, L., et al. (2017). Bipolar microsecond pulses and insulated needle electrodes for reducing muscle contractions during irreversible electroporation. *IEEE Trans Biomed Eng, 64*, 2924–2937. https://doi.org.10.1109/TBME.2017.2690624

Ye, Y., Luan, X., Zhang, L., Zhao, W., Cheng, J., Li, M., et al. (2020). Single-cell electroporation with real-time impedance assessment using a constriction microchannel. *Micromachines (Basel)*, 11. https://doi.org.10.3390/MI11090856

Yu, K., Shao, Q., Ashkenazi, S., Bischof, J. C., and He, B. (2016). In Vivo electrical conductivity contrast imaging in a mouse model of cancer using high-frequency magnetoacoustic tomography with magnetic induction (hfMAT-MI). *IEEE Trans Med Imaging, 35*, 2301–2311. https://doi.org.10.1109/TMI.2016.2560146

Zager, Y., Kain, D., Landa, N., Leor, J., and Maor, E. (2016). Optimization of irreversible electroporation protocols for in-vivo myocardial decellularization. *PLoS One* 11, 1–15. https://doi.org.10.1371/journal.pone.0165475

Zhang, L., Getz, S. A., & Bordey, A. (2022). Dual in Utero Electroporation in Mice to Manipulate Two Specific Neuronal Populations in the Developing Cortex. *Front Bioeng Biotechnol*, *9*, 1–9. https://doi.org.10.3389/fbioe.2021.814638

Zhang, X., & He, B. (2010). Imaging electric properties of human brain tissues by B1 mapping: A simulation study. *J Phys Conf Ser*, *224*, 474–481. https://doi.org.10.1088/1742-6596/224/1/012077

Zhao, Y., Zheng, S., Beitel-White, N., Liu, H., Yao, C., & Davalos, R. V. (2020). Development of a multi-pulse conductivity model for liver tissue treated with pulsed electric fields. *Front Bioeng Biotechnol*, *8*, 1–11. https://doi.org.10.3389/fbioe.2020.00396

Zimmermann, C. E., Faesser, H. A., Gassling, V., & Wiltfang, J. (2021). The role of electrochemotherapy with intratumoral bleomycin for early tongue carcinoma. *Acta Otolaryngol*, *141*, 424–431. https://doi.org.10.1080/00016489.2020.1871511

List of Scientific Publications by the Author on the Topic of the Dissertation

Papers in the Reviewed Scientific Journals

Novickij, V., Malyško, V., Želvys, A., Balevičiūtė, A., Zinkevičienė, A., Novickij, J., & Girkontaitė, I. (2020). Electrochemotherapy using doxorubicin and nanosecond electric field pulses: a pilot in vivo study. Molecules, 25(20), 4601DOI: https://doi.org/10.3390/molecules25204601 (ISI Web of Science)

Novickij, V., Zinkevičienė, A., Malyško, V., Novickij, J., Kulbacka, J., Rembialkowska, N., & Girkontaitė, I. (2020). Bioluminescence as a sensitive electroporation indicator in sub-microsecond and microsecond range of electrical pulses. Journal of Photochemistry and Photobiology B: Biology, 213, 112066. DOI: https://doi.org/10.1016/j.jphotobiol.2020.112066 (ISI Web of Science)

Novickij, V., Balevičiūtė, A., Malyško, V., Želvys, A., Radzevičiūtė, E., Kos, B., ... & Girkontaitė, I. (2021). Effects of time delay between unipolar pulses in high frequency nano-electrochemotherapy. IEEE Transactions on Biomedical Engineering, 69(5), 1726–1732. DOI: http://doi.org/10.1109/TBME.2021.3129176 (ISI Web of Science)

Perminaitė, E., Zinkevičienė, A., Malyško-Ptašinskė, V., Radzevičiūtė, E., Novickij, J., Girkontaitė, I., & Novickij, V. (2023). Killing bacteria using acetic acid and nanosecond pulsed electric fields—an in vivo superficial infection model study and immune

response. Applied Sciences, 13(2), 836. DOI: https://doi.org/10.3390/app13020836 (ISI Web of Science)

Malyško-Ptašinskė, V., Staigvila, G., & Novickij, V. Invasive and non-invasive electrodes for successful drug and gene delivery in electroporation-based treatments. Frontiers in Bioengineering and Biotechnology, 10, 2479. DOI: https://doi.org/10.3389/fbioe.2022.1094968 (ISI Web of Science)

Papers in Other Editions

Malyško, V., Novickij, V., Želvys, A., Balevičiūtė, A., Girkontaitė, I., & Zinkevičienė, A. (2021, May). Measurement and Evaluation of Electric Pulse Parameters to Improve Efficacy of Electrochemotherapy. In 13th International Conference on Measurement (pp. 127–129). IEEE. DOI: https://doi.org/10.23919/Measurement52780.2021.9446780

Summary in Lithuanian

Įvadas

Problemos formulavimas

Elektroporacijos reiškinys yra naudojamas įvairiose srityse, įskaitant biomedicininį gydymą, pvz., elektrochemoterapiją, genų pernašą ar audinių abliaciją. Elektroporacija pagrįstų technologijų, naudojamų biomedicinoje, efektyvumas tiesiogiai priklauso nuo elektros impulsų parametrų, dielektrinių audinių savybių ir ypač nuo erdvinio impulsinio elektrinio lauko pasiskirstymo audiniuose. Pagrindinis elementas paskirstant ir kontroliuojant elektrinio lauko pasiskirstymą audinyje yra elektrodas. Todėl nuolat atliekama naujų elektrodų struktūrų paieška.

Biologinių audinių elektroporacija vis dar yra gana sudėtinga dėl unikalios vėžinių ir sveikų audinių morfologijos ir jų atsako į impulsinį elektrinį lauką. Audinių elektroporacijos mechanizmus iš dalies galima paaiškinti imitaciniais modeliais. Todėl reikia sukurti realistiškus imitacinius odos ar giliai įsišaknijusių vėžinių audinių modelius.

Šiuo metu vėžio gydymo kontekste elektroporacija pagrįstos procedūros turi įvairių neigiamų veiksnių, tokių kaip raumenų susitraukimai, skausmo pojūtis, Džaulio šiluma arba netolygus erdvinio elektrinio lauko pasiskirstymas dėl audinių nevienalytiškumo. Minėti aspektai lemia nepakankamą veikiamų audinių atsaką ir dėl to neefektyvų gydymą, taip pat uždelstą gijimą ir diskomfortą, keliamą pacientams. Norint sumažinti neigiamus veiksnius, reikia pasirinkti tinkamą elektrodo struktūrą ir apsvarstyti tinkamus impulsinio elektrinio lauko parametrus.

Elektrochemoterapija iki šiol atliekama mikrosekundžių diapazono elektros impulsais, pagal ESOPE (100 μs × 8 impulsų) procedūras, susijusias su didesne impulsų energija, raumenų susitraukimais ar skausmu. Naujausi tyrimai parodė, kad trumpesni impulsai (submikrosekundžių trukmės) gali sumažinti nurodytus šalutinius poveikius. Nepaisant to, sutartiniai submikrosekundžių trukmės impulsų protokolai turi būti išvesti eksperimentiškai *in vitro* ir *in vivo* prieš taikant kliniškai.

Darbo aktualumas

Dažniausiai taikomų elektrodų struktūros yra trivialios, tačiau moderniausios technologijos tobulėja ir atsiranda efektyvesnių elektrodų, leidžiančių tiksliau valdyti priešvėžinį
elektrinių laukų poveikį. Norint sukurti tokius elektrodus, reikia atlikti išsamų tyrimą. Šiuo metu būtent poveikio prognozavimas ir neigiamų veiksnių (šilumos poveikio audiniuose, impedanso iškraipymų, raumenų susitraukimų, nepakankamo lauko homogeniškumo, tūrio ir kt.) mažinimas yra viena pagrindinių technologinių problemų elektrochemoterapijos srityje. Todėl naujų elektrodų ir impulsinio elektrinio lauko protokolų kūrimas leidžia spręsti šias problemas kontroliuojant priešvėžinio poveikio lokalizaciją ir rezultatų atkuriamumą, skatinant tolesnę elektroporacijos srities biomedicininę plėtrą.

Tyrimo objektas

Disertacinių tyrimų objektas – invaziniai ir neinvaziniai elektrodai bei impulsinio elektrinio lauko protokolai, skirti vėžiui gydyti taikant elektrochemoterapijos procedūrą.

Darbo tikslas

Disertacijos tikslas – ištirti įvairias elektrodų struktūras, pritaikytas biomedicininės elektroporacijos technologijoms, išanalizuoti erdvinio elektrinio lauko pasiskirstymą atsižvelgiant į audinių nehomogeniškumą bei elektrines audinių savybes ir pasiūlyti naujus elekktrodus ir submikrosekundžių parametrinius protokolus elektrochemoterapijai.

Darbo uždaviniai

Darbo tikslui pasiekti buvo sprendžiami šie uždaviniai:

1. Apžvelgti skirtingus komerciškai prieinamus elektrodus, elektrodų prototipus ir *in silicio* modelius, naudojamus elektroporacija pagrįstiems biomedicininiams pritaikymams *in vivo*.
2. Sukurti paviršinio naviko skaitmeninį modelį, skirtą erdviniam elektriniam laukui įvertinti, kad būtų galima tiksliau planuoti išankstinį gydymą, remiantis baigtinių elementų metodu.
3. Sukurti elektrodų struktūrą, tinkamą efektyvesniam elektrochemoterapijos gydymui *in vivo*.
4. Pasiūlyti naujus submikrosekundžių impulsinio elektrinio lauko parametrinius protokolus, kurie yra efektyvumo požiūriu yra geresni arba prilygsta standartiniam klinikiniam ESOPE gydymui,

5. Atlikti parametrinę vaistų pernašos *in vitro* analizę ir sukurti naujus submikrosekundžių protokolus taikomiesiems elektrochemoterapijos tyrimams.
6. Sukurtą elektrodo struktūrą pritaikyti elektrochemoterapijos tyrimuose *in vivo*.

Tyrimų metodika

Šiame darbe buvo taikomi skaitiniai ir eksperimentiniai metodai. Erdvinis elektrinio lauko paskirstymas atliktas naudojant COMSOL programinę įrangą. Skaičiavimai ir detalus modelio tyrimas naudojant MATLAB ir COMSOL LiveLink for MATLAB programinę įrangą. Rezultatai patikrinti eksperimentiškai *in vivo* ir *in vitro* tyrimų metu.

Darbo mokslinis naujumas

Disertacijos teorinio ir eksperimentinio tyrimo mokslinio naujumo aspektai yra tokie:

1. Sukurtas paviršinio naviko modelis sėkmingai panaudotas eksperimento rezultatams tiksliai įvertinti ir elektriniams elektrochemoterapijos protokolams *in vivo* tyrimams nustatyti.
2. Vertinant elektroporacijos potencialą bakterijoms naikinti odos paviršiuje, buvo taikoomas paviršinis odos modelis. Remiantis gautais rezultatais, parinkti tinkami impulsų protokolai paviršiniam odos gydymui nepažeidžiant giluminių audinių.
3. Sukurtos invazinio tipo elektrodo struktūros ir jo naudojimo metodikos veiksmingumas buvo patikrintas taikant elektrochemoterapiją SP2/0 auglio tipui *in vivo*.
4. Neinvazinio plokštelinio elektrodo modelis su laidžiu geliu buvo papildytas pasyvia švirkšto adata chemoterapinių vaistų injekcijai. Šis metodas leidžia sustiprinti elektrinį lauką ir užtikrinti homogeniškesnį elektrinio lauko pasiskirstymą.
5. Siūlomi submikrosekundžių trukmės elektros impulsų protokolai buvo išbandyti su LLC1 ir SP2/0 navikų ląstelių linijomis. Rezultatai parodė, kad pasiūlyti impulsų parametrai leidžia pasiekti ekvivalentinį arba geresnį bendrą gydymą, lyginant su standartiniais impulsų parametrais.

Darbo rezultatų praktinė reikšmė

Gauti disertacijos rezultatai prisidės prie saugesnės ir efektyvesnės vėžio gydymo terapijos, mažinančios raumenų susitraukimus, šiluminį poveikį ir kitus neigiamus veiksnius, atsirandančius atliekant elektroporacija pagrįstą gydymą. Baigiamojo darbo rezultatai panaudoti trijuose projektuose: „Aukšto dažnio dielektroforeze ir elektrosensibilizacija pagrįstų nanoelektroporacijos technologijų kūrimas tiksliniai vaistų ir genų pernašai“, S-MIP-19-13, Lietuvos mokslo taryba“; „Elektrochemoterapijos ir jos derinio su dendritinių ląstelių vakcinacija įtaka pelių navikų likvidavimui ir imuninio atsako formavimuisi“, S-MIP-19-22, Lietuvos tyrimų taryba; „Elektroporacija pagrįstas vėžio atsparumo vaistams valdymas naudojant naujas nanosekundžių asimetrines impulsų sekas“ S-LL-21-4, Lietuvos mokslo taryba.

Ginamieji teiginiai

1. Sukurti skaitiniai paviršinio naviko ir odos modeliai leidžia tiksliai (su ±10 % nuokrypiu) įvertinti erdvinio elektrinio lauko pasiskirstymą audiniuose ir audinių reakciją į įvairias impulsinio elektrinio lauko sąlygas.
2. Sukurta plokštelinio elektrodo konstrukcija su pasyvia adata leidžia sustiprinti elektrinį lauką centrinėje naviko dalyje, kas sukelia geresnį naviko atsaką į elektrochemoterapiją.
3. Siūlomi mažo tarpelio pinceto formos elektrodai ir pozicijos keitimo technika tinka žaizdoms gydyti, siekiant įveikti paviršines infekcijas, ir užtikrina sėkmingą žaizdos sterilizavimo metodą nepažeidžiant gilesnių audinių.
4. Siūlomi submikrosekundžių diapazono (100–900 ns) impulsiniai elektrinio lauko protokolai efektyvumo požiūriu yra pranašesni už ESOPE gydymą.

Darbo rezultatų aprobavimas

Tyrimo rezultatai paskelbti penkiuose moksliniuose straipsniuose *Clarivate Analytics Web of Science* žurnaluose su citavimo indeksu. Disertacijos rezultatai pristatyti 13-oje pranešimų 10-yje tarptautinių mokslinių konferencijų:

- Tarptautinėje mokslinėje konferencijoje „4th International Wroclaw Scientific Meetings“, 2020. Vroclavas, Lenkija.
- Tarptautinėje mokslinėje konferencijoje „Electroporation-Based Technologies and Treatments“, 2020. Liubliana, Slovėnija.
- Tarptautinėje mokslinėje konferencijoje „Open Readings 2021“, 2021. Vilnius, Lietuva.
- Tarptautinėje mokslinėje konferencijoje „8th IEEE Workshop on Advances in Information, Electronic and Electrical Engineering“, 2021. Vilnius, Lietuva.
- Tarptautinėje mokslinėje konferencijoje „MEASUREMENT 2021“, 2021. Bratislava, Slovakija.
- Tarptautinėje mokslinėje konferencijoje „1st International Scientific Conference “Advances in biomedical research with use of in vitro methods“, 2021. Liublinas, Lenkija.
- Tarptautinėje mokslinėje konferencijoje „9th IEEE Workshop on Advances in Information, Electronic and Electrical Engineering“, 2022. Ryga, Latvija.
- Tarptautinėje mokslinėje konferencijoje „Open Readings 2022“, 2021. Vilnius, Lietuva.
- Tarptautinėje mokslinėje konferencijoje „3rd Baltic Biophysics Conference (BBC2022) 2022“, 2022. Vilnius, Lietuva.
- Tarptautiniame moksliniame kongrese „4th World Congress on Electroporation“, 2021. Kopenhaga, Danija.

Disertacijos struktūra

Disertaciją sudaro trys pagrindiniai skyriai.

Pirmajame skyriuje aiškinamas pagrindinis elektroporacijos ir elektroporacija pagrįstų technologijų, įskaitant elektrochemoterapiją, veikimo principas biologiniuose audiniuose. Apžvelgiamos audinių dielektrinės savybės ir priklausomybė nuo impulsinio elektrinio lauko. Skyriuje pateikiama įvairių biomedicininio gydymo (elektrochemoterapijos, genų pernašos ar negrįžtamos audinių abliacijos) elektrodų santrauka. Skyrius baigiamas formuluojant pagrindinį šio tyrimo tikslą ir uždavinius.

Antrajame skyriuje pristatomas sukurtas paviršinio naviko modelis, skirtas tiksliam erdvinio elektrinio lauko pasiskirstymo vertinimui. Modelis jungia atskirų odos sluoksnių dielektrinių savybių priklausomybę nuo impulsinio elektrinio lauko. Taikant baigtinių elementų metodą tiriamas invazinių ir neinvazinių elektrodų kuriamas elektrinis laukas. Remiantis gautais rezultatais, tiriamas elektrodų tinkamumas disertacijos tikslams.

Trečiajame skyriuje pateikiami plaučių karcinomos (LLC1), pelių mielomos (Sp2/0) ir pelių melanomos (B16) navikų ląstelių linijų elektrochemoterapijos tyrimo rezultatai *in vitro* ir *in vivo* naudojant sukurtas elektrodų struktūras ir impulsinio elektrinio lauko protokolus. Taip pat tiriamos galimybės panaudoti elektroporaciją paviršinei žaizdų sterilizacijai.

Bendrosios išvados ir rekomendacijos tolesniems tyrimams apibendrina šį tyrimą.

Disertaciją sudaro įvadas, 3 skyriai, bendrosios išvados, šaltinių ir literatūros sąrašas, autoriaus mokslinių publikacijų disertacijos tema sąrašas ir santrauka lietuvių kalba. Disertacijos apimtis – 109 puslapiai. Disertacijoje yra 67 paveikslai, 12 lentelių ir 2 numeruotos formulės, disertacijoje panaudota 170 literatūros šaltinių.

1. Elektroporacija ir elektroporacija pagrįstos technologijos

Elektroporacija yra reiškinys, kai ląstelės membrana tampa pralaidi dėl trumpų didelio intensyvumo elektros impulsų. Toks ląstelių pralaidumo padidėjimas pastaraisiais metais plačiai naudojamas medicinoje, maisto pramonėje ar biotechnologijų srityse visame pasaulyje. Biotechnologijos srityje elektroporacija leidžia į biologinę ląstelę įterpti išorines molekules, kurios sukelia ląstelių inaktyvaciją (stabdo ląstelių aktyvumą, dalijimąsi ir augimą) arba aktyvaciją, kai prie ląstelės prilimpa išorinės medžiagos ir sustiprina jos dalijimąsi. Elektroporacija taip pat gali būti taikoma tiksliniam audinių ar medžiagų naikinimui be išorinių priemaišų. Procesai toliau kontroliuojami naudojant grįžtamąsias arba negrįžtamąsias elektroporacijos procedūras. Pastarosios priklauso nuo elektrinio lauko stiprio ir jo pasiskirstymo audinyje.

Pirmajame disertacijos skyriuje atlikta literatūros šaltinių disertacijos tematika apžvalga. Didžiąją skyriaus dalį sudaro esamų elektrodų, skirtų elektrochemoterapijai, genų terapijai ir negrįžtamai elektroporacijai, analizė ir elektrinio lauko pasiskirstymas. Apžvelgti pagrindiniai elektrodų trūkumai ir pritaikymas skirtingiems augliams ar audiniams gydyti. Išanalizavus žmogaus audinių elektrinius parametrus ir jų priklausomybę nuo naudojamų impulsų parametrų, nustatyta, kad elektrinis laukas yra stipriai iškraipomas dėl audinio sluoksnių nehomogeniškumo. Nustatyta, kad elektrinis laukas ir gydymo efektyvumas gali būti valdomas naudojant tinkamą elektrodų struktūrą. Remiantis gautais rezultatais apibrėžtas disertacijos tikslas ir iškelti darbo uždaviniai.

Skyriuje taip pat apžvelgiami elektros impulsų parametrai ir jų pritaikymas biomedicinos srityje, apžvelgiami pagrindiniai trūkumai ir neigiami padariniai žmogui

gydymo metu. Atsižvelgiant į literatūroje pateiktus duomenis buvo nustatyta, kad, keičiant elektros impulsų amplitudę, trukmę, kiekį ir dažnį, galima kontroliuoti elektroporacijos efektyvumą ir sumažinti šalutinius poveikius. Skyriaus pabaigoje apibrėžtas disertacijos tikslas ir iškelti darbo uždaviniai.

2. Elektroporacijos audinio modelio kūrimas gydymo numatymui

Antrajame darbo skyriuje pateikti autoriaus sukurti paviršinio odos auglio ir odos modeliai, leidžiantys tiksliai vertinti elektrinio lauko pasiskirstymą naudojant skirtingų tipų elektrodus ir elektros impulsų parametrus.

Atliktų tyrimų pirmajame etape buvo išspręstas vienas iš uždavinių, t. y. sumodeliuoti paviršinį auglį atsižvelgiant į atskirų odos sluoksnių ir auglio priklausomybę nuo elektrinio lauko. S2.1 paveiksle pavaizduotas sukurtas auglio modelis naudojant „COMSOL Multiphysics“ programinę įrangą.

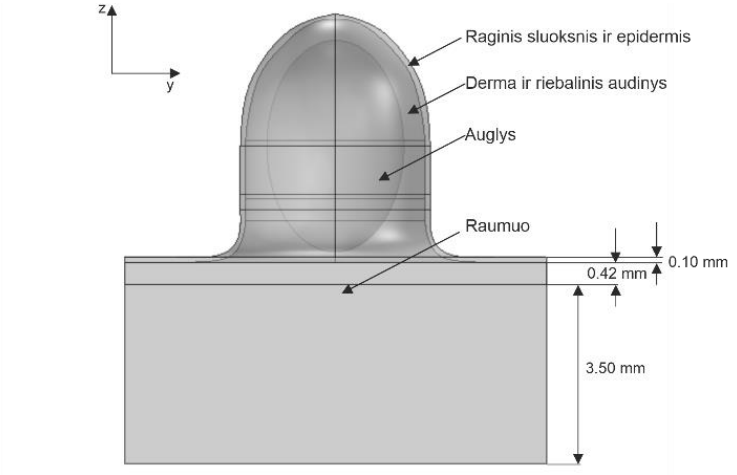

S2.1 pav. Paviršinio naviko modelis, skirtas erdvinio elektrinio lauko pasiskirstymui įvertinti

Odos modelis vertina audinių struktūros nehomogeniškumą, atsižvelgiant į tokius odos sluoksnius kaip raginis sluoksnis, epidermis, derma, riebalai, raumuo ir poodinis auglys. Gydomo audinio modelio geometrija yra labai sudėtinga ir nėra pakankamai duomenų apie atskirus odos parametrus, todėl buvo pasirinkti daugiasluoksniai audiniai, tokie kaip raginio sluoksnio audinys su epidermiu, dermos audinys su riebalais bei atskiri raumens ir poodinio auglio audiniai. Tai leidžia sumažinti klaidų tikimybę simuliacijos metu.

Taikant *in vivo* elektrochemoterapiją, reikia atsižvelgti į audinių laidumo dinamiką (santykinį σ padidėjimą). Todėl sukurtame modelyje vertinamas laidumo santykinis

padidėjimas dėl elektrinio lauko (neišeinant už grįžtamos E_{RE} ir negrįžtamos E_{IRE} elektroporacijos ribų).

Laidumo vertės buvo parinktos remiantis eksperimentiniais duomenimis, išmatuojant gautą naviko srovės ir įtampos kritimą. Eksperimentinė schema parodyta S2.2 pav. Gydymo metu buvo naudojamas ESOPE protokolas (1,4 kV / cm × 100 μs × 8). Išmatuotas elektros srovės padidėjimas, rodantis elektroporaciją.

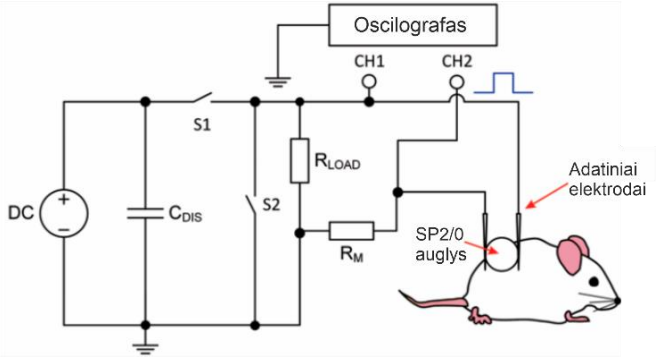

S2.2 pav. Srovės ir įtampos matavimo eksperimentinė schema (Novickij et al., 2020a)

Impulsai buvo filtruojami siekiant sumažinti pereinamuosius vyksmus. Apkrovos varža tarp elektrodų apskaičiuota pagal Omo dėsnį. Laidumo reikšmių ir elektrinio lauko slenksčio koregavimas modelyje buvo atliekamas tol, kol nuokrypis tarp eksperimentinių ir skaičiuojamųjų duomenų (išmatuotos ir apskaičiuotos srovės) neviršijo 10 %. Modelis taip pat buvo patikrintas su lygiagrečiais plokšteliniais elektrodais (Novickij et al., 2021).

Sukurtas imitacinis modelis gali būti naudojamas erdvinio elektrinio lauko pasiskirstymo analizei naudojant skirtingas elektrodų struktūras, tinkamas paviršiniam navikui gydyti. Tai taip pat patogus būdas analizuoti skirtingų elektrodų kuriamą erdvinį elektrinio lauko pasiskirstymą, išbandyti galimas jų tobulinimo galimybes ir kurti naujas elektrodų struktūras.

Antrajame disertacijos skyriuje parodyta, kad invaziniai elektrodai, sudaryti iš dviejų adatų, negali užtikrinti vientiso elektrinio lauko pasiskirstymo auglyje, ypač centrinėje jo auglio dalyje. Tai didina auglio ataugimo riziką ir sveikų audinių pažeidimo laipsnį. Todėl buvo pasiūlytas ir ištirtas elektrodų, sudarytų iš dviejų adatų, padėties keitimo metodas. Numatoma, kad adatiniai elektrodai yra įleidžiami į auglio centrą ir kraštą. Tada kraštinis elektrodas perkeliamas keturis kartus kas 90 laipsnių. Impulsinis elektrinis laukas yra generuojamas kiekvienoje adatos padėtyje, reguliuojant amplitudę pagal audinių varžą ir atstumą tarp adatų porų.

Modeliavimo rezultatai parodė, kad pasiūlytas metodas leidžia užtikrinti didžiausią elektrinio lauko vertę centrinėje auglio dalyje ir sumažina sveikų audinio pažeidimo galimybę. Metodo pritaikymas naudojant sukurtą paviršinio auglio modelį ir 1,4 kV/cm elektrinį lauką pavaizduotas S2.3 paveiksle. Elektrodų įtampa buvo pritaikyta atsižvelgiant į elektrodų tarpo dydį: 4 mm – 500 V ir 1,5 mm – 270 V.

Pagrindinis sukurto modelio trūkumas yra metodo invaziškumas. Be to, technikos pritaikymas, esant mažiems navikams, yra ribotas dėl galimo sveikų audinių pažeidimo.

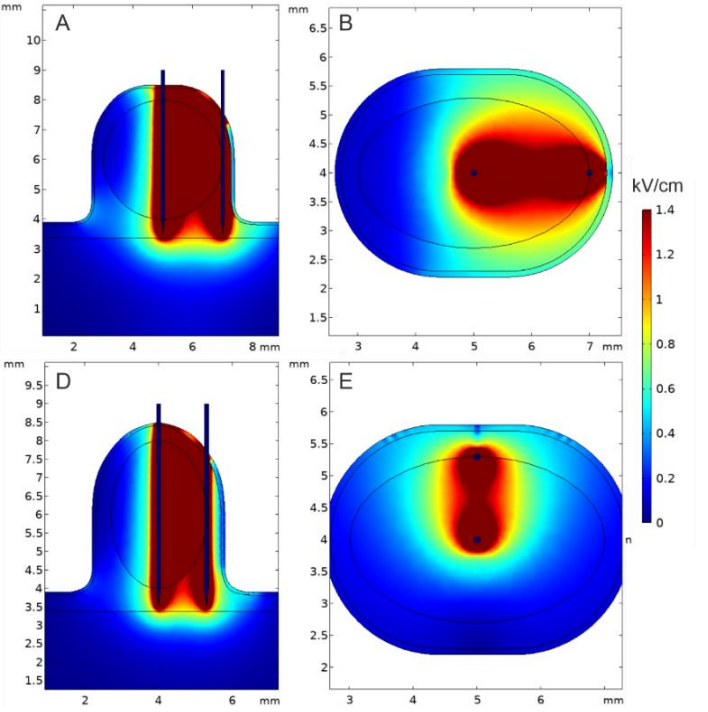

S2.3 pav. Modeliavimo rezultatai naudojant sukurtą invazinį elektrodą (1,4 kV/cm impulsas), kur A, D – elektrinio lauko erdvinis pasiskirstymas, vaizdas iš šono; B, E – elektrinio lauko erdvinis pasiskirstymas, vaizdas iš viršaus

Antrajame disertacijos skyriuje vertinamas elektrinio lauko pasiskirstymas naudojant plokštelinius elektrodus. Pagal gautus rezultatus, auglys nebus padengtas vienodu elektriniu lauku. Audinių sritys, kurios neturi tiesioginio kontakto su elektrodais, yra veikiamos perpus mažesnės vertės elektriniu lauku. Todėl galima daryti prielaidą, kad elektrochemoterapijos procedūra, naudojant plokštelinius elektrodus, negali garantuoti veiksmingo gydymo.

Norint padidinti procedūros efektyvumą, galima apsvarstyti impulso intensyvumo (impulso amplitudės) didinimą. Tai leistų visą auglį paveikti aukštesnės vertės elektriniu lauku. Sprendimas padidintų abliacijos plotą odos paviršiuje ir neturėtų jokios įtakos elektrinio lauko homogeniškumui. Remiantis literatūros apžvalgos duomenimis, plonas laidžiojo gelio sluoksnis tarp paviršinio naviko ir elektrodų leistų pasiekti homogeniškesnį elektrinio lauko pasiskirstymą. Todėl šiame skyriuje buvo ištirtas laidžiojo gelio veiksmingumas naudojant paviršinio auglio modelį ir neinvazinius plokštelinius elektrodus.

Siekiant sumažinti šunto srovės tarp elektrodų galimybę, laidžiojo gelio sluoksnis padengiamas taip, kad viršutinė paviršinio naviko dalis liktų neuždengta.Simuliacijai parinktas 4 mm atstumas tarp elektrodo plokštelių, pritaikant tokią pat 500 V įtampą. Sukurtas modelis ir erdvinis elektrinio lauko pasiskirstymas pavaizduotas S2.4 paveiksle.

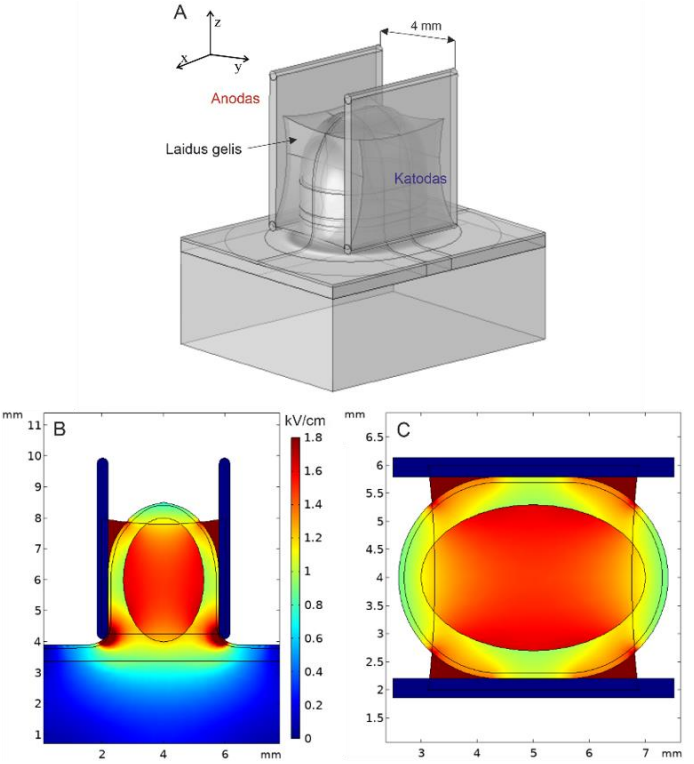

S2.4 pav. Modeliavimo rezultatai naudojant neinvazinį elektrodą su laidžiu geliu (1,4 kV/cm impulsas): A – simuliacijos modelis; B, C – elektrinio lauko erdvinis pasiskirstymas, vaizdas iš šono ir viršaus

Dėl odos struktūros ir elektrodų sudėties vienodas elektrinis laukas yra sunkiai pasiekiamas gydant paviršinius navikus plokšteliniais elektrodais. S2.4 pav., B ir C matoma, kad laidus gelis gali padidinti erdvinio elektrinio lauko pasiskirstymo homogeniškumą naviko viduje. Tačiau plokštelinių elektrodų su laidžiu geliu modelio kuriama elektrinio lauko vertė sumažėja viršutinėje ir apatinėje auglio dalyse. Norint tai kompensuoti, šiame darbe buvo pasiūlytas pasyvus centrinis adatinis elektrodas.

Įprastas gydymas, taikant elektrochemoterapiją, atliekamas naudojant vieną lokalią chemoterapijos vaistų injekciją į auglį steriliu švirkštu prieš poveikį impulsiniu elektriniu lauku. Atlikti tyrimai siūlo naudoti elektrodą su tuščiavidurėmis adatomis vaistui (Ritter et al., 2018) arba genams (Liu & Huang, 2002) įvesti ir impulsiniam elektriniam laukui perduoti.Elektrochemoterapijai naudojama nuimamoji švirkšto adata gali

sustiprinti naviko elektrinį lauką dėl santykinai didelio nerūdijančiojo plieno adatos laidumo. Hipotezei patvirtinti buvo sukurtas plokštelinio elektrodo ir pasyvios švirkšto adatos imitacinis modelis (S2.5 pav.). Galutinė adatos padėtis buvo pasirinkta atsižvelgiant į tipines eksperimentines procedūras. Todėl, pasyvios adatos padėtis buvo apibrėžta centrinėje naviko dalyje per visą auglio ilgį.

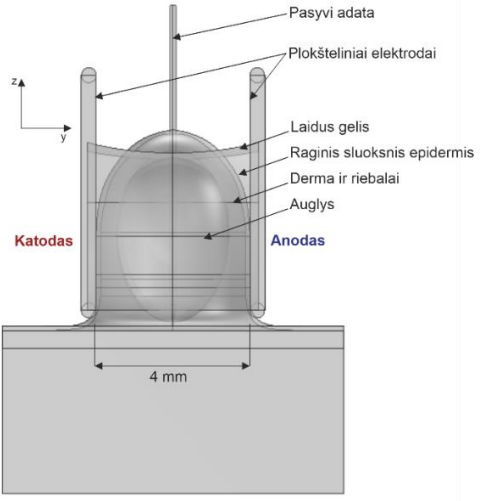

S2.5 pav. Paviršinio odos auglio modelis su neinvaziniais plokšteliniais elektrodais ir pasyvia adata

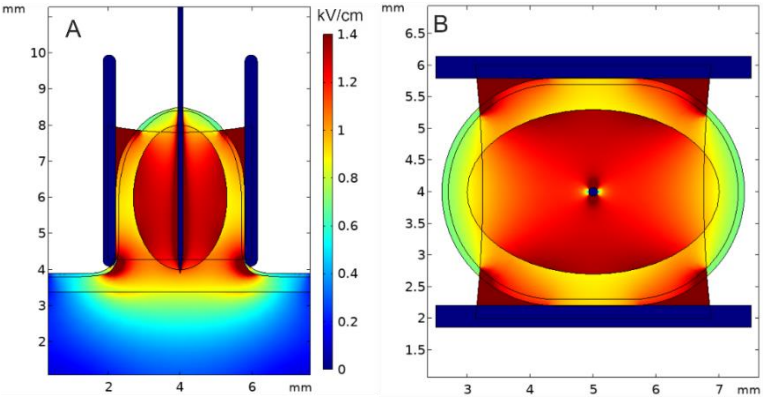

S2.6 pav. Erdvinis elektrinio lauko pasiskirstymas naudojant paviršinio auglio su plokšteliniais elektrodais ir pasyviąja adata imitacinį modelį: A – vaizdas iš šono; B – vaizdas iš viršaus

Erdvinio elektrinio lauko pasiskirstymo analizė atlikta esant 420 V gnybtų įtampai ir 4×10^6 S/m pasyvios adatos laidumui, išlaikant kitus modelio parametrus pastovius.

Pasiūlyta elektrodo struktūra leidžia sukurti homogeniškesnį erdvinio elektrinio lauko pasiskirstymą auglio viduje. Be to, pasyvi adata padidina elektrinį lauką apatinėje ir viršutinėje naviko dalyse (S2.6 pav.).

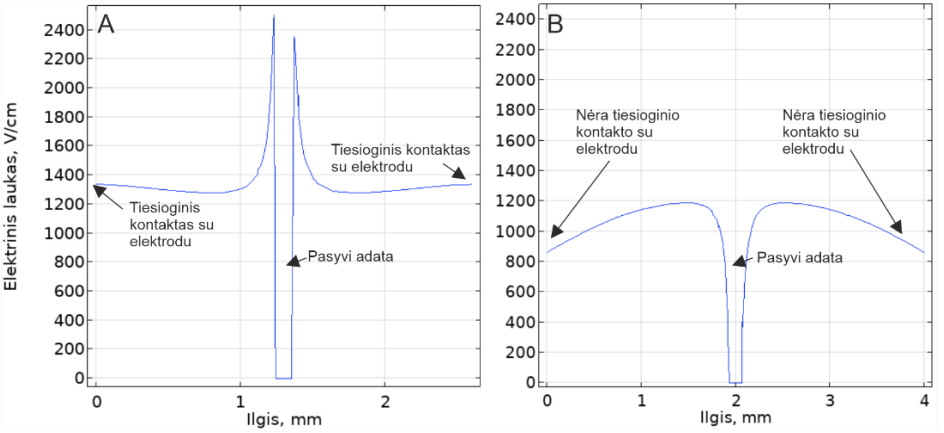

S2.7 pav. Elektrinio lauko verčių kreivės auglyje: A – YZ ašis; B – XZ ašis

Tačiau pagal S2.7 paveikslą pasiūlytas elektrodas neišsprendžia problemos auglio srityse, neturinčiose tiesioginio kontakto su elektrodais (S2.7 pav., B). Šiose ribose elektrinio lauko stipris nesiekia 0,9 kV/cm.

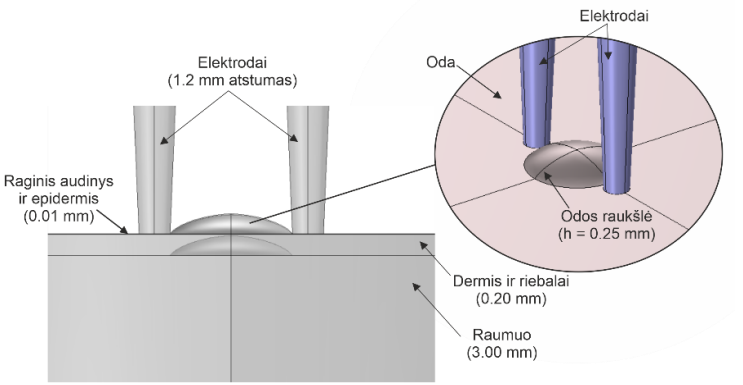

S2.8 pav. Beplaukių pelių odos imitacinis modelis, esantis tarp aštrių (kūgio formos) pinceto tipo elektrodų

Antrajame skyriuje taip pat sukurtas paviršinis odos imitacinis modelis, esantis tarp aštrių (kūgio formos) pinceto tipo elektrodų (S2.8 pav.). Modelis sudarytas iš dviejų daugiasluoksnių audinių, t. y. raginio sluoksnio ir epidermio, dermos ir riebalų, bei

raumens, atsižvelgiant į pradinį audinių laidumą ir laidumo pokyčius dėl taikomų elektrinio lauko impulsų. Nustatyta, kad raginis audinys yra kliūtis cheminiam ir fiziniam gydymui. Tačiau gauti rezultatai parodė, kad elektroporacija gali būti naudojama jo laidumui padidinti.

S2.9 paveikslo duomenimis, didžiausias elektrinis laukas yra sutelktas elektrodo ir audinio kontakto srityje. Tačiau po elektros impulsų perdavimo audiniai negrįžtamai elektroporuojami, tai rodo, kad laidumas didėja. Todėl S2.9 pav., B., parodytas tikrasis erdvinio elektrinio lauko pasiskirstymas, kai taikomas santykinai didelis impulsinis elektrinis laukas. Elektrinio lauko gylis gali būti valdomas keičiant elektrodo atstumą.

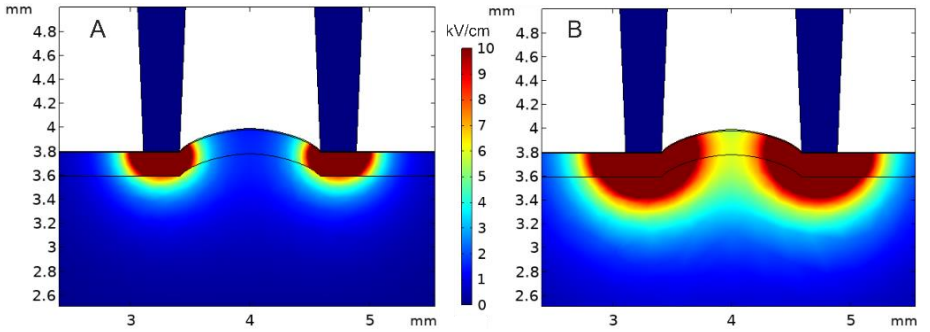

S2.9 pav. Erdvinis elektrinio lauko pasiskirstymas: A – audinių laidumas nepriklauso nuo impulsinio elektrinio lauko; B – audinių elektrinis laidumas padidėja dėl impulsinio elektrinio lauko sukelto pralaidumo

Remiantis modeliavimo rezultatais galima teigti, kad mažas tarpas (1,2 mm) tarp elektrodų užtikrina tik paviršinių ląstelių pralaidumą, nepažeidžiant gilesnių audinių, pavyzdžiui, raumens.

3. Taikomoji elektrochemoterapija su mikrosekundžių ir submikrosekundžių impulsiniais elektros laukais

Trečiajame skyriuje pateikti sukurtų elektrodų ir siūlomų submikrosekundžių impulsinių elektrinių laukų pritaikymo *in vivo* eksperimentinių tyrimų rezultatai. Tyrimų protokolai buvo sudaromi naudojant atliktus *in vitro* eksperimentinių tyrimų rezultatus.

Siekiant sukurti naujus ir veiksmingumo požiūriu efektyvius elektroporacijos protokolus, visų pirma buvo atliktas tyrimas *in vitro*, naudojant pelių liuminescencines mielomos SP2/0 ląsteles (SP2/0-Luc). Eksperimente buvo išbandyti 0,1–5 µs × 250 ir 100 µs × 1–8 pulsavimo protokolai 1–2,5 kV/cm diapazone.

Elektriniai impulsai buvo perduodami naudojant 1 mm tarpo kiuvetę su aliuminio elektrodais. Ląstelių atsakas į impulsinį elektrinį lauką buvo įvertintas naudojant morfologinę analizę su skirtingomis impulsų trukmėmis *in vitro*. Ląstelių morfologiniai pokyčiai ir fluorescencinio dažo (propidžio jodido) pasisavinimas parodyti S3.1 paveiksle. Rezultatų analizei įvertinti S3.1 paveiksle pavaizduotos nepaveiktos ląstelės (CTRL).

Vaizdai buvo naudojami elektroporacijos rezultatams ir negrįžtamos elektroporacijos riboms numatyti. Remiantis duomenimis, silpnas impulsinis elektrinis laukas sukelia beveik neaptinkamą ląstelių fluorescenciją. Negrįžtamą elektroporaciją vaizduoja ryški fluorescencijos signalo spalva.

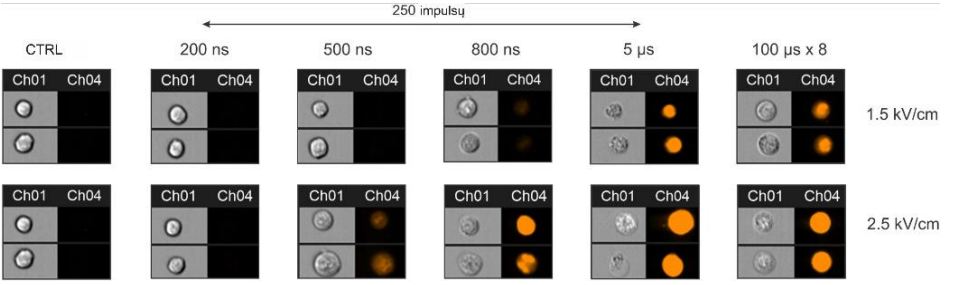

S3.1 pav. Ląstelių morfologijos pokyčiai priklausomai nuo impulsinio elektrinio lauko intensyvumo: Ch01 – šviesaus lauko vaizdas; Ch04 – fluorescencinis vaizdas naudojant 610–630 nm dažnių juostos filtrą (Novickij et al., 2020b)

Remiantis duomenimis, 1,5 ir 2,5 kV/cm impulsinis elektrinis laukas nesukelia aptinkamo pralaidumo su 200 ns trukmės impulsais, esant kHz dažniui. Tačiau, norint tiksliau apibrėžti elektroporacijos slenkstį, ląstelių pralaidumo priklausomybė nuo taikomų pulsavimo protokolų buvo tiriama naudojant srauto citometriją.

Buvo pastebėta, kad elektroporacija yra slenksčio tipo reiškinys. Taikant mikrosekundžių impulsus 1 kV/cm pakanka pasiekti visų ląstelių pralaidumą tik po 8 impulsų. Padidinus amplitudę, ląstelių pralaidumas pasiekiamas jau po 1–2 impulsų. Nanosekundžių trukmės impulsai yra veiksmingi tik su 2 ir 2,5 kV/cm elektriniu lauku. Lygiavertis ląstelių pralaidumas (~80 %) pasiekiamas naudojant 700 ns ir 300 ns × 250 impulsus su atitinkamomis 2 ir 2,5 kV/cm amplitudėmis. Rezultatus patvirtino pakartotinio matavimo duomenys gauti praėjus 1 valandai po gydymo.

Pastebėta, kad priklausomai nuo impulsų skaičiaus ir amplitudės elektroporacija gali būti negrįžtama tiek naudojant ESOPE, tiek trumpus mikrosekundžių ir submikrosekundžių trukmės impulsus. Visi tyrime naudoti submikrosekundžių protokolai rodė grįžtamąją elektroporaciją. Ilgėjant impulsų trukmei (pvz., 2 µs) ląstelių, kurių membranos negalėjo užsidaryti, skaičius siekia beveik 40 %. ESOPE impulsai, kurių amplitudė yra 1 kV/cm, sukelia grįžtamąjį pralaidumą visame 1–8 impulsų diapazone. Didėjant impulso amplitudei, didėja negrįžtamai pralaidžių ląstelių skaičius.

Ląstelių linija buvo naudojama bandomuosiuose *in vivo* eksperimentuose, siekiant nustatyti navikus ir išbandyti elektrochemoterapijos su bleomicinu pritaikymą. Elektros impulsai (1, 2 kV / cm × 100 µs × 8) buvo naudojami kartu su plokšteliniais neinvaziniais elektrodais.

Liuminescencijos sumažėjimas buvo pastebėtas po elektrochemoterapijos. Tai rodo naviko atsaką į gydymą. Tūrinė analizė reikšmingų skirtumų neparodė, nes prieš tikslius matavimus susidaro šašas. Todėl liuminescencija yra tikslesnė priemonė naviko augimo dinamikai įvertinti pirmosiomis dienomis po gydymo.Visi eksperimento protokolai buvo

patvirtinti Lietuvos valstybinėje maisto ir veterinarijos tarnyboje (patvirtinimas 2020-04-14 Nr. G2-145). Tyrimas atliktas griežtai laikantis laboratorinių gyvūnų priežiūros ir naudojimo vadovo rekomendacijų.

Sukurta invazinė adatinių elektrodų struktūra ir jos pritaikymo metodas buvo naudojamas SP2/0 auglio gydimui su 12 mg/kg doksorubicino. Gydymas buvo atliekamas naudojant 12 pelių, kurių augliai buvo pasiekę apie 150–500 mm^3 tūrį. Eksperimente buvo taikomi nanosekundžių (3,5 kV/cm × 800 ns × 250) ir mikrosekundžių (1,4 kV/cm × 100 μs × 8) elektros impulsai.

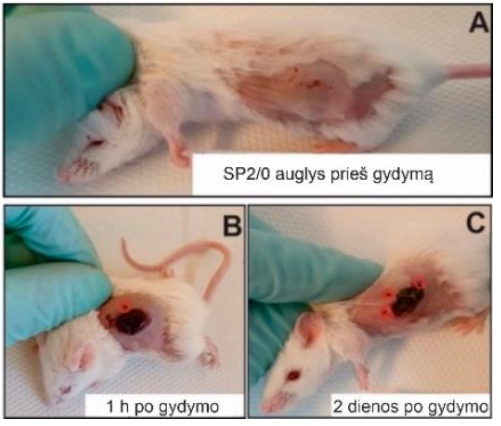

S3.2 pav. Reprezentatyvios pelių nuotraukos prieš gydymą (A), 1 valandos (B) ir 2 dienų (C) po gydymo (3,5 kV/cm × 800 ns × 250 impulsų doksorubicinu). Raudoni apskritimai (B, C) žymi matomus elektrodo įdūrimo taškus (Novickij et al., 2020a)

Submikrosekundinė elektrochemoterapija, taikant adatinių elektrodų metodiką, pateiktą antrajame skyriuje, parodė geriausią gydymo rezultatą. Pelių išgyvenamumas buvo dvigubai didesnis, palyginti su negydyta kontrole. ESOPE protokolų atveju taip pat buvo aptiktas reikšmingas naviko augimo sulėtėjimas, tačiau veiksmingumas buvo prastesnis nei submikrosekundžių trukmės protokolų.

Buvo patvirtinta, kad siūloma invazinio elektrodo struktūra yra veiksminga elektrochemoterapijai. Taip pat elektrodas gali užtikrinti gerai kontroliuojamą poveikio lokalizaciją. Gydyto gyvūno nuotraukos prieš ir po ECT pateiktos S3.2 paveiksle.

Siūloma nanosekundžių elektrochemoterapijos metodika su adatiniais elektrodais sumažino naviko augimo dinamiką. Remiantis gautais duomenimis, nanosekudžių trukmės impulsai buvo efektyvesni už standartinius mikrosekundinius impulsus.Išsamią metodiką pateikia Novickij et al. (2020a).

Sukurtas paviršinio naviko modelis su plokšteliniais elektrodais ir laidžiu geliu buvo panaudotas LLC1 ląstelių linijos C57BL pelėms gydyti taikant elektrochemoterapiją su bleomicinu (50 μl). Tyrimo metu buvo vertinamas vienpolių impulsų, perduodamų aukštesniu pasikartojimo dažniu (1 kHz ir 1 MHz), efektyvumas. Tyrime naudoti elektrinių impulsų protokolai pateikti S3.1 lentelėje.

S3.1 lentelė. Elektroporacijos protokolai (Novickij et al., 2021)

Grupės pavadinimas	Protokolų parametrai
CTRL	Gydymas netaikomas
nsPEF1	3,5 kV/cm × 200 ns × 200,1 kHz
nsPEF2	3,5 kV/cm × 200 ns × 200,1 MHz
nsPEF3	3,5 kV/cm × 700 ns × 200,1 kHz
nsPEF4	3,5 kV/cm × 700 ns × 200,1 MHz
µsPEF	1,3 kV/cm × 100 µs × 8,1 Hz (ESOPE)

Pastebėta, kad 700 ns trukmės impulsai, perduodami 1 MHz dažniu, sukelia prisotintą pralaidumą, panašų į ESOPE impulsus. Padidinus delsą tarp nanosekundžių impulsų (1 kHz), gydymo efektyvumas labai sumažėja. 200 ns impulsai sukelia mažą ląstelės membranos pralaidumą, tačiau jų efektyvumas padidėja taikant 1 MHz dažnį.

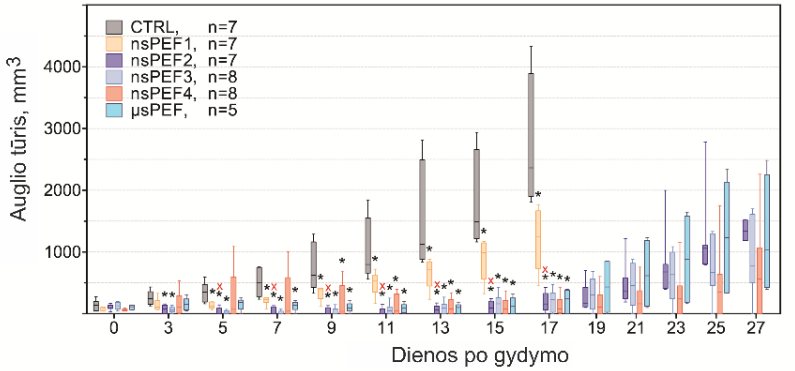

S3.3 pav. Auglių tūrio pokyčiai po elektrochemoterapijos bleomicinu; CTRL – gydymas netaikomas. * rodo statistiškai didelį (P < 0,05, Mann-Whitney U testas) skirtumą, palyginti su CTRL; X rodo statistiškai reikšmingą (P < 0,05) skirtumą, palyginti su nsPEF1 (Novickij et al., 2021)

Gydymo veiksmingumas buvo vertinimas keturias savaites matuojant naviko tūrį (S3.3 pav.). Dalinis arba visiškas atsakas į gydymą buvo stebimas visose gydytose grupėse, įskaitant ESOPE. 3 iš visų 16 pelių, gydytų skirtingomis sąlygomis, visiškai pasveiko. Šie navikai buvo veikiami 3,5 kV/cm × 700 ns × 200 impulsų protokolu, naudojant 1 MHz pasikartojimo dažnį. Buvo įrodyta, kad siūlomi submikrosekundžių elektrochemoterapijos protokolai yra veiksmingesni už standartines ESOPE nustatytas procedūras.

Išsamią metodiką galima rasti Novickij et al. (2021) darbe.Visi eksperimento protokolai buvo patvirtinti Lietuvos valstybinės maisto ir veterinarijos tarnybos (2020- 04- 14, Nr. G2-145). Tyrimas atliktas griežtai laikantis laboratorinių gyvūnų priežiūros ir naudojimo vadovo rekomendacijų.

Trečiajame skyriuje taip pat pateikti eksperimentiniai rezultatai naudojant plokštelinius elektrodus su pasyvia adata ir laidžiu geliu. Tyrimų metu buvo naudojamas pelių melanomos (B16) modelis taikant gydymą kalcio chloridu ($CaCl_2$) ir standartinį mikrosekundžių trukmės elektros impulsų protokolą (1,3 kV/cm × 100 μs × 8 (1 Hz). Objektyviam rezultatų vertinimui buvo atskirta pelių grupė, kuriai gydymas buvo taikomas naudojant tik plokštelinius elektrodus ir laidų gelį (CaPEF grupė). Rezultatai rodo, kad gydymas kalcio chloridu buvo efektyvus, lyginant su negydyta grupe (CTRL), nes vidutinis išgyvenamumas yra du kartus didesnis. Nustatyta, kad sukurta elektrodo struktūra su pasyviuoju elektrodu buvo efektyvesnė, palyginti su CaPEF grupe. Tai atitinka 2 skyriuje pateikto modeliavimo rezultatus.

Antrajame skyriuje sukurtas odos imitacinis modelis pritaikytas paviršiniam liuminescuojančios *P. aeruginosa* bakterijos žudymui impulsiniu elektriniu lauku ir 1 % (100 μL) acto rūgštimi. Užkrėsti bakterijomis pelių (BALB/C) odos audiniai (apie 78,5 mm^2) buvo veikiami taikant du impulsų protokolus: 15 kV/cm ir 25 kV/cm elektrinio lauko stiprio, 750 ns trukmės 1000 impulsų, pasikartojančių 15 kHz dažniu. Užkrėsti audiniai prieš impulsinio elektrinio lauko pritaikymą buvo sudrėkinti 1 % acto rūgštimi. Norint paveikti visą užkrėstą odos plotą, elektrodų padėtis buvo keičiama 14 kartų. Kita pelių grupė buvo gydoma tik 1 % acto rūgštimi (CTRL).

Bakterijų gyvybingumas vertinamas proporcingai bioliuminescencijos išspinduliuotų fotonų skaičiui. Bakterinio užterštumo analizė buvo atlikta kiekvienai pelių grupei 0, 3, 5, 7 dienomis po gydymo. Eksperimentas parodė, kad 25 kV/cm elektrinis laukas kartu su acto rūgštimi turi antibakterinį poveikį ir gali apsaugoti nuo tolesnės infekcijos plitimo 7 dienas po gydymo. Apibendrinant galima teigti, kad gydymas nanosekundžių impulsais yra perspektyvus žaizdų sterilizavimo metodas. Siūlomą gydymo metodą galima optimizuoti keičiant impulsų parametrus ir acto rūgšties koncentraciją.

Išsamią metodiką galima rasti Perminaitė et al. (2023) darbe. Protokolas patvirtintas Valstybinės maisto ir veterinarijos tarnybos (licencijos Nr. G2-48).

Bendrosios išvados

1. Sukurtas skaitmeninis paviršinio naviko modelis, remiantis baigtinių elementų metodu. Modelis leidžia tiksliai (rezultatų nuokrypis yra ±10 %) suplanuoti elektrochemoterapijos išankstinį gydymą, atsižvelgiant į atskirų odos sluoksnių laidumo dinamiką. Modelis yra tinkamas įvertinti erdvinio elektrinio lauko pasiskirstymą paviršiniame auglyje, naudojant skirtingas elektrodų konfigūracijas.
2. Sukurtas invazinis adatinis elektrodas su padėties keitimo technika gali būti sėkmingai pritaikytas elektrochemoterapijai. Elektrodai gali sukurti poveikį augliui, užtikrinant didžiausią elektrinio lauko vertę centrinėje jo dalyje. Tai leidžia efektyviai lokalizuoti poveikio sritį.
3. *in vivo* buvo pritaikyti aukštojo dažnio (MHz) nanosekundžių impulsai, rodantys kur kas geresnį veiksmingumą, nei šiuo metu naudojami klinikiniai protokolai, užtikrinant lėtesnį naviko augimą arba visišką pasveikimą.

4. Pasiūlyti pinceto tipo elektrodai ir jų naudojimo metodas yra tinkami žaizdoms gydyti kartu su acto rūgštimi. Metodas užtikrina paviršinį gydymą, nepažeidžiant gilesnių audinių.

Rekomendacijos

1. Rekomenduojama dar labiau suspausti elektros impulsus (>MHz), nes tai gali leisti pasiekti didesnį gydymo efektyvumą. Tačiau šis metodas reikalauja naujų elektroporacijos prietaisų kūrimo.
2. Norint palengvinti pasiūlytą žaizdų gydymo metodą naudojant impulsinį elektrinį lauką ir acto rūgštį, pinceto tipo elektrodus rekomenduojama pakeisti kelių adatų masyvu.

Veronika MALYŠKO-PTAŠINSKĖ

DEVELOPMENT AND RESEARCH OF INVASIVE AND NON-INVASIVE ELECTRODES FOR ELECTROCHEMOTHERAPY

Doctoral Dissertation

Technological Sciences,
Electrical and Electronic Engineering (T 001)

INVAZINIŲ IR NEINVAZINIŲ ELEKTRODŲ ELEKTROCHEMOTERAPIJAI KURIMAS IR TYRIMAS

Daktaro disertacija

Technologijos mokslai,
Elektros ir elektronikos inžinerija (T 001)

Lietuvių kalbos redaktorė Rita Malikėnienė
Anglų kalbos redaktorė Jūratė Griškėnaitė

2023 04 21. 10 sp. l. Tiražas 20 egz.
Leidinio el. versija *https://doi.org/10.20334/2023-010-M*
Vilniaus Gedimino technikos universitetas
Saulėtekio al. 11, 10223 Vilnius
Spausdino UAB „Ciklonas“,
Žirmūnų g. 68, 09124 Vilnius